# A Wearable Bioreactor to Study Limb Regeneration In Vivo using an Adult Murine Digit Amputation Model

A dissertation submitted by

Anne S. Golding

In partial fulfillment of the requirements for the degree of

Doctor of Philosophy

In

Chemical Engineering

Department of Chemical & Biological Engineering

Tufts University

Febuary 2019

Advisor: Dr. David L. Kaplan

## Abstract

In the United States approximately 185,000 people annually suffer from a limb amputation. Limb regeneration has been designated one of the top goals in fields of biomaterials and regenerative medicine, but is unattainable due to our lack of knowledge of the biology that drives limb regeneration. The fields of developmental and regenerative biology study the different pathways that define limb regeneration using animal models capable of this phenomenon. One of the few mammalian models of limb regeneration is the mouse digit tip amputation model. The resulting research has furthered our understanding of the fundamental mechanism that controls limb regeneration. However, in order to translate this fundamental knowledge into application, a system that can control activities at the amputation site, including hydration and drug delivery, is needed. In this thesis we present a solution to this issue with a wearable hydrogel based bioreactor for the studying limb regeneration *in vivo* using the mouse digit tip amputation model. The work presented demonstrates a robust system capable of handling the rough *in vivo* environment. The device was used to study the static and dynamic role of macrophage polarization towards limb regeneration. With static delivery, three different cytokines (interferon gamma, interleukin 4, and interleukin 10) were utilized to induce the different polarization states (M1, M2a, and M2c, respectfully). The different deliveries resulted in distinct immune profiles 5-day post amputation (DPA) that altered the wound healing and hydrogel interactions at later time-points (15 DPA and 28 DPA). Next we applied two methods of drug delivery to dynamically manipulate the local macrophage population with temporal and spatial control of two polarizing cytokines in a single treatment. The results confirmed the efficacy of both treatments at 5 DPA with differences in morphology in the wound bed, as well as variations in the immune profile (cell recruitment and macrophage polarization at the wound site). Overall the results

demonstrate the capabilities of this system to be used in mouse studies to further our understanding of limb regeneration.

.

## Acknowledgments

In my time here at Tuft's University I have learned many things. Some lesson were skillsets that I will utilize in my future career choice, others were valuable lessons on how to do research properly, and even some were friendly reminders of the rules of laboratory procedure, social norms, and common sense that will prevent my early death and possible jail time. While the lab I worked in taught me the necessity of self-reliance, it also taught me the value of collaboration. One needs a mentor to grow, and I am beyond grateful for the people who provided me that needed mentorship and friendship. They never gave up on me. Thank you Lorenzo, Jeannine, Dana, and Jon. For you I am beyond grateful and you have my respect and love. In particular I want to thank Lorenzo and Dana. Dana was the kind and patient teacher who helped me get over my own insecurities. And Lorenzo who was the friend and mentor that defined my PhD. Words cannot describe how grateful and blessed I am to have you shaped who I have become through this journey.

To the lab mates who were there during those late nights in the lab. They were a precious source of strength. Disha, Sarah LV, Sarah B., Meg, and Nicole, if not for you guys I am pretty sure I would not be where I am today. I thank my family; they gave the greatest gift of letting me go. They loved me even when I was absent, which a true gift of unselfish love. I also like to thank my advisor David Kaplan. While we had our differences, in the end I know he was the right advisor for me. He is the extremely rare combination of someone who is successful and intelligent, but still humble and kind. No matter where I go in life you will always be my advisor who I respect deeply. Someday I

hope you will explain how you have tolerated all my one-liners, without having resorted to murder.

## Dedication

I dedicate this to my Aunt who died from B-cell lymphoma while I was here. I promised her before she died I would do my best to make sure that others would have a chance to live where she did not. I hope I did her well. I dedicate this to my brother whose life has been defined and limited by an autoimmune disease. I hope that someday that things will be better for you and in some small way I can help with that.

## Table of Contents:

## List of Tables:

## List of Figures:

# Chapter 1: Introduction

## 1.1. Introduction

Whole organ and limb regeneration has been one of the goals of tissue engineers since the field began. In 2010 it was designated as one of the "Biomaterials Grand Challenges" set by the biomaterial field[1]. In the United States alone approximately 185,000 people annually suffer from a limb amputation with a predicted doubling of this number by 2050[1]**.** On top of the health issues, there is also a financial burden for the community and the family to accommodate for the loss of limb[2]. While advances in bio-electronic technologies and interfaces have created prosthetics that return some capability to the user[3], even the most advance models cannot completely replace the lost limb.

While limb regeneration has been a defined goal of the field for nearly a decade, there is still a long way to go. One of the road blocks that face engineers in this pursuit is the knowledge gap in the biological pathways that control limb regeneration. Without at least a working understanding of the biology, the situation remains a black box problem with too many unknown variables. The field of developmental and regenerative biology focuses on characterizing the different pathways that define limb regeneration. Most organisms are capable of near perfect regeneration during development, but few maintain this ability after birth[4]. The few animals that are capable of complex regeneration into adulthood have become models in studying the mechanisms that define this phenomenon. This information can be taken and applied to the next generation of materials used in tissue engineering.

.

There are a variety of different animal models used to study limb regeneration with many of these animals being aquatic or amphibian. The most commonly used animal model is *Ambystoma mexicanum* or axolotl salamander[4,5] The axolotl is capable of complete limb regeneration, even after multiple amputations[4,6]. Work with this model has provided insight to many important aspects of the limb regeneration event such as the importance of the wound epithelium[5] and the role of the immune system in initiating limb regeneration[6,7]. Yet, work has also shown that the mechanism that drives limb regeneration in amphibian models, like the axolotl, can differ in mammals[8]. For example, axolotl limb regeneration is nerve dependent, while results with mammal models remain uncertain regarding the role for innervation in the process[9].

### 1.2. Limb Regeneration in Mouse and Factors that Play Critical Roles in Limb Regeneration

One of the few established adult mammalian limb regeneration models is the mouse digit tip amputation model. Mouse digit tip regeneration is an epimorphic event that is spatially dependent[10]. If a mouse digit-tip is amputated distal to the nail bed on the farthest phalange bone (P3), the bone will regenerate[11,12]. If the cut is proximal to the nail-bed (typically a cut at the distal end of the second farthest phalange bone P2) then the digit will not regenerate[12]. This type of spatial dependent regeneration has also been observed in individual cases of digit tip regeneration in human children[13], making the information even more applicable for regenerative medicine.

Both the non-regenerative and regenerative models share similar initial biological steps right after amputation (inflammation and histolysis), but deviate around wound closure or initial blastema formation at 7 – 9 days post amputation (DPA)[12]. While these models do diverge at the 7 – 9 DPA, even the divergent steps are similar in nature. Both types of mouse digit models go through progenitor recruitment, differentiation, and a cartilage to bone transition phase that are akin to remodeling[14]. However, at the anatomic level what becomes clear is that while the P2 amputation represents an attempt at regeneration, it ultimately fails due to the lack of a distal organizing influence in these divergent steps[15]. Researchers can utilize both models to characterize how the P2 non-regenerative model differs from the P3 regenerative model, then use that information to modulate the non-regenerative model in an attempt to alter the regenerative outcome. This spatial approach can provide a power tool for us to understand and promote mammalian limb regeneration. Areas that are important for limb regeneration include the immune response, wound closure and its microenvironment, progenitor recruitment, and innervation.

### *1.2.1. Immune Response and Macrophages*

The immune response, and in particular macrophages, play an essential role in limb regeneration. In both the axolotl and mouse amputation models, if the local macrophage population is depleted from the limb prior to amputation the limb will not regenerate[7,16]. The parts that macrophages play in the initial stages of regeneration is multifaceted. The first and most fundamental role which macrophages play is to protect the body from foreign entities and removal of damaged tissue[14,17]. Beyond that, macrophages also secrete growth factors and chemotactic compounds that are essential for recruitment of

progenitor cells and initial blastema formation, as well as signaling other tissue systems to return to the digit tip (e.g. epithelium, vasculature, and nerve)[10,16,18,19].

One of the key features of macrophages for a successful role in limb regeneration is plasticity. A macrophage's ability to participate in processes towards limb regeneration is time and location dependent[16]. How a macrophage accomplishes this capability is through a concept called macrophage polarization. This is the process through which macrophages express different functional phenotypes in response to micro-environmental cues[20]. Little is known as to how macrophage polarization occurs during wound healing events. What is known is that if macrophages are not polarized correctly at the right times and in the right location then regeneration will not occur[20,21]. It is important to clarify the specific role that macrophage polarization plays in limb regeneration.

*1.2.2. Wound Environment, Closure, and Healing*

The wound-bed environment and initiation of the wound healing events play a major role in the final regenerative outcome for the both the regenerative and non-regenerative mouse digit-tip amputation models. Following amputation, Lehoczky et al. showed that the fibrin clot that forms initially will act as a hub for needed progenitor, and regeneration is hindered when the clot is removed prematurely[22]**.** Hypoxia is also an important factor in the initial stages of limb regeneration. The hypoxic environment acts as an environmental cue for macrophages to secrete needed signaling for cell recruitment, and initial blastema formation requires a low oxygen environment[23]. Extracellular matrix composition also plays an important role in limb regeneration. The types and orientation

of collagen in the regenerative amputation are different than what is observed in the non-regenerative limb amputation model[24].

The wound epithelium and wound closure are key events associated with the divergent step observed between the two amputation models[10]. Closure of the wound epithelium over the amputation site signals the end of the hysteria phase of regeneration. Simkin et al. demonstrated that early closure of the wound epithelium resulted in less bone degradation, and the final bone volume was closer to the initial bone volume compared to the typically observed denser version resulting from amputation and regeneration[18]. In axolotl limb regeneration, which is nerve dependent, the skin was shown to act as a bridge for the nerves to the area of the blastema[4]. Wound closure can also be inhibitory depending on what stage the wound epithelium is closed. If the wound fails to close at all then limb regeneration does not occur, but if the wound is stitched closed too early, limb regeneration will also not happen[4].

*1.2.3. Progenitor Recruitment, Distal Signaling, and Patterning*

Dawson et al. demonstrated the importance of progenitor recruitment when comparing regenerative P3 cut, non-regenerative P2 cut, and femur bone fractures in relation to progenitor recruitment. Both the P3 cut and bone fracture are considered regenerative, while the P2 cut non-regenerative. One of the major factors that let both the bone fracture and the P3 regenerative cut regenerate was the availability of pattern able progenitor cells[25]. The role of progenitor cells is not only to provide a source of undifferentiated cells, but also to provide patterning information which allows for digit formation. Lin et al demonstrated that grafting limb progenitor cells to the amputation site

in another regenerative model, laevis xenopus results in the growth of a partially formed limb with signs of digits[26]. This work also shows that these cells recruited a large population of endogenous cells intp the regenerative event. This demonstrated that progenitor cells promoted limb, patterning in cell types typically not capable of limb regeneration.

*1.2.4. Innervation*

Limb regeneration in axolotl is a nerve dependent event[27]. If an axolotl limb is denervated, it loses its ability to regeneration[27]. However, in the mammalian mouse digit tip model, the importance of the nervous system for digit tip regeneration is still under debate. Work by Johnston et al. demonstrated in the regenerative mouse amputation model that if a limb is denervated prior to amputation then it will not regenerate. In particular, they associated this with the local Schwann progenitor cell population which either directly or indirectly acted as a source of chemotactic cytokines and growth factors[28]**.** However, these denervated limbs were rescued with application of cytokine oncostatin m (OSM) or growth factor platelet derived growth factor AB (PDGF-AB)[28]**.** Both of these proteins are produced by macrophages or neighboring cells types regardless of the presence of nerves[29–31]. In addition, work by Dolan et al. demonstrated that nerve regeneration in the digit occurs independently of the blastema formation event[9]. He also showed that the progenitor Schwann cell population will follow vasculature, while the cells which form the blastema will follow signaling created by the local macrophage population and the hypoxic environment that they help create[9]**.**

## 1.3. Limitations in Using the Mouse Digit Tip Amputation Model and Current Druge Delivery Systems Used.

The mouse digit tip model overall is a robust model that has been utilized in the fields of regenerative and developmental biology to characterized the different key elements that facilitate and define limb regeneration. However, this model cannot be utilized to its full potential with current technology used to study this event. Current methods to deliver different stimuli to the wound bed are limited to small molecules and certain biomolecules, and generally only provide a single burst upon delivery[32]. More advanced methods have been attempted, but tend not to work due to animal tampering. Discussed below is the currently used technology to deliver stimuli to amputation sites and recent attempts to improve delivery.

### *1.3.1. Affinity chromatography beads*

Agarose affinity chromatography beads (affi-beads) are the gold standard for drug delivery in the mouse digit-tip amputation model. The beads are soaked in a solution with a high concentration of a desired compound. After this, the beads are implanted under the skin at the amputation site[32]. This is a well-established method of delivery that can be easily reproduced[32]. Affi-beads can deliver both small molecules, such as the C-X-C chemokine receptor type 4 (CXCR4) inhibitor AMD3100[32] and some bio-molecules, such as the morphogen bone morphogenetic protein 2 (BMP2)[33]. More than one compound can be loaded at a time, and additional beads can be implanted to increase the amount of a desired compound(s) to be delivered.

While affi-bead implants are a well-established method of drug delivery to the mouse digit amputation system, the method of loading and release, and the need for it to be implanted limits capability. The amount of drug delivered to the amputation site per bead is unknown and usually reported in terms of the concentration of drug in which the bead was soaked[34]. This makes it difficult to determine an optimized dose for the given delivery, which is critical when a given treatment has a small therapeutic window. The mode of implantation also limits the time which a bead can be implanted without suturing shut the amputation site (typically 3 – 5 days wait is reported in literature[33,34]). This makes studying the initial biological signals nearly impossible.

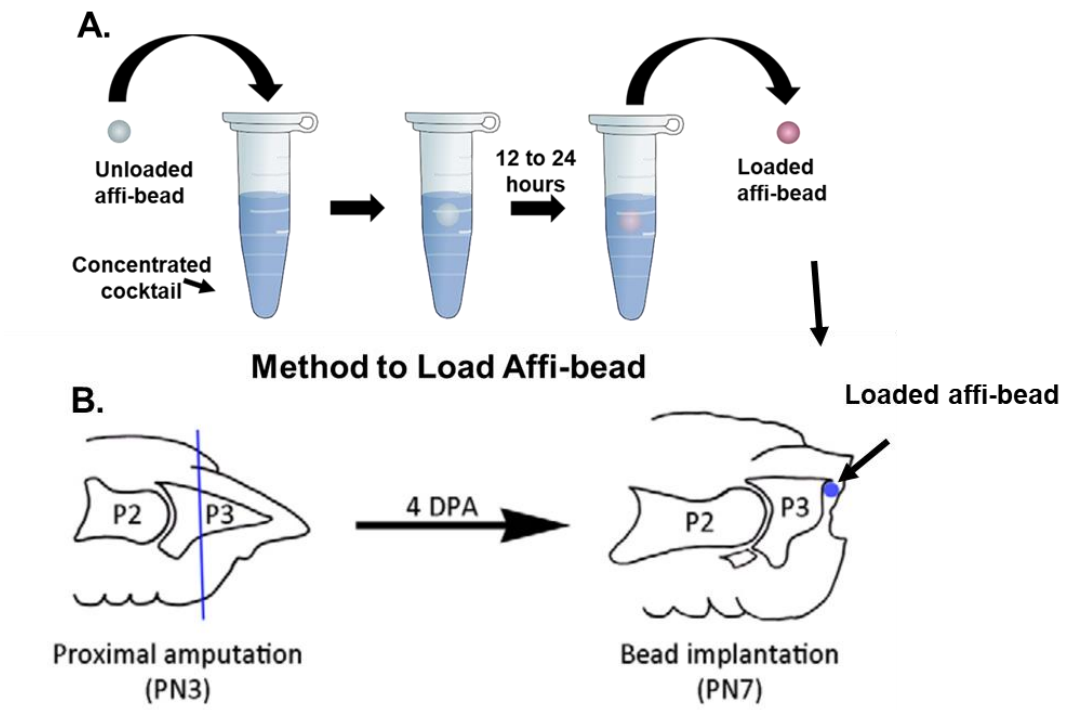


**Figure 1.2. Agarose Bead Drug Delivery System. A,** Schematic of Affi-bead loading. **B.** Example of Affi-bead implantation[33]. While the figure presents a P3 regenerative amputation this method can also be used for a P2 non-regenerative amputation as well. Implantation is usually performed using a sharp needle and a dissection scope.

*1.3.2. Fibrin Patches for Limb Progenitor Delivery*

Recent work has applied a more materials engineering approach in order to reach this middle ground[35]. The researchers utilized a two-stage system to study the effect of delivering mouse embryonic limb progenitor cells to the amputation site to induce limb regeneration[35]. After digit amputation, the wound was covered with a Hyphecan cap bandage to facilitate the necessary wound closure and healing[35]. Twelve days after wound closure (about 2 weeks post amputation) the bandage was removed and a fibrin gel loaded with the limb progenitor cells was grafted under the now closed amputation site[35]. Results from this work showed successful incorporation of the cells into the amputation site of the immune compromised mice, and bone growth distal from the cut site was observed in the cell treated groups[35]. However, the stage at which the regenerative P3 and non-regenerative P2 amputation response deviates occurred around 7 to 9 DPA[36]. As mentioned earlier this is when the wound epithelium closes over the cut site and either blastema formation begins (the P3 regenerative amputation), or the initial recruitment of osteochondral progenitor cells at and around the amputated bone that will be needed to form the soft fracture callus (non-regenerative P2 amputation) is observed[35]. The mechanisms that define what results in limb regeneration versus typically observed wound healing must happen before this 7 to 9 DPA event. Thus, the results observed from this work may not reflect the role that progenitor cells play in the limb regeneration process. In addition, both the Hyphecan cap and fibrin gel were susceptible to premature removal by animal tampering[35].

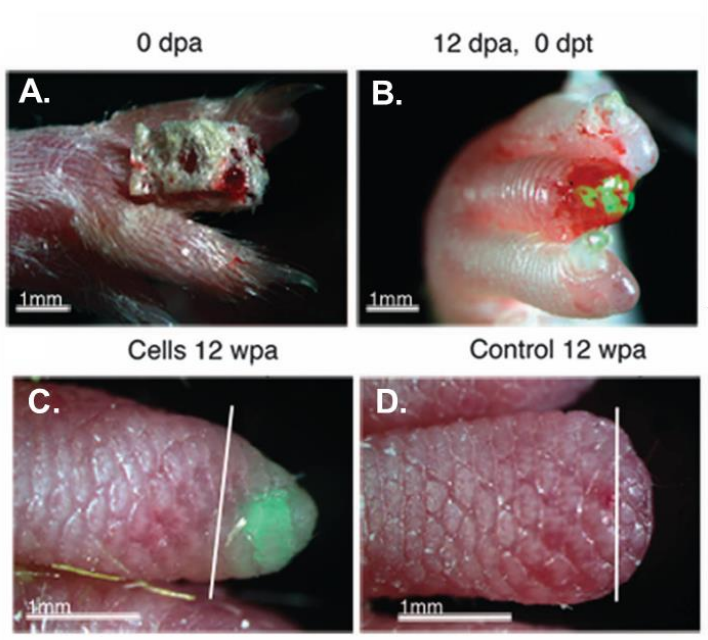


**Figure 1.3. Fibrin Patch for Limb Progenitor Delivery**[35]. **A.** Image of the digit right after amputation with the Hyphecan cap bandage attached. **B.** Hand after the GFP labeled limb progenitor cells were implanted at 12 days post amputation (DPA). **(C -D).** Mouse digits 12 weeks' post amputation with (C) and without (D) the implanted limb progenitor cells. The limb progenitor cells are GFP labeled and can be tracked. While this method showed success many of the mice prematurely removed the bandage or implanted fibrin path presented in figures (A) and (B).

### *1.3.3. Wearable Bioreactor Biodome*

The device known as Biodome was a wearable bioreactor that was a clear plastic reservoir attached to the amputated mouse digit via cyanoacrylate adhesive (super glue). The hard plastic reservoir was meant to house a liquid base cocktail of desired compounds to the amputation site. The Biodome design allowed for the insertion of a needle at the proximal end of the reservoir so that the cocktail solution could be exchanged over time. The Biodome was the first attempt to create a wearable bioreactor capable of being attached to the mouse externally for extended periods of time. Pilot technical studies for the Biodome device showed that it was able to stay attached for approximately 14 days' post amputation without removal[37]. However, issues of necrosis and severe tissue damage from device attachment arose from the need for a liquid tight seal, the location of device attachment, and the mode of attachment of the device. Also, many animals were able to remove the device before the desired end point[37].

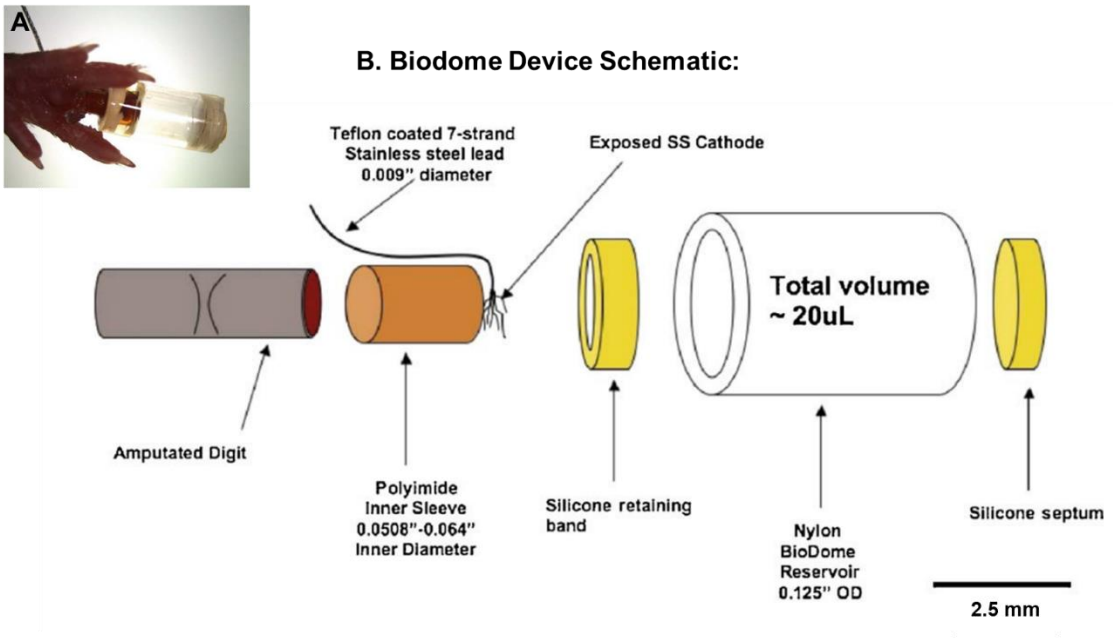


**Figure 1.4. Biodome wearable bioreactor[37]**. **A.** Image of the device being worn. Device is attached to the digit-tip of a mouse using cyano-acrylate based glue. **B.** Device schematic of the different components use in the Biodome device. The soft silicone sleeve is what is attached to the digit, while the hard plastic reservoir is what held the liquid cocktail. Cocktail could be injected and removed from the reservoir via a syringe through the rubber septum port of the device on the distal part of the device.

## 1.4. Thesis Goals and Chapter Outline

### *1.4.1. Scope of Thesis*

The purpose of this thesis was to develop, characterize, and optimize a wearable bioreactor for the study of limb regeneration *in vivo* using a mouse digit amputation model. Previous methods used to study limb regeneration lacked the capability to deliver the diverse stimuli to the amputation site with the tunability needed to mimic the steps that define limb regeneration. Previous work that attempted to rectify this issue proved ineffective due to animal tampering. To address these issues, three design criteria were established. First, the device must protect the mode of delivery from animal tampering without hurting the animal. Other methods, like the Biodome device, were able to remain attached for extended periods of time but would often lead to necrosis of the digit. Second, the delivery vehicle must be able to deliver a wide range of stimuli (i.e. small molecules, biomolecules, and cells) in a tunable manner that does not hinder wound healing. Scientists will need to be able to explore a plethora of different stimuli that will need to be delivered in a controllable manner. However, work has shown that limb regeneration will not occur if wound healing is block, so the device cannot hinder that event. Finally, the delivery system and methods used with it must be robust, scalable, and be able to be used by a wide audience. Animal studies require reproducibility with reasonably sized populations to verify a hypothesis. *We hypothesized that we could generate a wearable bioreactor to study key events in the wound healing cycle that define limb regeneration in a mouse digit-tip model. The work presented focuses on the static and dynamic role of macrophage polarization in limb regeneration*. The hypothesis was accomplished with the following aims:

**Aim 1:** Design a wearable bioreactor capable of studying limb regeneration *in vivo* with a mouse digit tip amputation model. In order to study the complexity of limb regeneration, a technical device and scaffold capable of providing dynamic stimulation is required. The first goal of this aim was to design, fabricate, and optimize the proposed hardware, baseline scaffold, and standards of procedure that will be used to study limb regeneration in the mouse digit tip model.

**Aim Two:** Utilize the device to study the role of static macrophage polarization and its role in limb regeneration. In order assess the ability of the device to study key events in limb regeneration, the role of macrophage polarization was assessed. Little is known as to how macrophage polarization during the initial wound healing events effects the limb regeneration process. In this work we used the device to deliver the cytokines interferon gamma (IFNy), Interleukin 4 (IL-4), and Interleukin 10 (IL-10) to polarize the local macrophage population into the M1, M2a, and M2c, respectfully. We hypothesized that we could alter the initial wound healing environment and secretome generated by the macrophages to alter further regenerative steps in the overall wound healing cycle.

**Aim Three:** Optimizing hydrogel design for dynamic modulation of macrophage polarization. In order to be an effective drug delivery system to study limb regeneration in the mouse digit-tip amputation model, the ability to tune delivery in both a temporal and spatial manner is required. Spatial delivery was achieved by a composite hydrogel with silk particles absorbed with IL-4, encapsulated into a silk hydrogel with either IFNy or IL-10 bulk loaded silk hydrogel. Temporal control was achieved by attaching two differently loaded cytokine hydrogels. We hypothesized that by manipulating the

temporal and spatial delivery of different polarizing cytokines we could alter the polarization macrophage recruitment profile observed in static bulk delivery of the same cytokines.

### *1.4.2. Thesis Outline*

Chapters 3 focus on the technical design of the external hardware of the device and optimizing design for *in vivo* application needed to accomplish aim 1. The work here demonstrated a working device and hydrogel delivery system capable of multi-week attachment with effective delivery of the drug Ivermectin to the amputation site with the additional benefit of observed hydrogel incorporation into the wound-bed allowing for longer term treatment. Chapter 4 focuses on characterizing how different macrophage polarization states could impact the macrophages role in the overall wound healing. Chapter 5 focused on optimizing hydrogel design and application to temporally and spatially manipulate macrophage polarization. Chapter 6 concludes and proposes future work on scaffold design for limb progenitor cell delivery with preliminary data showing that the device is capable of delivering limb progenitor cells.

# Chapter 2: Wearable Bioreactor Design, Fabrication, and Experimental Application

## 2.1. Introduction

The goal of this thesis was to apply the fundamentals of chemical engineering in the design of a drug delivery system to study limb regeneration. However, to accomplish this *in vivo* a device was needed. For the delivery system, the various methods and material sections provide the protocols used to create this device. The purpose of this chapter is to provide methods, relevant history, and theory behind the different protocols used to fabricate the system to study limb regeneration. In addition, the limitations of the current protocols with proposed methods of improvement is provided in order to aid in future improvements. A general overview is given to all aspects of the process so that this device could be used by engineers and biologists.

### *2.1.2. Benefits of the Wearable Bioreactor System*

The technical hardware of the system provides a means of attachment and protection for the hydrogel drug delivery system. All components are made from materials approved by the Federal Food and Drug Administration (FDA) and can be sterilized using an autoclave. Given the automated method of hardware fabrication and the simple method of attachment and removal, the device can be scaled up to allow for the needed population numbers to assess biological changes *in vivo*. The devices haves remained attached to the animals for up to 2 weeks (with minimal to no necrosis, a major improvement over the previously reported systems). While longer attachments are most likely feasible, they have not been attempted. In addition, the wound epithelium has a

tendency to heal and incorporate the silk hydrogel into the amputation site around 7 to 9 days' post amputation (DPA), thus making longer attachments mostly unneeded.

### *2.1.3. Benefits of a Silk Based Hydrogel Delivery System for the Wearable Bioreactor*

A hydrogel is a material composed mostly of water entrapped in a polymer mesh. The high water content of hydrogels combined with their elastic properties and shape retention makes it an effective delivery system to study limb regeneration *in vivo*. The first and most fundamental benefit is that the hydrogel is a material that will hydrate the amputation site without a need for a water tight seal. This will decrease the chance of tissue necrosis and animal tampering that would result in loss of attempting to make this seal. Since the hydrogel is both a solid and a liquid it processes tunable properties that can manipulate the micro-environment of the amputation site to alter biological outcomes. Some of these areas include mechanical properties like (e.g. stiffness), material (cross-linking density), and even biological functions are all tunable with these hydrogels. (addition of biological active compounds such as collagen).

In the area of delivery, hydrogels can provide improved means of temporal and spatial control versus that a solid material, allowing for a hydrated wet environment for the needed delivery of biologically sensitive molecules (e.g., proteins and cells) that a more liquid based reservoir can provide. It's this combination of spatial and temporal control while still maintaining a hydrated environment that is critical in understanding the dynamic events that drive limb regeneration. Finally, the hydrogel itself will be incorporated into the amputation site during wound closure, avoiding tissue damage

during removal and providing additional options to track regenerative outcomes. This allows for longer term delivery and experimental design.

## 2.2. Technical Device Design and Fabrication

The device concept is based on previous work addressed in Chapter 1, while the designs, fabrication, method of delivery, and capabilities are unique to this new device. All materials used and their respective vendors are included in in the supplementary section of this chapter. The hardware of the device can be broken down into 4 components: the hard outer sleeve, the protective cover cap, the soft insert that houses the hydrogel reservoir, and the bio-adhesive that is used to attach the components together and to the mice.

### *2.2.1. Outer Protective Sleeve*

As seen in Figure 2.2, the hard outer sleeve is composed of a two pieces which wrap around the hind-paw of the mouse. All materials were designed first in a CAD based program (either Solidworks or Autocad). The first version of this device was machined out of Polyether ether ketone (PEEK) and was held together by two screws. This model could be autoclaved and reused multiple times. However, due to the material and method of fabrication used, this version of the device was cumbersome and hindered mouse movements.

The next version of the outer sleeves was printed using a stereolithography 3D printer (Form 2, Formlabs, Somerville MA). The high resolution of this printer allowed for the

design to be modified so that the screws could be replaced with a key and lock design at the wrist in Figure 2.2. This design is lighter than the previous model, and as a result was a better fit for the mouse. Since the components are printed, this part of the device can be scaled up in a uniform manner. The material used to print the device was a methacrylate based resin (Dental SG resin, Formlabs, Somerville MA) that is autoclavable and FDA approved for medical device use. One benefit lost from the previous version of the device is that the sleeves are not as durable and can typically be used only once. Despite this limitation, speed and reproducibility for component printing and the decrease in attachment time resulted in more effective animal studies.

Additional post-printing steps are required before this component can be autoclaved. After the components are removed from the printer, the components need to be washed with isopropanol for 10 minutes twice to remove excess polymer. After the components are dried, they are UV cured to complete the polymerization reaction (MelodySusie 36W UV Nail Dryer, Amazon, Seattle WA). The outer sleeve parts need to be cured for 1.5 to 2 hours prior to autoclaving.

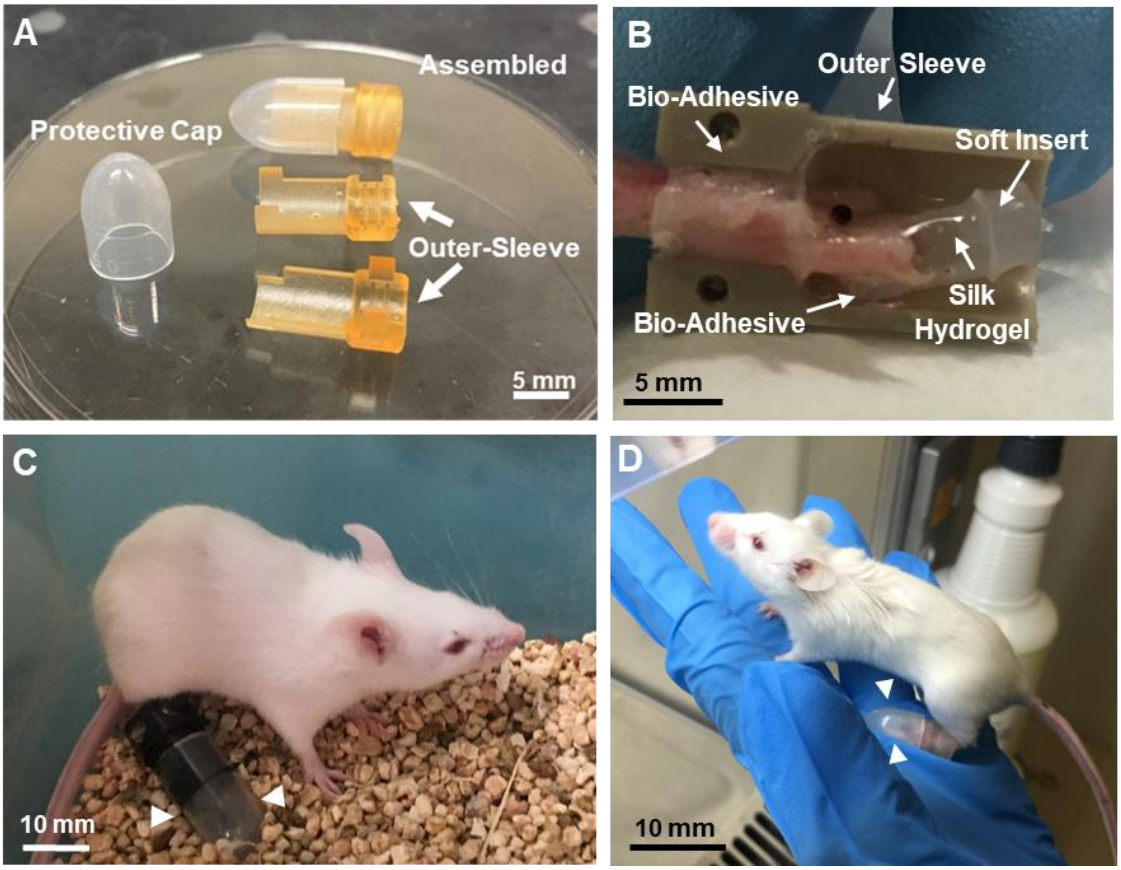


**Figure 2.1. Device Hardware Components. A**. Current protective sleeve and end cap of the device. The lock and key design of the two components allows for the device and cap to create a secure fit while the glue dries without the need of additional support. **B.** Device opened up to show the soft silicone insert (loaded with hydrogel) and bio-adhesive applied to the hind-paw. The paw, insert, and device is secured in place without damage to the tissue surrounding it. The hydrogel provides a hydrating environment to the amputation site. while the insert and adhesive allows for a secure but flexible attachment. **C.** Mouse wearing old device design. **D.** Mouse wearing new device. As shown in the figure, the improve design is lighter and smaller than the original device. The printed components add foe ease of movement and full use of the hind-paw to move.

.

### *2.2.2. Outer Protective Cap*

The end cap is used to cover the end of the outer protective sleeve. The cap is separate from the rest of the outer sleeve for removal and replacement while the rest of the sleeve remains attached to the animal. The dome shape lacks edges, which makes it less prone to chewing and animal tampering. The component is fabricated from a USA Scientific 2.0 mL flat cap tube (catalog no. NC9558509, Fischerscientific, Hampton, NH). This brand is slightly wider than the standard 2 ml micro-centrifuge tube, wide enough to fit over the outer protective sleeve. The in house design blueprints are included in the supplementary portion of this chapter. The cap is fabricated by cutting off the bottom of the tube at the 0.6 to 0.7 mL line with a razor blade. A fabrication diagram is presented in Figure 2.3.

### *2.2.3. Soft Silicone Insert*

The soft silicone insert is cast out of Dragon Skin™ 10 NV silicone polymer (Smooth-On, Harrisburg PA). Polymerization is achieved following the manufacturer's directions where an equal volume of the two components are mixed together and poured into Teflon molds. The molds are then placed into a descanter and vacuum applied to remove bubbles in the mold for 10 minutes. After 10 minutes, the molds are removed from the descanter and left on the bench-top to solidify for 1.5 to 2 hours. The cured silicone is removed from the molds and a 4 mm biopsy punch is used to punch out each individual insert (each mold is designed to make 4 inserts per cast). At this point the inserts can be placed into an autoclave bag for sterilization and later use. A fabrication diagram is presented in Figure 2.3.

### *2.2.4. Skin-Tite Bioadhesive*

The final component of the hardware is the glue used to attach the device components to the mouse paw. SkinTite (Smooth-On, Harrisburg PA) is a two-part silicone bioadhesive that is approved for external medical device use. Previous work had surgically stitched device components to the animal or cyanoacrylate (super glue) based glues. Both systems could be removed during attachment and damaged the tissue of the hind-limb. Super glue resulted in tissue damage and necrosis due to the hard and abrasive material of the dried glue on the skin**.** The silicone based glue is approved by the Federal Food and Drug administration (FDA) for medical device attachment. When applied, this material provides a flexible but secure fit of the device components to the mouse that can be easily removed by peeling away the silicone from the limb. This material reduces damage to the mouse during attachment and removal.

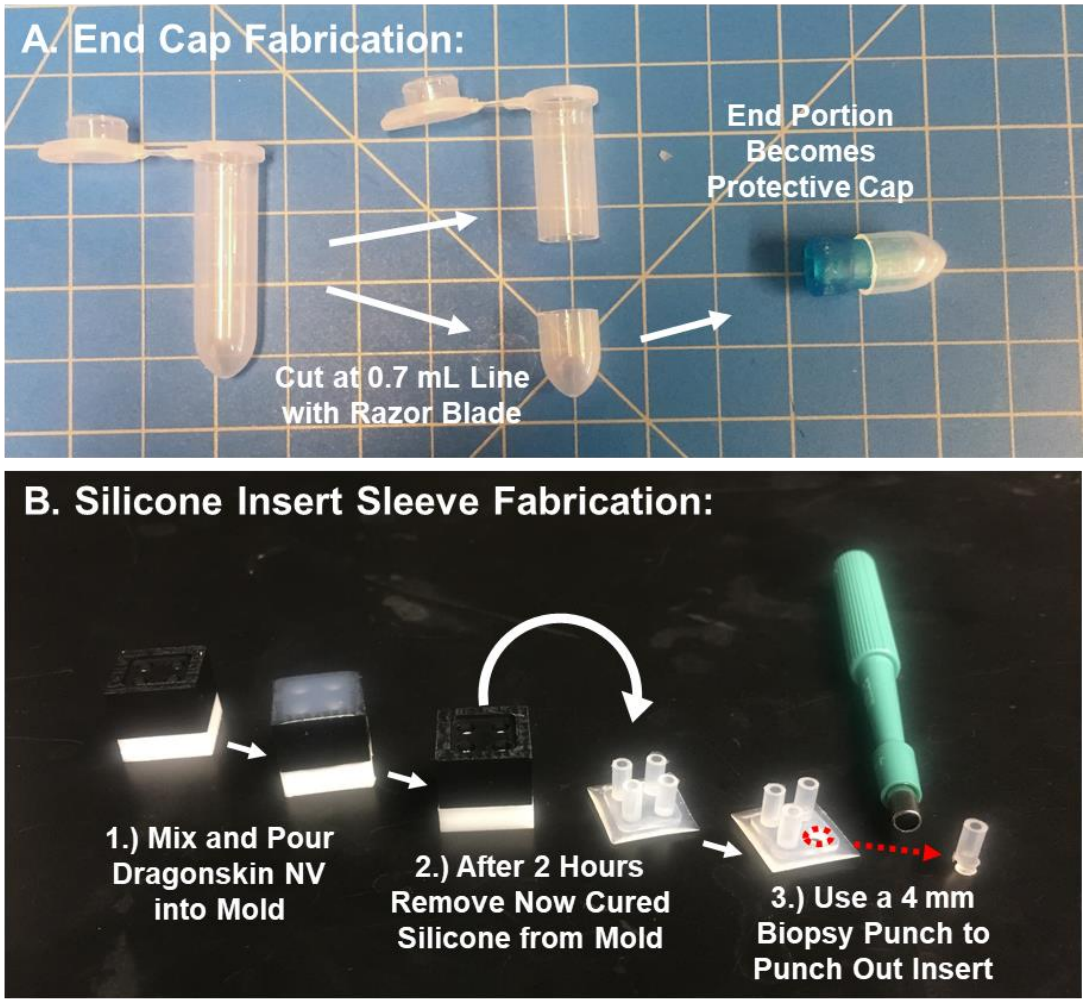


**Figure 2.2. Protective Cap and Soft Silicone Insert Fabrication. A.** End Cap Fabrication Process Diagram. A razor blade is used to cut the end portion of the micro-centrifuge tube to be used as the cap. **B.** Silicone Insert Sleeve Fabrication Process Diagram. The two part dragonskin silicone polymer is mixed then poured into the molds. These molds are degassed for 10 minutes to remove bubbles then placed for 2 hours to cure. After curing, the now solid polymer can be removed from the mold and each individual insert can be punched out for use.

## 2.3. Silk HRP Hydrogel Delivery System

The reservoir is the main component of the bioreactor device with direct stimulation at the amputation site. The hydrogel-based component is an enzymatically crosslinked silk protein using horseradish peroxidase enzyme (HRP)[38]. To improve tissue viability and hydrogel incorporation into the wound site, the protocol and base hydrogel was modified. In addition, a protocol to load the hydrogel into the soft insert of the device was developed. The method of hydrogel loading was modified in order to accommodate different release profiles and different loaded components.

### *2.3.1. Silk HRP Hydrogel Gelation and optimization for in vivo use*

The HRP enzyme facilitates covalent crosslinking via the free tyrosine amino acid side chains to create a di-tyrosine peptide bonds[38]. The reaction is initiated by the addition of HRP and hydrogen peroxide ($H_2O_2$) to the silk solution. The concentrations typically used in this gelation reaction are 10 U of HRP/mL silk hydrogel solution and a final concentration of 0.01% of $H_2O_2$[38]. The concentration was dependent upon hydrogel loading. In this study, the HRP concentration is halved and the $H_2O_2$ concentration is used at two-thirds of the above mentioned amount to decrease crosslinking density to improve hydrogel incorporation into the wound-bed.

### *2.3.2. Hydrogel Gelation and Drug Loading*

The silk HRP hydrogel reaction contents used in the device are presented in Table 2.1. The formulation was optimized from protocols used for 3D culture using the silk HRP hydrogel. These types of media additions to hydrogels are common for *in vivo*

implantation and *ex vivo* explants, examples including the delivery of limb progenitor cells to the amputation site of a mouse digit model using a fibrin hydrogel[26,28,35].

For the gelation solution, the media, dextrose, hanks buffer, and glutamax are mixed and the pH is adjusted to ~7.0 with sodium bicarbonate (the phenol red in the media should look peach-pink/salmon pink color) prior to the addition of the silk or other components. Then the silk is added and the solution is adjusted to pH ~7.0 again, and then the components to be delivered are added last. This process minimizes potential denaturation to the compounds that could arise from the acidic pH. A diagram showing the recommended component addition is presented in Figure 2.4. The desired delivered compounds can be added to the bulk solution before gelation. Certain molecules and proteins will react with HRP, or binds to the silk, which can affect reactivity, gelation, and/or release. Different compounds and biomolecules will escape from the HRP silk hydrogel with varying levels of success. It is recommended that for each desired component that the release profile is characterized. Protocols for *in situ* drug release analysis will be presented later in the chapter.

Silk mechanical and material features can be tuned based on the time that a person boils the cocoons during processing (this time period is referred to as minute boil or mb). The standard time that researchers tend to boil silk is 30 minutes (30 mb) for biomaterial application. Higher minute boils (such as 60-minute boil or 60 mb) are easier to sterilize in solution and are preferred for animal work. The minute boil used in this work is 60-minute boil or 60 mb.

Stock volumes for each component to achieve the desired concentration in the formulation as well as the compound in the final gelation solution can be calculated using dilution equations ($C_1V_1 = C_2V_2$ or $V_1 = (C_2V_2)/C_1$) where $C_1$ is the stock concentration of the component, $V_1$ is the volume to added of the component, $V_2$ is the final volume of the gelation solution, and $C_2$ is the desired final concentration of the added component in the gelation solution.

**Table 2.1.** Silk Hydrogel Base Formulation

| Item | Final Concentration | Purpose |
|---|---|---|
| Silk (60 mb) | 1 to 3% (w/v) | Polymer that creates hydrogel[38] |
| Media (10x) | 1:9 of Final Volume | Provides nutrients and helps with osmolality[38] |
| Glutamax (200 mM) | 2 mM | Essential nutrient for nucleic acid synthesis and help with cell removal of ammonia and oxidative species[39] |
| Dextrose (100 mg/mL) | 4.5 mg/mL | Additional sugar source that brings the concentration to typical levels found in DMEM media. |
| Sodium Bicarbonate (1 M) | till ~6.5 to 7.0 pH | Used to Adjust pH to ~7.0 |
| Hanks Balance Solution | Until Desired Final Volume is Obtained | Buffer Solution |

**Table 2.1. Silk Hydrogel Base Formulation.** The above table presents all components used in the base hydrogel formulation with final concentrations and description of the purpose of each component.

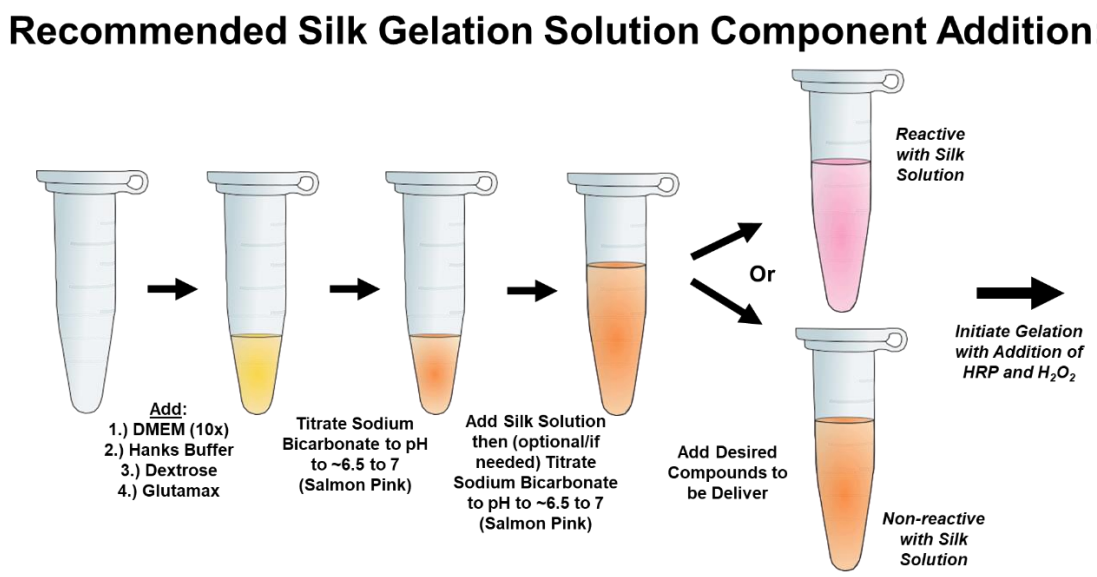


**Figure 2.3. Base Silk Gelation Solution Fabrication.** Presented schematic details of the silk hydrogel solution formula. The order presented minimizes damage to the desired delivred compound by adding in the base components, altering the pH, adding the silk, then adding the desired compounds last. If the compound reacts with the silk solution a color change sometimes be noticed. This is not always the case, but if the compound reacts with the silk solution or participates in the HRP reaction, then the gelation process could be altered.

## 2.4. Hydrogel Insert Fabrication Protocols

*2.4.1. (General Method) Bulk Loaded Hydrogel Fabrication*[a] *(Process Diagram Presented in 2.5)*

1) (prior to gelation) Have silicone sleeves ready to be loaded. Remove the insert sleeves from the autoclave bag and place them in a petri-dish. Gelation happens quickly and this will minimize wasted time[b,c].

2) Add 0.75 uL of HRP stock solution into the hydrogel solution and mix by pipetting the solution.

3) Add 0.5 uL of $H_2O_2$ stock solution into the hydrogel solution and mix by pipetting the solution.

4) Using the 1 – 10 uL micro-pipetter take 9 uL of the hydrogel solution and pipette it into the silicone insert sleeve.

5) Using the fine-tip forceps place the solution loaded insert into the 0.5 mL micro-centrifuge tube and close the lid. Place this tube onto the mini-centrifuge, balance the tube, and spin it down for ~30 seconds to removed trapped bubbles in the gel solution.

6) After spinning down the solution, check the insert, make sure that there are no bubbles, and enough solution in the insert to fill 5/6 of sleeve. Add or remove silk solution to achieve desired volume. If there are still bubbles trapped, then spin down the insert again for ~30 seconds. The space left empty will allow for the insert to be attached to the mouse digit tip securely. If the solution has solidified, then use a pair of fine-tip forceps to remove any excess silk hydrogel from the insert.

7) Once the desired volume is achieved for the hydrogel, place filled insert back into the centrifuge tube. After gelation is complete then the hydrogel insert can be used for *in vivo* work.

### *2.4.2. (Modification 1) Cell Loaded Hydrogel Fabrication*[d]

1.) (prior to gelation) Spin down cells and re-suspend them in DMEM so the cell gelation density of 1.5 x $10^6$ cells/mL can occur at the desired final volume[d] .

2.) Initiate gelation of hydrogel solution. Wait 1 - 2 minutes then add the cells to the gelation solution. Wait an additional minute then follow steps 4 – 7 in section 2.3.1. The final cell population per insert should be ~ 10,000 cells per insert.

3.) (optional) in a 96 well cell culture plate, cast 3 cell loaded hydrogels. The cell suspension homogeneity can be assess using a light microscope. If these cast gels are kept alive *in vitro*, then additional assays can be performed and correlated to the loaded cells.

### *2.4.3. (Modification 1) Composite/Layered Hydrogel Fabrication*[e]

1) Pipette 2 uL of bulk loaded only gelation solution into the insert[f]. Spin the inserts down if needed and wait for gelation to be completed.

2) Initiate gelation prior to addition of micro-particles. After gelation solution is well mixed then add in the desired components in a hank's buffer solution. Mix well, then add 7 ul to the insert. Place the insert back into the micro-centrifuge tube and wait for gelation to finish[g].

*2.4.4. Notes:*

a) Volumes of HRP and $H_2O_2$ are based on a silk hydrogel solution with a volume of 0.1 mL

b) Divide the hydrogel solution into 0.05 to 0.1 mL volume aliquots. The HRP silk reaction can be faster than predicted which can result in solution gelling before all the inserts are completed. Having aliquots will allow the researcher to repeat gelation and continue loading the inserts with minimal waste of materials.

c) Have labeled 0.5 mL micro-centrifuge tubes ready to go before fabrication occurs. The hydrogel can be placed into the designated tube, spun down to remove trapped bubbles and transported to surgery in a sterile manner with confidence in what treatment that hydrogel houses.

d) Cells loading density and time between start of gelation and addition of cells to gelation solution will depend upon the cell's size and general morphology. The larger and more amorphous the cell type is the lower the loading density and longer the time between start of gelation and addition of cells to the gelation solution will be. It is recommended that cell encapsulation with this hydrogel is optimized for each cell type *in vitro* before attempting to load the cells into the device. The presented protocol will use the optimized loading protocol for limb progenitor (LP) cells, which are small and circular. Additional cell types can be found in literature[38,40]

e) The layered/composite fabrication method is used when the researcher will want to load heavier components (such as the presented silk micro-particles), or if the researcher would want to include multiple treatments into one gel. The

process is designed to remove the centrifugation step used in the basic protocol, which can drag heavier added components to the bottom of the hydrogel (which limits the success of the desired treatment).

f) The purpose of the base layer is to “wet” the insert inside to help promote easier loading with minimal bubble formation.

g) The wait time between addition of hydrogel composite solution and gelation should be minimal. As with the cell encapsulation protocol, timing between initiation of gelation in the silk HRP solution and addition of the component the researcher wishes to have suspended in the hydrogel will need to be optimized prior to *in vivo* use.

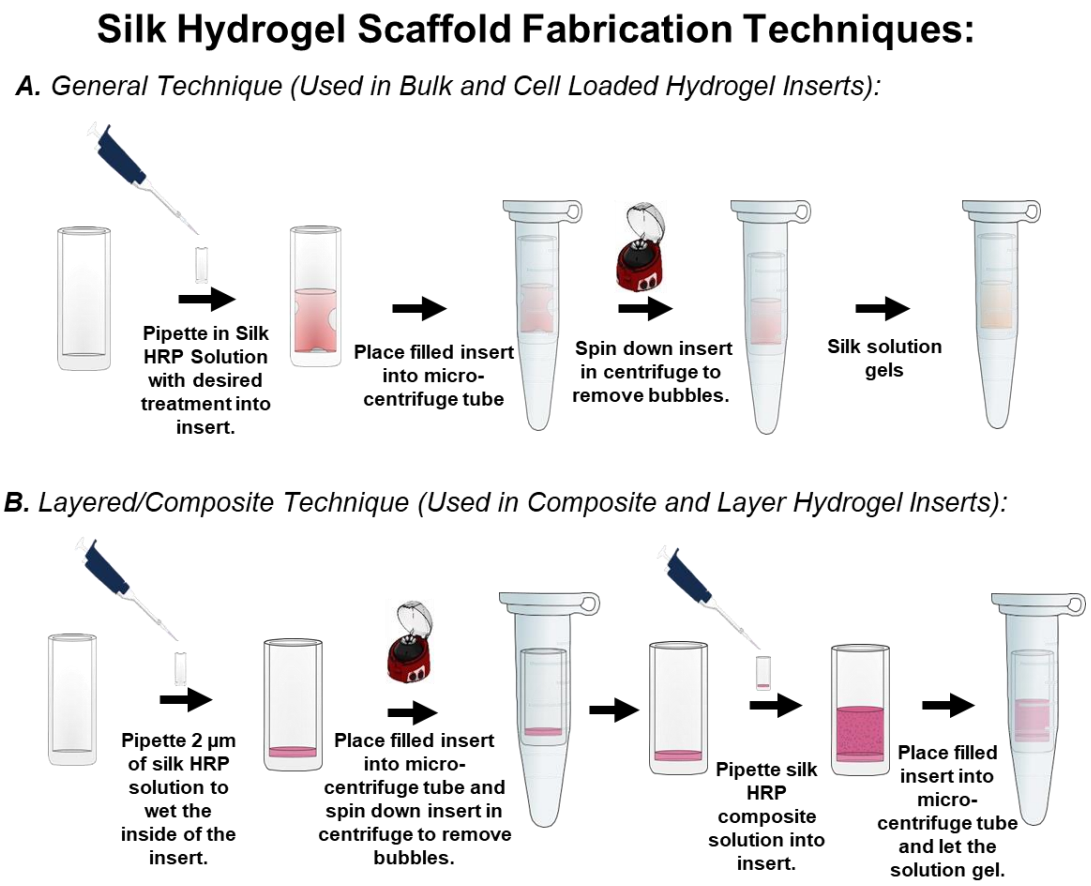


**Figure 2.4. Silk Hydrogel Insert and Fabrication Methods.** Process diagrams for the most commonly used silk hydrogel insert fabrication techniques **A.** The general technique used to load the silk hydrogel is recommended for bulk loaded homogenous solutions. After the 9 µL of hydrogel is injected into the insert the insert is then spun down to remove trapped bubbles before gelation is complete. **B.** The layer and composite technique removes the need for centrifugation to remove trapped bubbles by introducing a wetting step. By removing the centrifugation step, this requires more skill and time per insert that the general procedure to avoid bubbles. This protocol is recommended for layered or encapsulation protocols.

## 2.5. Surgical Technique

Presented below are the surgical protocols designed and optimized for the wearable bioreactor use *in vivo*. A visual summary of the experimental design is presented in Figure 2.6. A non-regenerative P2 digit amputation is performed followed by attachment of a silk hydrogel treatment to the amputation site. After the desired attachment time is reached then the device is removed with the potential of an additional hydrogel treatment proceeding this removal (reattachment). The attachment time is based on both drug release studies as well as the wound epithelium healing around the hydrogel insert around 5 to 9 DPA. Having the hydrogel incorporated into the wound-bed allows for longer term delivery design as well as better incorporation of cells in cellular delivery.

This chapter focuses on surgical techniques for three types of delivery protocols followed by a set of protocols for wound site care during attachment. The first is the typical bolus delivery which involves a single attachment and removal protocol (this includes cell delivery and composite hydrogel delivery). The second is for reattachment of a second hydrogel insert to allow for temporal control of delivery. The third protocol set replaces the hydrogel based reservoir for a liquid one. This last protocol allows for a control group to be compared to the hydrogel. Finally, a set of methods to allow for observation and limb maintenance during attachment is provided. Please note; before any animal procedure, protocols must be approved by the institution review committee.

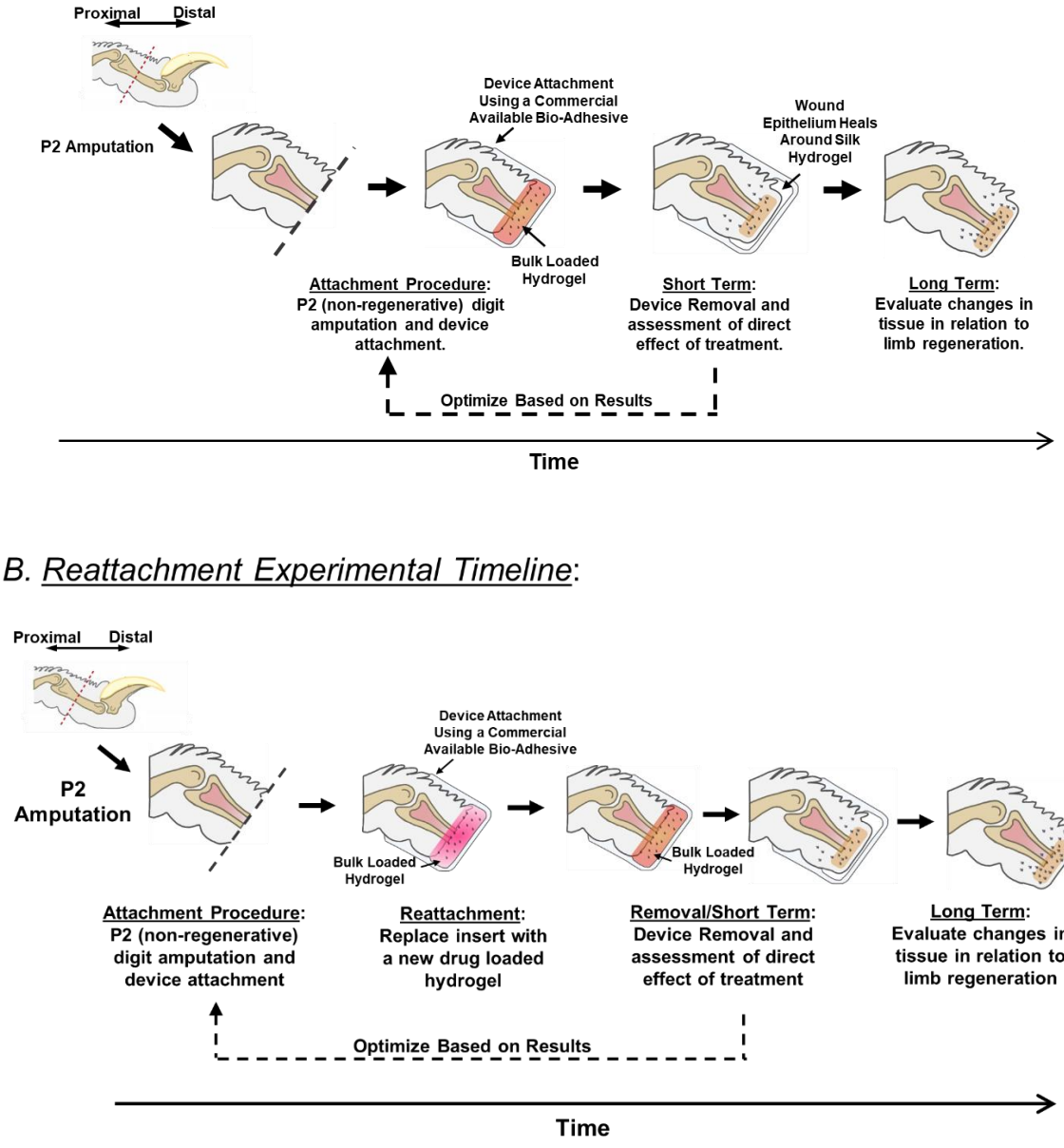


**Figure 2.5. General Experimental Design**. The above schematic the two types of surgical techniques used with the device. (A). Displays the typically used single attachment method which only attach one device while (B) demonstrates multiple reattachments. The benefit of B is that reattachment allows for multiple hydrogel treatments given in a desired sequential order.

*2.5.1. Amputation and Device Attachment (A process diagram is presented in Figure 2.7)*

1.) (Prior to surgery) To prevent mess and minimize error, prepare a station away from the surgical area to mix the bio-adhesive. It is recommended to have the two-part glue components aliquoted out in a ready to mix format before the procedure begins.

2.) Prepare mouse for amputation. (application of anesthesia, analgesic, and sterilization of the amputation site with ethanol and beta iodine washes.)

3.) Using the spencer suture scissors amputate the middle digit at the P2 bone. This particular type of scissors have a notch in the blade that the researcher can place the digit in to help with facilitating a clean and spatial repeatable amputation[a]. Staunch any bleeding with a gauze for 2 to 5 minutes.

4.) After bleeding is minimized, mix the two-part bio-adhesive at the glue station and bring the glue to the surgical area for use.

5.) With a pair of fine tip forceps remove the silk hydrogel insert from the 0.5 mL micro-centrifuge tube and place the hydrogel insert onto the digit-tip. The empty space at the top of the insert should help hold the insert in place and protect the amputated site from the glue.

6.) Using the surgical probe apply glue on the amputated hind-paw and outside portion of the hydrogel insert to glue to the insert to the paw.

7.) Grab one of the two part components of the outer sleeve. With the surgical probe add bio-adhesive to inner cuff area of the component. Place the glue

painted component face up, then place the amputated hind-paw with insert attached into the component.

8.) Take the opposite part of the out protective sleeve component, add glue to the cuff region of it, then attach it to the mouse's hind-paw.

9.) Take the protective cap and with the surgical probe add bio-adhesive to half of the circumference of the inner edge. Slide this onto the end of the outer-protective sleeve (distal end).

10a.) (If isoflurane is used as anesthesia) Wait for the glue to cure before moving the mice off the isoflurane (~2 - 5 minutes). The researcher can monitor this by checking how cured the unused glue in the pot is (this can be done with the surgical probe). While it easier to keep the mouse at the surgical site while waiting, the researcher can also move the animal to the knock-out box if they wish to move onto the next mouse. Remember to remove the mouse from the knock-out box once the glue is cured.

10b.) (If an injection of ketamine and xylazine is used as anesthesia) Carefully move the mouse to the recovery cage and wait for the mouse to recover. Make sure that the recovery cage has a paper towel or Wypal place inside the cage to prevent the bedding from getting into the glue of the device.

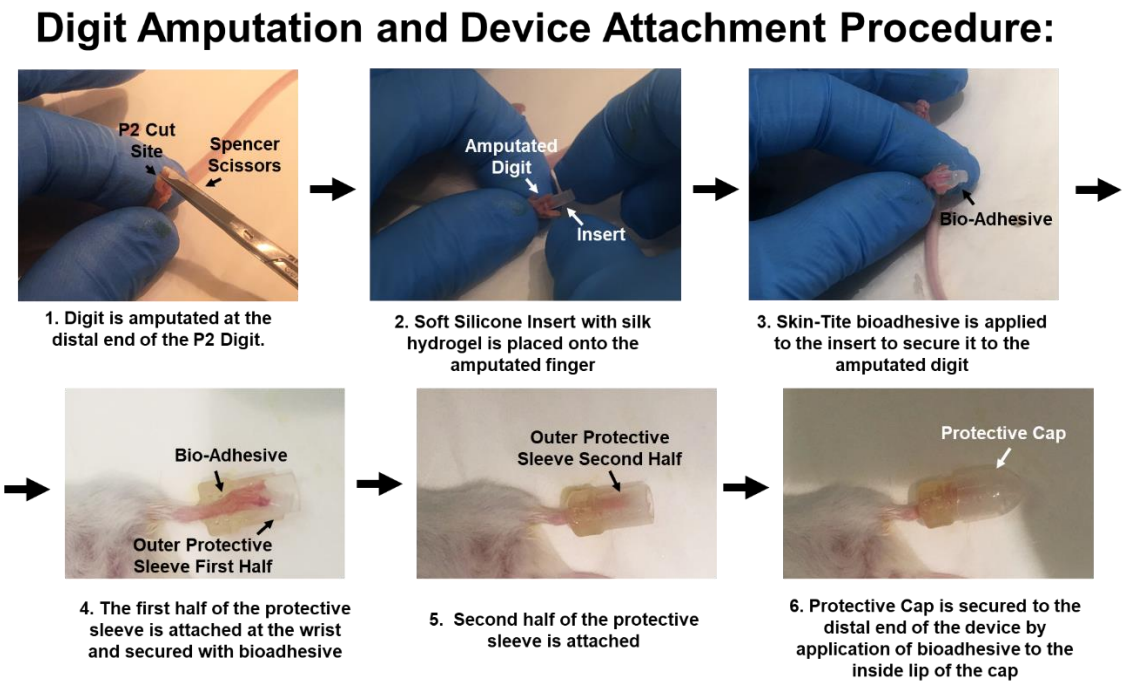


**Figure 2.6. Protocol Diagram of Device Attachment Protocol**. Amputation is performed using a spencer scissor which after the blood is staunched then the insert is attached with bio-adhesive followed by the rest of the device.

### *2.5.2. Observation and Limb Maintenance During Attachment*[b]

To remove any built up liquid without removing the end-cap of the device:

1.) Take a 23 gauge need and at the top of the attached protective cap drill a hole into the end. Be careful to not injure the mouse.

2.) Using a diabetic syringe, insert the needle into the hole and remove excess liquid by pulling back on the plunger on the syringe.

Remove and Replace End-Cap of Device:

1.) The end cap can be removed by lightly twisting and lifting the cap from the device. Use a pair of forceps and fine-tip scissors to remove any residual glue on the outer portion of the protective sleeve.

2.) The amputation site can be cleaned while the device remains attached by using a piece of Kim-wipe and forceps.

3.) Replace old cap with a new cap and bio-adhesive when completed[c].

### *2.5.3. Removal and Reattachment (A process diagram is presented in Figure 2.8)*

1.) Remove the end-cap by lightly twisting and lifting the cap from the device. Use a pair of forceps and fine-tip scissors to remove any residual glue on the outer portion of the protective sleeve.

2.) Using the bent surgical probe, very carefully pry apart the two parts of the device at the edges. Remove one component of the outer sleeve then the other. This should leave you with the dried glue and insert attached to the hind-paw.

3.) Using a pair of small surgical scissors and bent forceps carefully remove the glue surrounding the wrist and paw. Make sure to not perturb the insert or hydrogel inside itself.

4.) After most of the glue has been removed, carefully remove the insert itself. While this can be taken off the mouse by physically removing the insert, it is recommended that the outer silicone sleeve is removed using the surgical scissors if possible[d].

5.) For reattachment follow steps 5 – 10 of the amputation and device attachment protocol.

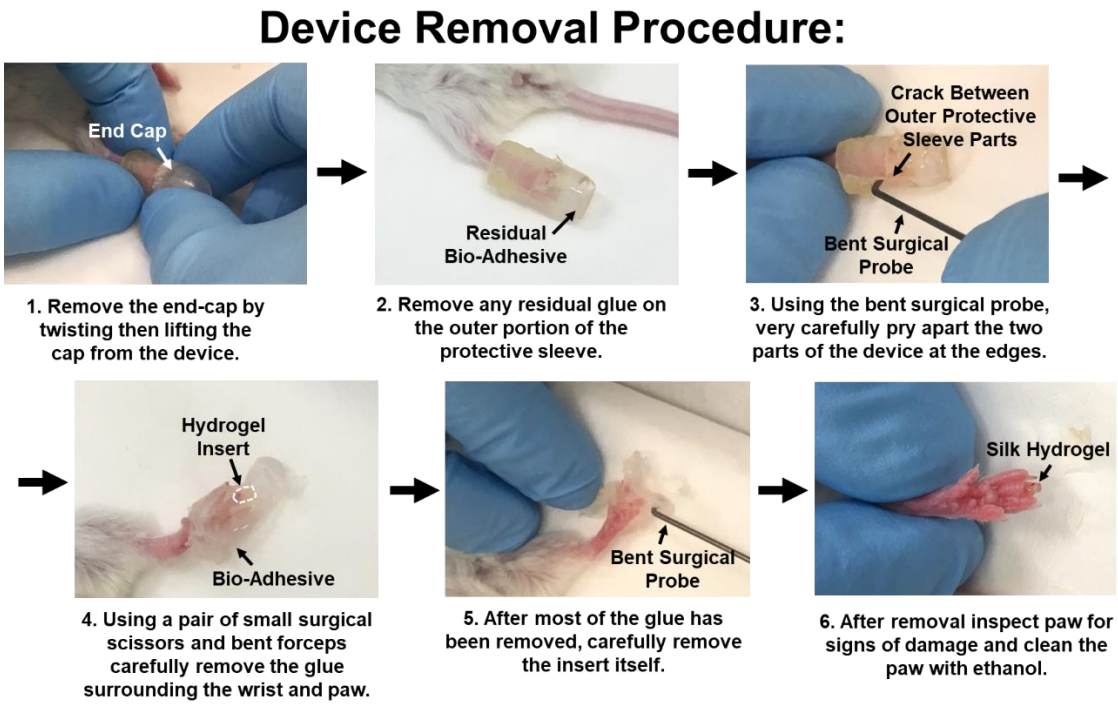


**Figure 2.7. Process Diagram of Device Removal.** Once the end cap is twisted off then the device can be carefully removed either with the surgical probe or a pair of surgical scissors and bent tweezers. To prevent the tissue and incorporated hydrogel from being ripped apart from the each other latter technique is recommended.

*2.5.5. Liquid Based Reservoir Attachment*[e]

1.) Proceed with steps 1 - 4 in the amputation and attachment protocol.

2.) Attach an empty insert to the amputated digit site in a similar fashion as described in step 5 and 6 of the amputation and attachment protocol. Leave the equivalent space of the hydrogel in the insert distal to the amputation site. Make sure that the glue is dried before proceeding.

3.) Take 2 - 3 insulin syringes. Remove the plunger from one and with another draw up the desired reservoir solution. Stick the syringe with no plunger on one side of the soft silicon insert (this will be used to vent air and allow from the liquid reservoir to be injected into the device).

4.) If there is blood in the insert, use the third syringe to remove the blood from the insert by inserting the needle of the syringe on the opposite side of the soft silicone insert from the venting syringe and very carefully pulling back the plunger. If there is no blood in the insert, then insert the needle with the reservoir solution on the side opposite of the venting syringe. Carefully inject ~ 9 – 10 uL of solution into the device.

5.) Once the desired solution is injected into the soft silicone insert, remove the solution syringe followed by the venting syringe.

6.) Follow steps 7 – 10 of the amputation and attachment protocol.

*2.5.6. Notes*

a.) If the researcher places the digit into the scissor notch proximal to the cut site and moves distally towards the tip of the digit the scissors will naturally stop near

the distal end of the P2 joint. This natural catch point is in a similar location on similarly aged mice and will decrease variability in cut site location.

b.) This set of procedures are done more on a “as needed” basis. The protocol is in case the researcher sees a build-up of liquid in the reservoir or sees the need to remove the cap to clean or inspect the area prior to device removal.

c.) If there is an issue of liquid build up in the device one solution for longer term attachment is to replace the end-cap with a new one that has a hole drilled into the top of the dome of the protective cap. This provides some ventilation and helps with the issue. It should be noted that this is not recommended upon initial attachment of the device, given that this might dry out the attached hydrogel prematurely.

d.) Depending on the treatment the wound epithelium and wound tissue can interact and attach itself to the hydrogel. Forceful device removal can result in the digit being ripped away from the hydrogel with part of the tissue still attached to the hydrogel itself.

e.) This is a modification to the attachment procedure that allows for liquid to be inserted into the insert instead of a hydrogel. This should be used as a control for the hydrogel and is not recommended as a replacement for the hydrogel in treatment. This method is prone to potential error, has a higher rate of tissue damage to the mouse, the liquid might leak out or dry out in longer term attachments, and stability of the compounds loaded into the solution is questionable.

## 2.6. Conclusion and Future Work on Protocols and Device Design

This system was capable of the task of studying limb regeneration *in vivo* using a murine digit tip amputation model. Furthermore, the hydrogel-based delivery system provides a means of delivery with tunable options for spatial and temporal control of a very diverse set of deliverable items (e.g. small molecules, biomolecules, and cells). However, there are areas that can be improved upon. In particular, future improvements should focus on the material design of the hydrogel and the methods used to assess the difference that the treatment cause to the final biological outcome**.** These areas will have the most influence on making this wearable bioreactor an effective tool to study limb regeneration.

# Chapter 3: A Wearable Bioreactor to Study Limb Regeneration in an Adult Murine Digit Amputation Model

### 3.1 Abstract

In the U.S., over 2 million people suffer from limb amputations and associated co-morbidities. A wearable bioreactor with a contained silk hydrogel was designed to study limb regeneration in an adult mouse metacarpal amputation model. Current methods for limb regeneration typically require wound closure prior to device implementation, while the device reported here can be attached immediately upon amputation and remains affixed during healing. The results demonstrated that hydrogels in the device and affixed to the wound bed provided a pro-regenerative environment by facilitating wound closure and improving tissue healing when compared to the no device controls. Changes in digit morphology and protein expression at the wound site demonstrated the ability of the device to deliver selective chemical stimuli capable of altering biological responses known to play key roles in limb regeneration. Specifically, the small molecule ivermectin was delivered and resulted in increased expression of nerve marker PGP9.5 and macrophage marker F4/80 at 9 days post amputation (DPA). These responses were followed by changes in morphology at the wound site at 15 days post amputation (DPA). In combination with increased expression of osteoblast marker osterix and decreased cartilage ECM marker collagen type II in the ivermectin study group, the results suggested that ivermectin treatment accelerated typical wound healing cycles. While these differences in responses between the ivermectin, sham, and no treatment study groups did not persist at longer time points, the results verify that the device and system

can stimulate the amputation site and manipulate the wound healing cycle, a critical feature for the study of limb regeneration.

**Key words:** Hydrogel, *In vivo regenerative models, limb regeneration, tunable, silk.*

### 3.2. Introduction

Regeneration is the processes of tissue repair and remodeling that returns the body to homeostasis[4]. Complete regeneration requires that the healed tissue is morphologically and functionally equivalent to its pre-injured state, otherwise, wound healing is the result. While all living organisms are capable of wound healing, few animals achieve true regeneration once they have developed past embryonic state. Furthermore, the quality of healed tissue varies based on many factors including, age, pre-existing medical conditions, and/or complexity of the injured tissue. In some situations, the injury fails to heal at all, such as in chronic wounds. In the US alone, around ~2.4 million people are affected by chronic wounds[2]. For more complex injuries, such as amputations, poor wound healing or non-healing often leads to further clinical complications. With current technology, even the most advanced care can only minimize these risks and manage the damaged site.

Engineers and scientists in the fields of bioengineering and regenerative medicine have studied options to encourage regeneration and/or improved wound healing in damaged tissues with the use of advance biomaterials and therapeutic treatments. These approaches have worked to varied degrees in specific tissue types, such as bio-glass scaffold implants for bone regeneration[41], or skin grafts for burns[42]. Some of the products involved in the above successes utilize de-cellularized amniotic extra-cellular matrices (ECM) or specific ECM components (such as hyaluronic acid or collagen) to generate

bandage meshes or cell support matrices to promote wound closure and to initiate healing. These materials improve wound closure[43], however, the results can be limited[44], as little is known about the fundamental biological pathways that define wound healing versus regeneration. Until these pathways are better understood, designing capable materials for regenerative medicine remain a challenge.

The field of developmental and regenerative biology can help provide insight into the biological mechanisms that define limb regeneration. These fields employ a variety of animal models in order to glean insight into different key pathways that are putatively involved in regenerative outcomes. However, most of these animal models utilize amphibians, planaria, frogs, and axolotls, which provide some insight, but are limited in terms of the more complex events observed in mammals. In the case of complex regeneration, and in particular, limb regeneration, the mouse digit tip amputation model has been the system of choice for such studies[34]. Adult mice are capable of regenerating an amputated digit as long as the amputation is distal from the nail-bed[12]. One advantage of this model is that it is spatial dependent; if the amputation is proximal to the nailbed on the most distal digit (P3), or occurs in any phalange proximal the P3 nail-bed (i.e. P2 or P1), then limb regeneration does not occur[12]. This location-dependent regeneration allows for studies of both a gain-of-function and loss-of-function, both of which are key for isolating and studying specific aspects of the regenerative process.

By utilizing both the gain and loss of function capabilities of the mouse digit tip model different factors that influence the final biological outcome have been identified (e.g., if the amputation results in regeneration, wound healing, or a non-healing event). Some

Examples include the immune response[16], ECM composition[24,45], fibroblast-mediated signaling[46], angiogenesis[19], wound closure and clot formation[18], innervation[28], progenitor recruitment[47], reactive oxygen species and hypoxia[11],and the balance between ossification and chondrogenesis[25]. While there are many diverse factors that determine success in these regenerative-related process, many are correlated to typical wound healing and not necessarily to true regenerative goals. For example, a typical non-regenerative P2 amputation followed a similar trend as that typically observed during femur fracture healing[25]. With this in mind, many of the observed trends that characterize successful regeneration in this amputation model mirror femur fracture healing. However, there are subtle, but critical differences between the two processes that define if a limb will regenerate, or merely heal. One example can be seen in the role that angiogenesis plays in digit regeneration and bone fracture healing. In the mouse regenerative P3 amputation, if vascularization is introduced prematurely via administration of vascular endothelial growth factor (VEGF) to the amputation site, then blastema formation is retarded and the digit does not regenerate[25,48]. In femur fracture, if the fracture site fails to vascularize in a timely manner, then the two ends of the broken bone will not meet, resulting in a non-union outcome[48]. Nonetheless, even with these important differences, the general similarities can allow for the developed biomaterials and techniques used to study and promote bone regeneration to be applicable to the field of limb regeneration.

Typically, two experimental setups are utilized for regenerative animal models. The first is a gain/loss of function model. This type of model will either inhibit or activate a given receptor that is known to promote or inhibit the biological pathway being investigated. By “rescuing” the animal from the initial gain/loss a direct correlation can be attained for that

given pathway to the observed change in biological outcomes [49]. However, the results from these types of models can be taken out of context of the overall regenerative event and thus may not reflect the needs and goals in this context [49]. The other type of experimental setup takes the opposite approach and uses an exogenous cocktail to promote regeneration. This cocktail includes a variety of known pro-regenerative stimuli (e.g., growth factors, drugs, progenitor cells, or genetic information[50]) which result in some degree of change to what is assumed related to the biological outcomes [50]. This method might provide a desired result, but with no means to correlate the result to an actual cause, makes it irrelevant[50]. The first method emphasizes correlation of a cause and effect with limited applicability, while the second approach might achieve a result, but lacks the ability to correlate the result to any specific cause. A middle ground is needed to understand the mechanisms that drive regeneration in an applicable manner. Moreover, regeneration is a dynamic process which requires temporal control over inputs, which neither current approach or model can fully offer.

Recent work has applied a more material engineering approach in order to reach this middle ground[35]. The researchers utilized a two-stage system to study the effect of delivering mouse embryonic limb progenitor cells to the amputation site to induce limb regeneration[35]. After digit amputation, the wound was covered with a Hyphecan cap bandage to facilitate the necessary wound closure and healing[35]. After 12 days after wound closure (about 2 weeks post amputation) the bandage was removed and a fibrin gel loaded with the limb progenitor cell's grafted under the now closed amputation site[35]. Results from this work showed successful incorporation of the cells into the amputation site of the immune compromised mice, and bone growth distal from the cut site was observed in the cell treated groups[35]. However, the stage at which the regenerative P3

and non-regenerative P2 amputation response deviates occurred around 7 to 9 DPA[36]. This is when the wound epithelium closes over the cut site and either a collection of undifferentiated cells appears at or just distal cut site known as a blastema (the P3 regenerative amputation), or the initial recruitment of osteochondral progenitor cells at and around the amputated bone that will be needed to form the soft fracture callus (non-regenerative P2 amputation) is observed[35]. The mechanisms that define what results in limb regeneration versus typically observed wound healing must happen before this 7 to 9 DPA event. Thus, the results observed from this work may not reflect the role that progenitor cells play in the limb regeneration process. In addition, both the Hyphecan cap and fibrin gel were susceptible to premature removal by animal tampering[35]. To utilize these types of materials in an effective manner a method of attachment needs to be designed to meet the demands of the *in vivo* system.

Nevertheless, the above research demonstrated the benefits of a material engineering approach for the study of limb regeneration in the mouse digit amputation model. While there are many different types of materials to consider, there are few options that can provide tunable properties, biological compatibility and independence from intrinsic biological interactions (e.g., does not inherently cause cell-specific responses independent of any loaded compound). Biomaterials derived from biologically synthesized sources (e.g., collagen and fibrin) have an intrinsic ability to interact with the cells, and therefore can initiate off-target biological feedback loops that could potentially bias the regenerative processes. Silk fibroin is an exception. As a protein biomaterial it is non-toxic, offers tunable properties, and is devoid of specific biological signaling. There are a wide variety of methods to tune the mechanical properties of silks, including concentration[51], chemical conjugation[52], or bioengineered variants using genetically

modified silks[51]. In particular, silk hydrogels have certain material properties useful for the study of limb regeneration. Since hydrogels are composed mostly of water, they can provide hydration to the wound-bed and amputation surface. In addition to more diversified release profiles, the mechanical and material properties of silk hydrogels can provide stimulation (e.g., via material stiffness and/or added biological ligands) to the wound-bed. Enzymatically crosslinked silk hydrogels, formed via horseradish peroxidase catalyzed free radical reactions, provide elastic hydrogels[38]. In previously published work, a wearable system was used to study regeneration *in* vivo using the mouse digit amputation model[37]. This "proof-of-concept" device was attached to the stump of an amputated mouse digit and delivered a cocktail of different regenerative compounds via solution to the wound site[37]. However, technical issues made application of this device for experimental use difficult along with the limitation of a liquid-only delivery system.

In the present work, a new design is introduced that incorporates an elastomeric silk crosslinked hydrogel. The device design, fabrication, and attachment protocol were designed and optimized to resolve issues of attachment, necrosis, and other limitations observed in the earlier design[37]. The silk hydrogel scaffold provides a tunable medium to deliver physical, chemical, and biological stimulants to manipulate the wound healing process in a controlled fashion. The results showed that the hydrogel scaffold promoted wound closure and supported wound healing patterns that were not observed in animals without the device. The elastomeric silk scaffolds were also incorporated into the wound-bed during healing and did not hinder the wound healing process. In addition, the hydrogel was able to deliver the small molecule ivermectin (a molecule known to activate biological pathways associated with limb regeneration and improve innervation in a skin

wound healing model) to the amputation site in an effective manner to alter the typically observed wound healing cycle, overall proving the functional capability of the device.

## 3.3. Methods and Materials

### *3.3.1. Silk Processing and Hydrogel Scaffold Fabrication*

The method used to process the silk for the hydrogels was previously described[38]. For scaffold fabrication, silk solution was diluted to a working concentration of 3% (w/v) using Hanks buffer solution with phenol red (Sigma-Aldrich, St. Louis MO). Additional components were added to the silk, including concentrated DMEM (1:10 dilution of stock, Sigma-Aldrich, St. Louis, MO), Glutamax (1:100 stock solution, Fischer Scientific, Waltham MA) and, dextrose (final concentration at 4.5 mg/mL gel solution, Sigma-Aldrich, St. Louis, MO). The system was then enzymatically cross-linked at the tyrosine side chains using horseradish peroxidase enzyme (HRP) at 10 U/ml (Sigma-Aldrich, St. Louis, MO) with hydrogen peroxide at 0.01% overall volume (or 10 µl/1mL solution)[38]. Sodium bicarbonate was added to balance the pH of the hydrogel based on the color of the gel generated by the phenol red present in the supplemented Hank's buffer solution and concentrated DMEM. For the drug loaded conditions, stock solutions of ivermectin (IVM, Sigma-Aldrich, St. Louis, MO) were diluted to 10 µM final concentration. The concentration was determined based on previous work showing that this concentration was effective to improve nerve regeneration in a mouse skin biopsy punch wound model[37].

### *3.3.2. Device Fabrication and Scaffold Loading:*

The device hardware and fabrication included two parts. The first part, the outer protective sleeve, was designed to protect the silk hydrogel from animal tampering. The

design was drafted using Solidworks 3D-CAD software (Dassault Systems, Waltham MA) and was printed using the Form 2 laser stereolithograph 3D printer (Formlabs, Somerville MA). This part of the device consisted of a two-part methacrylate case. The second part, a silicone removable insert, housed the hydrogel scaffold that interacted with the wound-bed. The insert was fabricated out of DragonSkin Silicone polymer (Smooth-On, Harrisburg PA). The inserts were cast into a 3D-printed acrylonitrile butadiene styrene polymer mold coated with an acrylic lacquer to prevent curing retardation from the mold material. Prior to scaffold loading, all materials and tools used in the experiment (e.g. surgical tools and device components) were autoclaved to ensure sterility. Scaffold gelation was performed in a sterile hood to maintain sterility of the scaffold components. HRP was mixed thoroughly into the solution prior to gelation, which was then initiated with the addition of the hydrogen peroxide. The solution was then allowed to sit in the sterile hood for 2 minutes, after which 10 µL of hydrogel solution was pipetted into the insert. After loading, the inserts were placed into sterile 0.6 mL mini-centrifuge tubes. Trapped bubbles in the insert were removed by centrifugation using a mini-centrifuge (Artec Educational, Osaka Japan). The scaffold loaded inserts were left to sit in the sterile hood until gelation was complete.

### *3.3.3. Release Studies for Ivermectin*

The method used to characterize Ivermectin release has been described in previous work[53]. In brief, 10 µM of ivermectin was loaded into the gelation solution. After gelation was initiated, 0.05 mL of each solution was pipetted into a 2 mL centrifuge tube and allowed to solidify in a 37$^{o}$C oven. After gelation was complete, 1 mL of PBS was added to each centrifuge tube and the samples where then placed in the oven. The PBS elution solution was then collected and replaced at specific time points (1, 2, 4, 8, 24, 48, and

72 hours) and stored at -80$^{o}$C and a spectrometer was used to assess the amount of ivermectin. The maximum absorbance for ivermectin was at 225 nm. Each group had an N = 3 samples with 2 technical replicates for each sample. Concentration was established with a standard curve with a blank of PBS to reduce noise due to the elution buffer. A control group of unloaded hydrogels was included.

*3.3.4. Amputation Surgery and Device Attachment and Removal*

All experiments were performed under the approval of Tuft's IACUC. All animals were housed in 12-hour light and dark cycles and fed using recommended feed. Female FVB/NJ mice 8 - 9 weeks of age were used in the work (Jackson Laboratories, Bar Harbor, ME). Animals were anesthetized with isoflurane administered at 2 to 2.5% air composition. After anesthesia, the middle digit was removed using surgical scissors. The dragonskin insert containing the silk hydrogel was then attached to the amputated digit using Skin-Tite Bioadhesive (Smooth-On, PA). Devices were attached for 3 days post amputation (3 DPA) and then removed. For short term analyses, animals were sacrificed at 5 and 9 DPA. For longer term assessments, animals were sacrificed at 15 and 28 DPA. Four study groups were used. The first group (controls) where animals that had the digit amputated but had no device attached (ND). The second group were animals that wore the device with a silk hydrogel scaffold without drug (sham). The third group wore the device that had either 10 of 20 uM of ivermectin loaded into the silk elastomeric scaffold (IVM). The final group were animals with the device, but no gel but with drug.

*3.3.5..Tissue Processing*

Animals were sacrificed using $CO_2$ asphyxiation and spinal dislocation. Amputation digits were collected and fixed for 12- 24 hours using a 4% paraformaldehyde solution

(Sigma-Aldrich, St. Louis, MO). The tissue was then moved to a decalcification solution for 12 hours (Decal I, Roche, Basel, Switzerland) and preserved in 30% wt. sucrose for 24 hours or until the tissue sunk to the bottom of the solution. The samples were then acclimated to Optimal Cutting Temperature Compound (OCT) using a (1:1) ratio of 30% wt. sucrose to OCT solution for 2 to 4 days. After tissue acclimation the digits were embedded in OCT and allowed to set for at least 48 hours at -80ºC. Following this process, 10 um sections were taken using a cyrotome (Model CM1950, Lecia Biosystems Buffalo Grove, IL).

*3.3.6. Histology and Immunohistochemistry*

The tissue sections were rehydrated in PBS before staining. For general morphology and collagen fiber alignment, samples were stained with Masson's Trichrome (Sigma-Aldrich, St. Louis, MO) according to the manufacturer's instructions. Sections were then mounted with permount mounting medium (Fischer Scientific, Waltham MA) and left to dry in a fume hood for 24 to 48 hours before imaging. To assess the amount of proteoglycan within the fracture callus, samples were stained with histological dye Safranin O (0.1%, SO, Sigma-Aldrich, St. Louis, MO) with Wiegert Iron Hematoxylin (WH, Sigma-Aldrich, St. Louis, MO) and Fast Green (0.05%, FG, Sigma-Aldrich, St. Louis, MO) as the nuclear and counter stains, respectfully.

For immunohistochemistry analysis, antigen retrieval was carried out either by a (1:1) ratio of methanol and acetone for 10 to 20 minutes at -20ºC or 1% sodium dodecyl sulfate solution for 5 minutes at room temperature. Non-specific antibody binding was blocked using a buffer that consisted of 10% goat (Sigma-Aldrich, St. Louis, MO), 0.1% triton-10X (Sigma-Aldrich St. Louis, MO), and 0.1% sodium-azide (Sigma-Aldrich St. Louis, MO). The slides were then incubated at 4ºC overnight with the following primary antibodies: CD31 (10 µg/ml, mouse anti-human Cat# 555444, BD Bioscience Franklin

Lakes, NJ), F4/80 (5 ug/mL, rat, anti-mouse, Cat# ab6640, Cambridge, MA), PGP9.5 (1:250 dilutions, Cat# NE1013, Millipore Sigma, Billerica, MA), K14 (1 ug/mL, Cat# ab7800, Cambridge, MA), OSX (2 ug/mL, Cat# ab22552, Cambridge, MA), and col II (5 ug/mL, Cat# ab7778, Cambridge, MA). Primary antibodies were conjugated to Alexa Fluor 488 nm (Abcam, Cambridge, MA) or 594 nm (Thermo-Scientific, Waltham, MA).

*3.3.7. Image Analysis*

All Images from the *in vivo* work were taken using a Keyence microscope (model BZ-X710, Keyence, Osaka, Japan) at 10x and 20x. Image analysis was carried out using ImageJ (National Institute of Health Rockville, MD)[54], or by the manufacture's software. For immunohistochemistry analysis, the regions of interests (ROI) were define within the tissue surrounding and distal the amputation site of the P2 bone. Histological and immunohistochemistry analysis used 20X images. Three to five 20x images takes within the ROI were taken as a representative sample of the tissue and used for analysis. For immunohistochemistry analysis, the total area of the fluorescent signal was calculated and then normalized to total 4',6-diamidino-2-phenylindole (DAPI) area (i.e. % Counted Cell Area = (Positive Fluorescent Signal of Antibody in ROI)/ (Total Area of DAPI in ROI)).

ImageJ was used to measure the area of the fracture callus at 15 DPA. The area of the fracture callus was determined by Masson's Trichrome and the IHC stain for the vascular marker PECAM/CD31. The fracture callus was mostly avascular at 15 DPA[55] and thus CD31 negative expression could be used to demarcate the callus fracture area from the rest of the tissue. Examples are presented in supplementary Figure S1. Since

the fracture callus is formed both around the P2 bone and distal the cut site, the calculated fracture callus area was normalized to the combined area of the callus and the P2 bone to minimize differences due to variation in the cut site along the P2 bone. The area of healed tissue of the tissue was normalized over the area of the callus. “Healed tissue” in the callus was tissue that visually looked like cartilage or calcified tissue in masson’s trichrome. This was further verified with antibodies for osteoblast marker (OSX), collagen type II, a cartilage ECM protein, and Safranin O, a histological stain for proteoglycans.

The percentage of Safranin O expression was calculated with previously described methods[37]. In brief, 20x merged images of the P2 bone and fracture callus were converted into an RGB image. Using ImageJ the green and blue color channels were subtracted away from the image, leaving on the red color channel. This area was taken as the Safranin O positive stain and normalized over the combined P2 bone and fracture callus area.

### *3.3.8. Statistical Analysis*

ANOVA statistical analysis followed by a student’s t-test was performed to determine statistical significance of the different sub populations. This process was accomplished using the data analysis package added to excel (Microsoft, Seattle, WA). All trials, unless otherwise indicated, had at least a population (N) of 4. Statistical significance was rated at $p<0.05$, 0.01, and 0.001 and this is indicated in the Figures by one, two, and three stars, respectively.

## 3.4. Results

### *3.4.1. Device and Scaffold Technical Assessment and Characterization:*

The method of device attachment can be broken down to three steps. First, the soft insert and hydrogel is attached to the amputated finger. Next, the two-part outer protective sleeve is placed over the insert and amputated paw. Finally, the end cap is inserted onto the distal end of the device. All components are attached and secured using the bio-adhesive Skin-Tite. The devices remained attached to the animals for up to 2 weeks with minimal to no necrosis, a major improvement over the previously reported system. The outer methacrylate protective sleeve, in combination with the polypropylene domed cap, protected the site and scaffold from tampering and premature removal by the animal (Figure 1C). The use of Bio-Adhesive Skin-tite was effective for device attachment. In addition, all the device components were autoclavable (technical hardware) or could be sterile filtered (the silk hydrogel scaffold components).

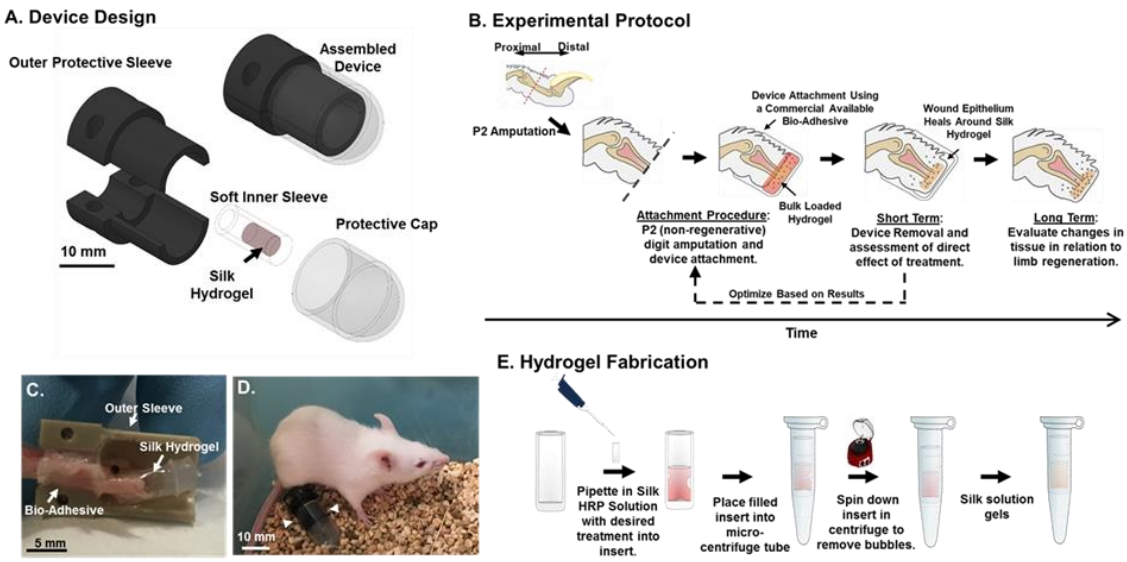


**Figure 3.1. Wearable Bioreactor Device and Experimental Design. A.** Schematic of device design. **B.** General Experimental Design with the hydrogel being incorporated into the wound-bed around 5 to 7 DPA. **(C and D).** Images of the device being worn *in vivo*. **C.** General schematic of the different components of the bioreactor. **E.** Procedure of loading the hydrogel into the insert.

The hydrogel inserts provided a hydrating barrier that promoted wound closure to facilitate regeneration (Figure. 2). Histologically, all device wearing animal groups showed increased wound closure at earlier time-points of 5 and 9 DPA (Figures. 2A and 2C). In addition, the 'no device' animals showed signs of calcification in the marrow pocket, which was not observed in the animals wearing devices. Phenotypically, there was an increase of OSX expressing cells (associated with osteoblasts and osteocyte cells) and accelerated vascularization into the newly formed tissue area in the device wearing animals. These results are essential for proper wound healing for a P2 amputation[18,19,25]. While the wound is closed at 15 DPA, results show improvement in the tissue quality between device and no device wearing animals. While the device wearing animals present the typically observed fracture callus at 15 DPA, the no device animals do not and show evidence of calcification in the actual marrow pocket of the P2 bone (as presented in Figure 4).

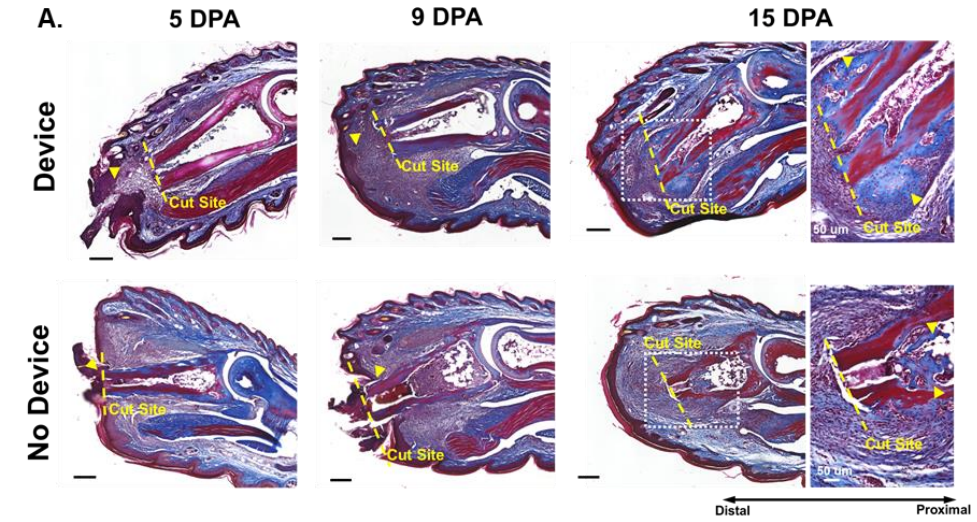


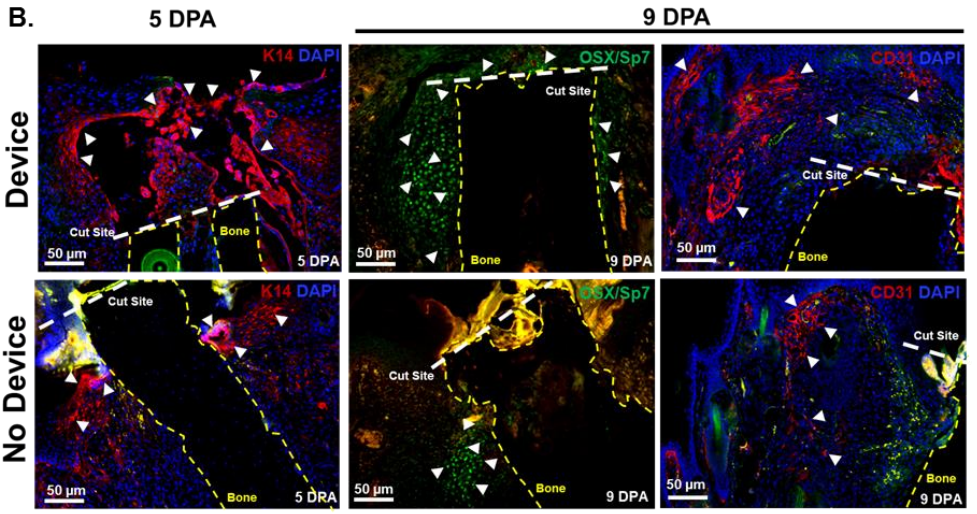


**C.** Ratio of Closed Amputations

| Time | Device | No Device |
|---|---|---|
| 5 DPA | 4/5 | 1/5 |
| 9 DPA | 5/5 | 0/5 |
| 15 DPA | 4/4 | 4/4 |
| 28 DPA | 5/5 | 6/6 |

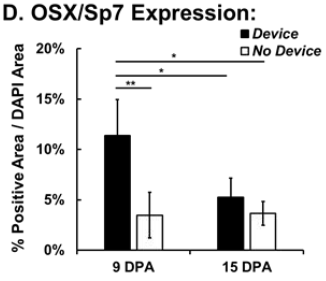


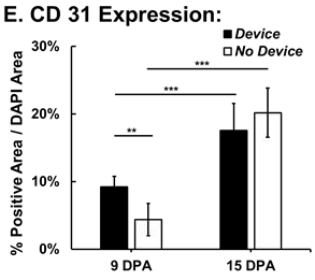


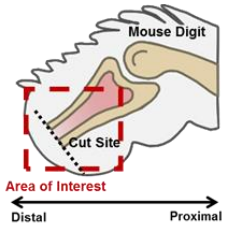


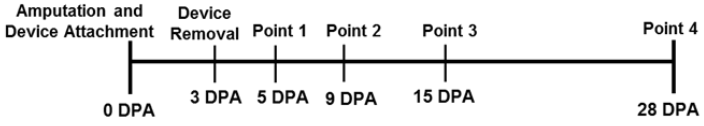

**Figure 3.2. Wearable Bioreactor is Capable of Promoting Key Wound Healing Events. A.** Histological analysis taken over the different time points. Yellow arrows at 5 and 9 DPA points to the wound epithelium, while the yellow arrows at 15 DPA points to the bone formation in the two representative images. **B.** Immunohistochemistry of device versus no device. Stains from left to right are the wound epithelium marker Cytokeratin 14 (K14), the osteoblast and osteocyte marker Osterix/Sp-7 (OSX/Sp7), and the vascular endothelial marker PECAM/CD31 (CD31). **C.** The number of closed amputation wounds at the time removal over the total population of either the device or no device group. **D.** Quantification of OXS/Sp7 expression between device and no device groups at 9 and 15 DPA. **E.** Quantification of CD31 expression between device and no device groups at 9 and 15 DPA. Statistical Analysis was performed using ANOVA single factor followed by a student's t-test to compare groups. Significance to the control group is measured as following p-values * ≤ .05, ** ≤ .01, and *** ≤ .001. Population is at n ≥ 4.

*3.4.2. Ivermectin Treatments*

Ivermectin release was characterized *in situ* to confirm delivery of Ivermectin to the amputation site. The results demonstrated that delivery was similar to a bolus injection at the wound site, with 89 ± 4% of the loaded ivermectin released by 3 DPA, with the majority within 24 hours of the application. There were two shared short term critical time points, 5 and 9 DPA, in the regenerative and non-regenerative mouse digit tip amputation model[11]. Five DPA takes place during macrophage infiltration, and 9 DPA is when the regenerative and non-regenerative models differ morphologically with blastema formation in the regenerative model[11,16]. Thus, these two time points were assessed to see if the ivermectin treatment had a phenotypic or morphological effect at the amputation site. Variability in wound closure times between animals made it difficult to conclude if the observed differences in macrophage expression were due to the drug treatment or inherent differences in wound closure times.

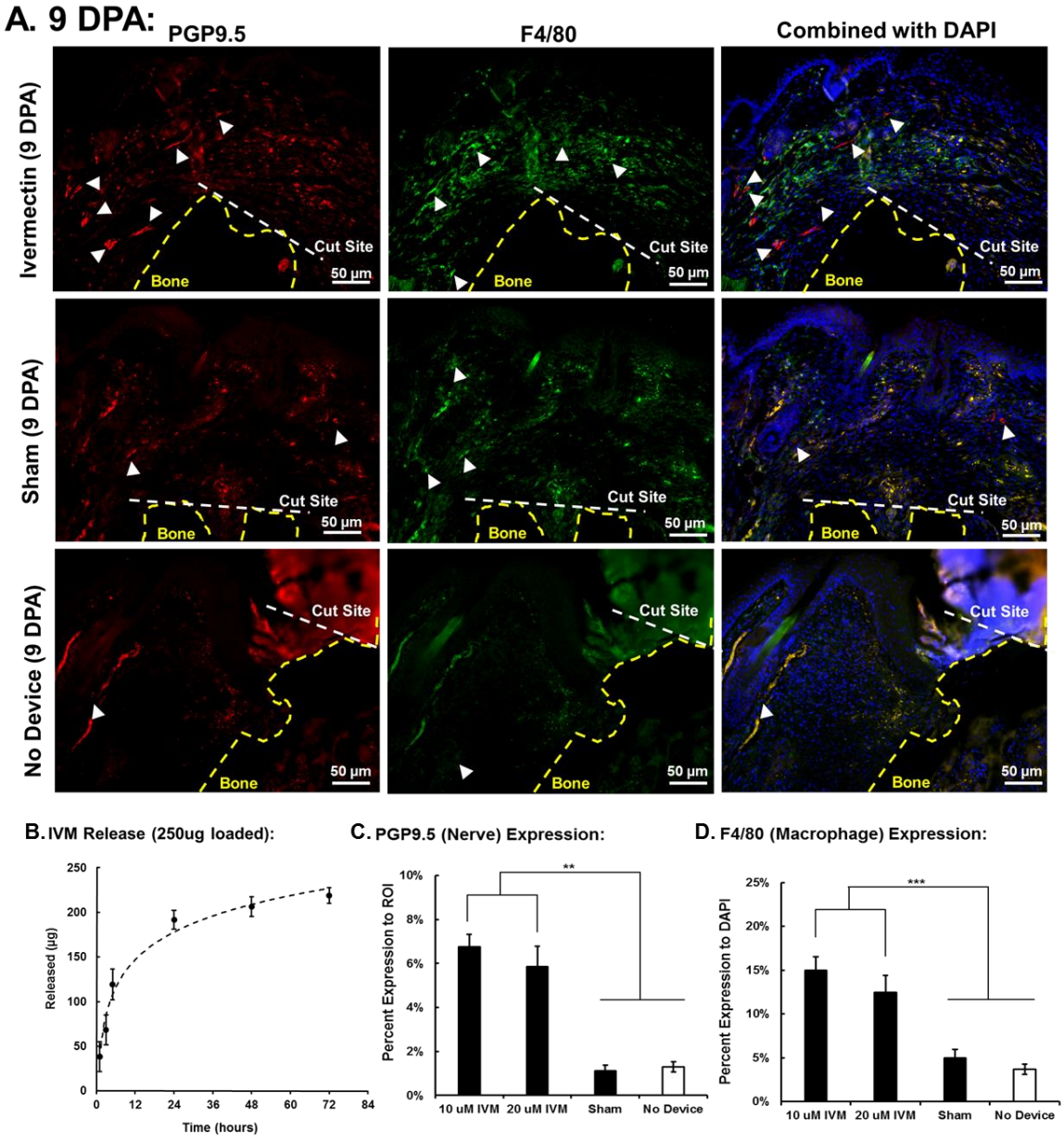
A. 9 DPA:
PGP9.5
F4/80
Combined with DAPI
Ivermectin (9 DPA)
Sham (9 DPA)
No Device (9 DPA)
Cut Site
Bone
50 µm
B. IVM Release (250ug loaded):
Released (µg)
Time (hours)
C. PGP9.5 (Nerve) Expression:
Percent Expression to ROI
**
D. F4/80 (Macrophage) Expression:
Percent Expression to DAPI
***
10 uM IVM
20 uM IVM
Sham
No Device

**Figure 3.3. Effective Delivery of the Small Molecule Ivermectin with the Wearable Bioreactor. A.** Immunohistochemistry of Ivermectin, unloaded device (sham), and no device animals. The red (which is pointed out by white arrows) is for the peripheral nerve marker PGP9.5, while the green is the mouse macrophage marker F4/80. **B.** Release profile of Ivermectin from the silk hydrogel over a 3-day period. **C.** Quantification of PGP9.5 expression between the groups at 9 DPA. **D**. Quantification of F4/80 expression between the groups at 9 DPA. Statistical Analysis was performed using ANOVA single factor followed by a student's t-test to compare groups. Significance to the control group is measured as following p-values * ≤ 0.05, ** ≤ 0.01, and *** ≤ 0.001. Population is at n ≥ 4. For drug release there was a population of n = 4 with 2 technical replicates for each sample.

Morphologically, at 9 DPA there were slight variations in cell morphology and calcification of the ivermectin versus the sham and no device control groups around the remaining P2 bone**.** Changes in nerve and macrophage expression were explored with immunohistochemistry. The results showed a statistically significant increase in the expression of the macrophage marker F4/80 and nerve marker PGP9.5 at or distal to the cut site compared to the sham ($p = 0.001$ and 0.003 for F4/80 and PGP9.5, respectively) and the no device control group ($p = 0.0005$ and 0.002 for F4/80 and PGP9.5, respectively). To see if this difference persisted at longer time points, immunohistochemistry for nerve and macrophages were performed. The results demonstrated that the increase of nerve and macrophage expression disappeared by 15 DPA (Supplementary Figure. 3.3).

*A*t the 15 DPA time point, changes in gross morphology of the amputated digits were evident. Overall, differences in morphology and size of the fracture callus was evident between the three groups (Figure 3). To evaluate if the morphological changes were associated with deviations in the wound healing cycle, histology and immunohistochemistry were conducted.

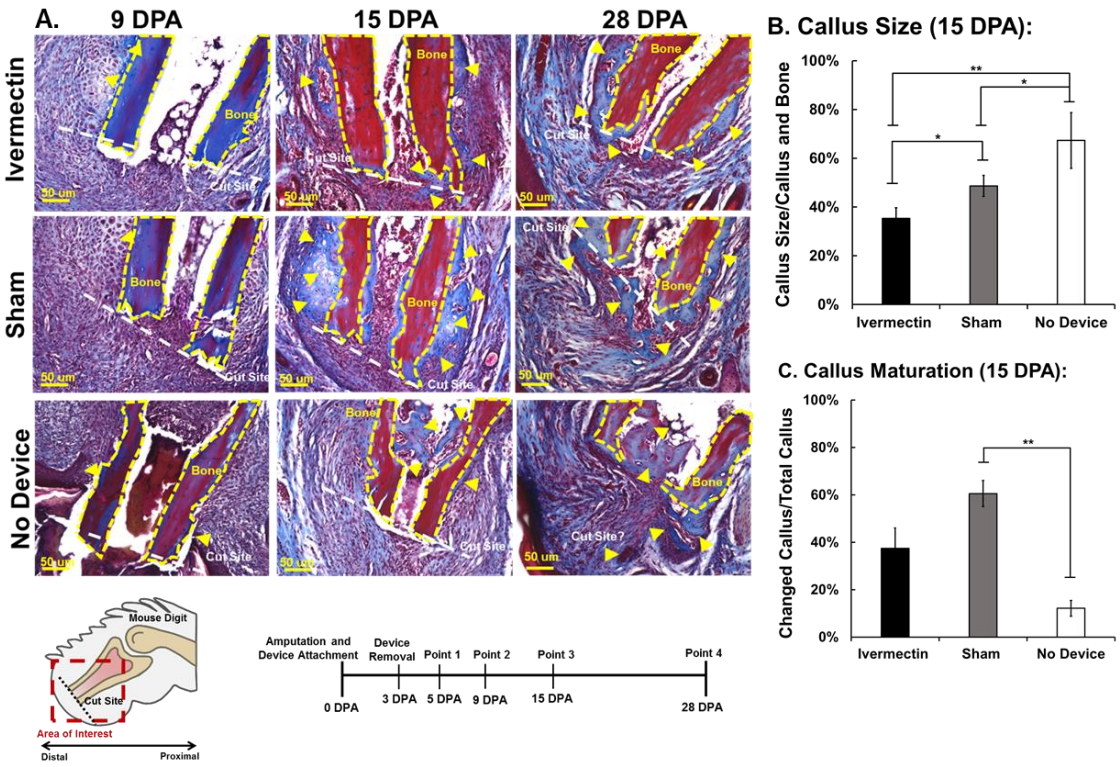


**Figure 3.4. Changes in Gross Morphology Due to Ivermectin Treatment at 15 DPA.** **A.** Histological analysis of the cut site of the different animal groups of the wound healing event. **B.** Semi-quantitative analysis of callus area for the different animal groups at 15 DPA. Callus area was normalized over the total area of both callus and P2 bone combined. **C.** Semi-quantitative analysis of callus *maturity* of the different animal groups at 15 DPA. Mature callus was normalized over total area of callus. Statistical Analysis was performed using ANOVA single factor followed by a student's t-test to compare groups. Significance to the control group is measured as following p-values * ≤ 0.05, ** ≤ 0.01, and *** ≤ 0.001. Population is at n ≥ 3.

Histologically, the callus in the sham group showed similar morphology to hypertrophic chondrocytes compared to the ivermectin treated group. The area of fractured callus was normalized to callus fracture and P2 bone was quantified Overall, there was a statistical increase of fracture callus size between the groups, with the largest increase with the no device group (67± 4%), followed by sham (49 ± 4%) and ivermectin groups (35 ± 5%). To quantify more mature callus tissue**,** the changed callus was normalized to the ROI of the total fracture callus and the P2 bone area combined**.** The callus was larger in the 'no device group', while both the ivermectin and sham animal groups had a more developed fracture callus, with a statistical significance between the sham and no device groups (Figure 4). Safranin O (SO) stains for proteoglycans and the results in Figure 7 showed that only the sham group showed SO staining within the fracture callus.

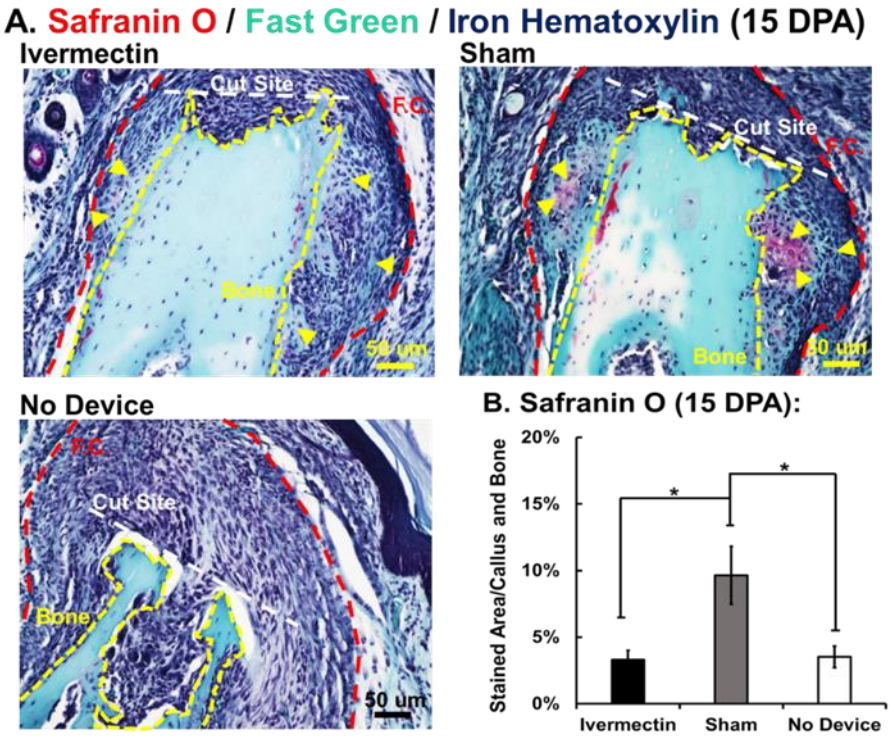

**Figure 3.5. Safranin O Stain for Proteoglycan Content of the Fracture Callus at 15 DPA. A.** Safranin O (red) stain for proteoglycan content of the fracture callus at 15 DPA. Fast Green (aqua) and Weigert's Iron Hematoxylin (Black) are used for the counter and nuclear stain respectfully. **B.** Quantification of Safranin O stain normalized over the combined area of the P2 bone and fracture callus. Statistical Analysis was performed using ANOVA single factor followed by a student's t-test to compare groups. Significance to the control group is measured as following p-values * ≤ .05, ** ≤ .01, and *** ≤ .001. Population is at n ≥ 3.

To provide more quantitative analysis of the morphological differences at 15 DPA, immunohistochemistry was performed for the osteoblast marker OSX/sp7 and the chondrocyte related ECM marker collagen type II (col II). The results showed a statistically significant increase in OSX/sp7 expression in the callus of the ivermectin treated animals compared to both control groups at 15 days ($p = 0.04$ and 0.01 for sham and no device animals, respectively) (Figure. 5,6). It should be noted that the expression of OSX/Sp7 was isolated to the fracture and bone of the animal. Due to the defined ROI included in all DAPI areas around the amputated bone, the actual expression appears low. However, the differences are distinct and can be seen in the represented IHC for each group (Figures. 5/6). For col II, the 'no device' and sham animals showed similar trends in expression, while the ivermectin treated animals typically showed a lower level. These results reflect what was seen qualitatively in the histology (Figure 4). At 28 DPA little differences were observed between the ivermectin and Sham animal groups.

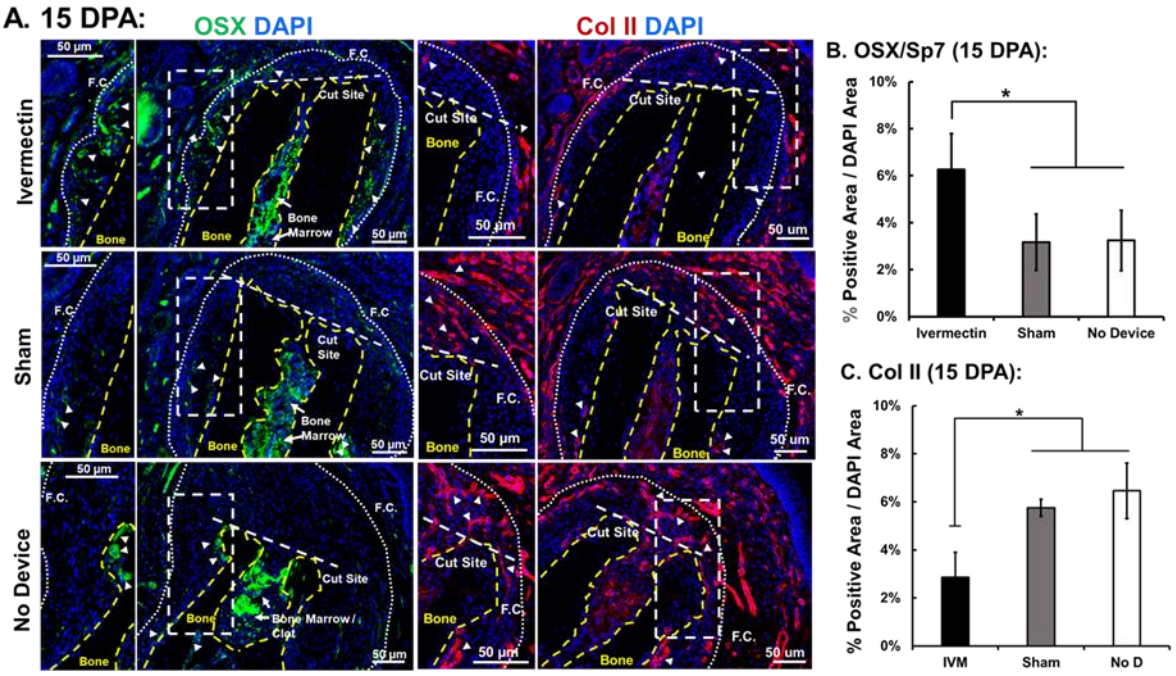


**Figure 3.6. Changes in Phenotypic Expression of the Fracture Callus at 15 DPA. A.** Immunohistochemistry of Ivermectin, unloaded device (sham), and no device animals. Stains from top to bottom are the osteoblast and osteocyte marker Osterix/Sp-7 (OSX/Sp7) and cartilage associated ECM marker collagen type II (col II). **B.** Quantification of OSX/Sp7 expression between the groups at 15 DPA. **C.** Quantification of Col II expression between the groups at 15 DPA. Quantification of F4/80 expression between the groups at 9 DPA. Statistical Analysis was performed using ANOVA single factor followed by a student's t-test to compare groups. Significance to the control group is measured as following p-values * ≤ 0.05, ** ≤ 0.01, and *** ≤ 0.001. Population is at n ≥ 3.

## 3.5. Discussion

Limb regeneration involves a series of interlocking events that requires specific temporal and spatial activation and inhibition of biological pathways. By understanding what drives and controls limb regeneration; engineers can then design better materials to be used in regenerative medicine. While progress has been made in characterizing the individual contributions of some pathways or tissue systems towards limb regeneration, their dynamic role in the overall process remains obscure. The work presented here attempts to bridge this gap through the use of a materials engineering approach. While the technical device (i.e., the outer protective sleeve and inner soft silicone insert) provide protection for the scaffold from animal tampering, the hydrogel scaffold allows for tunable control of mechanics and drug delivery, along with hydration of the wound bed.

### *3.5.1. Device Capability*

The device and silk hydrogel scaffold were successfully used as a research tool to study limb regeneration in the mouse digit tip amputation model. The device remained attached for up to 2 weeks without signs of necrosis at the amputation site or premature removal by the animal. It should also be noted that the wound tends to heal around a portion of the hydrogel by 1 week, thus longer wearable times may not be required. In addition, the hydrogel was incorporated into the healing wound. This trait could be useful for further stimulation post wound closure. Silk as a biomaterial is mechanically tunable by varying different features (e.g. concentration of silk used in the hydrogel or chemically decorating the polymer backbone). In combination with drug delivery, these features would allow for a wide range of impacts to manipulate the amputation site to study limb regeneration in the mouse digit tip model.

One of the major causes of necrosis with these types of devices is cyanoacrylate often used in adhesion[37]. This issue was mitigated by using the bio-adhesive skin-tite as the

mode of attachment. Additional benefits of this new system include the two methods used to sterilize the device components and the scaffolds (autoclaving and sterile filtration, respectively), methods that are readily available to most laboratories. Another advantage of the silk is the biocompatibility without activation of specific biological pathways. The sham animals showed improved healing and growth distal from the wound-bed. Histologically there also appears to be an increase in some ECM deposition. Besides these features, there was little innate interaction between the scaffold and tissue in the sham group. This means that observed changes in future treatments can be attributed to the added components and their effect on the tissue.

One of the benefits of the hydrogel insert was the ability to act as a delivery system as well as an occlusive bandage. Wound closure plays an essential role in initiating both wound healing and limb regeneration[18]. This event requires mitogenic factors and the entry of desired cells to the amputation site[56]. In the axolotl, the wound epithelium allows for innervation in limb regeneration[56]. Wound healing will not occur until wound closure, and without this event will result in non-healing wounds, such as diabetic ulcers[57]. In larger wounds, such as digit amputations, if wound closure is not facilitated, then either the wound will not heal or the speed of healing will be slowed, which can result in loss of tissue[58]. Yet, it is also well established that if the wound is forcibly closed in a limb amputation, then limb regeneration is hampered or will not occur[59]. Given that many critical events that define limb regeneration versus wound healing are during the initial wound healing process, it is advantageous that the material used to cover the wound-bed is also able to stimulate the site. The hydrogel inserts in the wearable bioreactor here was effective as both a medium to deliver the drug, and also as a hydrating bandage to facilitate wound closure and healing.

*3.5.2. Drug Delivery*

Previously published work demonstrated the capability of silk to release a wide range of small molecules and biological compounds[52]. In addition, silk stabilizes sensitive biomolecules (e.g. RNA and proteins) and can act as excipient for long term storage and drug release[52]. This is a desired trait, given that many of the key signaling molecules used to facilitate and control limb regeneration have short half-lives (typically ranging from minutes to hours in plasma[60]). As a proof of concept of the drug delivery capability of the wearable bioreactor, Ivermectin was loaded into the hydrogel of the device and delivered to the amputation site**.** Past work showed that this small molecule improved innervation in a skin wound healing model[37]. The release study confirmed a bolus release within the first 24 to 48 hours, thus a 3-day attachment time was chosen for the study.

Trials were conducted in which the small molecule ivermectin (IVM) was delivered to the wound site via the hydrogel insert. IVM is a macrocyclic lactone known to interact with a wide range of ligand gated channels including GABA, glycine, histamine, and nicontinic acetylcholine receptors[61]. IVM has shown to induced chloride influx in neuronal cells[62], decreased proliferation and migration in cancer cells[63,64], and have immune modulating effects on both macrophages and T-cells[65–68]. Studies have shown this drug to affect the WNT-TCF pathway in cancer cells[63]. This pathway is essential in developmental biology and limb regeneration. In addition, recent work has shown that application of IVM in a mouse skin injury model resulted in improved innervation at the site of injury by 12 day's post wounding[37].

Limb regeneration is nerve dependent in the axolotl model[4]. Recent work also showed that Schwan progenitor cells were required for limb regeneration in the mouse limb regeneration model; if the digit was denervated or if the Schwan progenitor cells were depleted from the amputation site then the limb did not regenerate[28]. In addition, one of the major differences in the non-regenerative mouse digit amputation model and the regenerative frog limb regeneration model was the lack of innervation of the amputation site from the skin in mouse compared to frog[69]. Previous work showed that ivermectin increased the expression of the nerve makers PGP9.5 and GFAP 12 days post wounding in a mouse biopsy skin wound model[37]. The results in the present work showed statistically significant increase in expression of nerve markers at 9 DPA in the IVM treated group compared to all other groups. As mentioned earlier, this is one of the earliest time points that the non-regenerative and regenerative models of the mouse digit-tip amputation model diverge morphologically. In addition, innervation is required in blastema formation in axolotl limb regeneration[4]. At the next time point there was a change in morphology. In addition to increased expression of the nerve marker PGP9.5 at the amputation site at 9 DPA, there was also an increase in the macrophage marker F4/80. The immune response is the gate keeper to both limb regeneration and basic wound healing in almost all animal models of limb regeneration. If the local macrophage population is depleted in both the axtolol and mouse regenerative limbs, then both limb regeneration and basic wound healing will not occur until that cell population is replenished[7,16]. In the previously mentioned work in which limb regeneration was prevented by denervation and depletion of the Schwann progenitor cell populations, those limbs were rescued by delivery of the cytokine oncostatin M[28]. This cytokine is known to improve nerve regeneration by facilitating macrophage recruitment and phagocytosis of damage nerve cells, as well as to attract nerve progenitor cells to the site of injury[70].

The morphological changes observed at 15 DPA were associated with the developing fracture callus. The fracture callus is the area in which fibroblasts, chondrocytes, and eventually osteoblasts coalesce and facilitate wound healing and new bone formation. The make-up of this callus changes over time from connective tissue to cartilage, and finally to bone[55]**.** These series of steps define the typically observed wound healing cycle for both fracture healing in long bones and wound healing in the mouse non-regenerative digit amputation model[25,55]**.** Changes observed in the fracture callus between the different animal groups could correlate to the stage of healing. Fracture callus formation observed in typical wound healing events for the mouse digit amputation were nerve independent and macrophage dependent[69]. The observed changes at 15 DPA were observed on the fracture callus. At that time point, markers for other tissue systems, such as CD31 for vasculature and PGP9.5 for nerve, showed little or no difference between the sham and ivermectin treated groups. The changes observed at 15 DPA were transitory and lost by 28 DPA. Also, the differences seen at 15 DPA were fracture callus related with the Ivermectin study group showing the highest expression of the osteoblast marker OSX/Sp7, followed by the sham and then the no device study groups. An inverse relationship was found for collagen type II expression. Finally, the proteoglycan histological stain SO, which would stain the proteoglycan rich intermediate stage fracture callus, only showed significant staining in the sham animal group when compared to the Ivermectin or no device groups.

Collagen type II is upregulated in cartilage and in the formation and composition of initial soft fracture callus[48]. The production and expression of collagen type II decreases as the cartilage rich callus matures and proceeds into terminal differentiation[48,55]. This later

stage of the cartilage fracture callus is composed mostly of proteoglycan-rich ECM[48]. While both the sham and no device animals showed an increase in col II expression, only the sham animal group presented a positive stain for the proteoglycan stain Safranin O. This makes sense, since the hydrogel improved the wound healing process by facilitating wound closure, be it not as accelerated as the ivermectin treated animals. Finally, the fracture callus increases in bone and calcifies as it matures to hard callus, as seen in the later stages of fracture healing. This hard callus is mostly bone and would show increased expression in bone markers, like OSX/Sp7[71]. The 15 DPA results most likely indicate that both the hydrogel alone, and the ivermectin study group, accelerated the naturally occurring wounding healing process. However, ivermectin accelerates this rate of healing more than the device alone.

Macrophages are essential for the initiation of fracture formation and maturation of soft callus to bony hard callus[71,72]. If the fracture site of a broken bone has its local macrophage population depleted at the time of injury, then the fracture callus will not form until that population is replenished[71]. Likewise, when the macrophage recruiting cytokine, Macrophage Colony-Stimulating Factor (M-CSF), was added to the fracture site of a broken femur in mice upon injury, there was an increase in macrophage population at the fracture site as well as an acceleration of callus formation and maturation[71]. On the other hand, innervation drives cartilage to bone transitions in both healing and development[73]. In development, bone patterning is shaped as the nerves develop[73]. Nerve and immune systems also are known to interact during bone healing[74]. Each event triggers the secretion of different growth factors or chemotactic signaling that affect each other[74]. So while the results are most likely related to increased rates of fracture healing, the causes, such as increased macrophage populations and/or

innervation, would need to be further investigated. However, this study demonstrates the ability of the wearable bioreactor to deliver a compound in an effective and controlled manner that can subsequently alter wound healing events, key features for the study of limb regeneration.

### 3.6. Conclusions

The work details a wearable bioreactor for use to study limb regeneration using a mouse limb amputation model. The device was attached directly after amputation and remained attached throughout the desired attachment time of 3 days, and has shown the ability to be attached for longer periods of time. The silk hydrogel promoted wound closure and healing and was able to deliver the small molecule ivermectin to the wound bed and alter typically observed wound healing events. While this work shows technical capability of the wearable bioreactor, more work is needed to assess the biological responses. The further optimization of the hydrogel in the device will depend on what tissue system or biological pathway is being studied and the target pathways for stimulation. Mechanical and chemical properties of the hydrogel can be altered to provide added control of the biological outcomes. Similarly, the hydrogel can be optimized for drug delivery (e.g., proteins, cells, DNA, RNA), with control of spatial and temporal factors.

### 3.7. Acknowledgements/Funding

Funding was provided by the NIH (R01AR055993 and PA-15-322), the W. M. Keck Foundation and the Paul Allen Foundation. The funders had no role in study design, data collection and analysis, decision to publish, or preparation of the manuscript.

# Chapter 4: Silk Hydrogel Design to Study the Role of Immune Modulation in Limb Regeneration.

## 4.1. Abstract

Macrophages play an essential role in limb regeneration, while the specific role of macrophage polarization in this process is not clear. However, the ability to study this has been limited due to a lack of a tunable drug delivery system to be used with the mouse digit amputation model *in vivo*. The work in this chapter focuses on the delivering three polarizing cytokines, interferon gamma (IFNy), interleukin 4 (IL-4), and interleukin 10 (IL-10), to the amputation site of a mouse digit tip amputation model and assess the effect on the regenerative outcome. Results at 5 DPA demonstrated effective delivery of the cytokines that was confirmed with the polarization markers iNOS (M1), CD206 (M2a), and CD163 (M2c), as well as enhance macrophage recruit and distinct morphologies per each cytokine treatment group. At 15 DPA differences between groups and their interactions with the hydrogel could be observed with improved innervation with the interleukin treated animals. Finally, improved hydrogel breakdown could be observed at 28 DPA compared to the sham group. Overall, the work shows the ability of the hydrogels to locally polarize the macrophage population and evidence of altered wound healing cycles longer term.

### 4.2. Introduction

Regeneration and wound healing follow the same initial steps of inflammation and histolysis, but diverge after wound closure[10]. What happens within these initial steps

dictates what will regenerate and what will only heal. Macrophages, large phagocytic immune cells, and have been shown to be a key to starting limb regeneration processes[7,16]. The part that macrophages play in the initial stages of regeneration is multifaceted. The first and most fundamental role is to protect the body from foreign entities and removal of damaged tissue[14,17]. Beyond that, Macrophages also secrete growth factors and chemotactic compounds that are essential for recruitment of progenitor cells and initial blastema formation as well as signaling other tissue systems to return to the digit tip (e.g. epithelium, vasculature, and nerve)[10,16,18,19].

One of the key features of macrophages for a successful role in limb regeneration is plasticity. A macrophage's ability to participate in limb regeneration is time and location dependent[16]. How a macrophage accomplishes this capability is through a concept called macrophage polarization. This is the process through which macrophages express different functional phenotypes in response to micro-environmental cues[20]. Little is known as to how macrophage polarization occurs during the wound healing event. What is known is that if macrophages are not polarized correctly at the right time, and in the right location then regeneration will not occur[20,21]. Thus, it is important to clarify the specific role that macrophage polarization plays in limb regeneration.

Three polarization states have been associated with limb and/or tissue regeneration: inflammatory polarization state M1, regenerative polarization state M2a, and inflammatory resolution polarization state M2c. The typical wound healing response starts with M1 at injury and transition to M2 as the wound progresses through the healing process[75]. The M2c state helps with the transition process to the regenerative

M2a state and later on with improved remodeling of the newly formed tissue[76]. M1 can be induced with application of the cytokine interferon gamma (IFNy), M2a with interleukin 4 (IL-4), and M2c with interleukin 10 (IL-10). Work has been done both *in vitro* and *in vivo* to understand how these polarization states relate to regeneration. However, *in vitro* experiments lack the complexity that determines the effect of macrophage polarization seen *in vivo* is an issue, yet most *in vivo* systems lack the tunability needed to understand what is observed[21]. A middle ground is needed in order to study the complexity of macrophage polarization in limb regeneration.

In Chapter 3 it was demonstrated that our wearable bioreactor was capable of providing that link between the tunability of *in vitro* applied materials to the *in vivo* mouse limb regeneration model. The work presented in this chapter uses this system to study the link between macrophage polarization and limb regeneration. Utilizing the bulk loading capability of the hydrogel, we were able to optimize and deliver three polarizing cytokines to induce M1, M2a, and M2c macrophage polarization states in a non-regenerative P2 mouse limb amputation model. Results at 5 DPA demonstrated proof of this concept and provided the ability to tune the dose of cytokines for optimal results. Longer time points indicated changes in hydrogel interaction with enhanced hydrogel incorporation with IL-10 and improved innervation with the interleukin groups compared to the other device wearing animals. Finally, improved hydrogel breakdown could be observed at the later time points at 28 DPA.

## 4.3. Methods and Materials

### *4.3.1. Silk Processing and Hydrogel Scaffold Fabrication*

The method used to process the silk for the hydrogels was previously described[38]. For scaffold fabrication, silk solution was diluted to a working concentration of 3% (w/v) using Hanks buffer solution with phenol red (Sigma-Aldrich, St. Louis MO). Additional components were added to the silk, including concentrated DMEM (1:10 dilution of stock, Sigma-Aldrich, St. Louis, MO), Glutamax (1:100 stock solution, Fischer Scientific, Waltham MA) and, dextrose (final concentration at 4.5 mg/mL gel solution, Sigma-Aldrich, St. Louis, MO). The system was then enzymatically cross-linked at the tyrosine side chains using horseradish peroxidase enzyme (HRP) at 5 U/ml (Sigma-Aldrich, St. Louis, MO) with hydrogen peroxide at 0.01% overall volume (or 10 µl/1mL solution)[38]. Sodium bicarbonate was added to balance the pH of the hydrogel based on the color of the gel generated by the phenol red present in the supplemented Hank's buffer solution and concentrated DMEM.

### *4.3.2. Release Studies for Murine IFN-y, IL-4, and IL-10*

Interferon gamma (IFNy), Interleukin 4 (IL-4), and Interleukin 10 (IL-10) were loaded into the gelation solution at a concentration at 5 µg/mL. After gelation was initiated, 0.05 mL of each solution was pipetted into a 1.5 mL centrifuge tube and allowed to solidify in a 37$^{o}$C oven. After gelation was complete, 1 mL of PBS was added to each centrifuge tube and the samples where then placed back into the oven. The PBS elution solution was then collected and replaced at specific time points (1, 3, 5, 7, and 15 days). The collected solution was stored at -80$^{o}$C for later assessment. Once all time points were collected, protein concentrations were measured by ELISA (PreproTech, Rocky Hill, NJ) following the manufacturer's instructions. Each group had an N = 3 with 2 replicates for each sample.

*4.3.3. Scaffold Loading*

Interferon gamma (IFNy), Interleukin 4 (IL-4), and Interleukin 10 (IL-10) were loaded at a final concentration of 50 ng/gel for all three cytokines or 250 ng/gel for IFny and IL-4 into the hydrogel solution prior to gelation. Gelation was performed in a sterile hood to maintain sterility of the scaffold components. HRP was mixedthoroughly into the solution prior to gelation, which was then initiated with the addition of the hydrogen peroxide. The solution was then allowed to sit in the sterile hood for 2 minutes, after which 10 µL of hydrogel solution was pipetted into the insert. After loading, the inserts were placed into sterile 0.6 mL mini-centrifuge tubes. Trapped bubbles in the insert were removed by centrifugation using a mini-centrifuge (Artec Educational, Osaka Japan). The scaffold loaded inserts were left to sit in the sterile hood until gelation was completed.

*4.3.4. Amputation Surgery and Device Attachment and Removal*

All experiments were done under the approval of Tuft's IACUC. All animals were treated fairly and housed in 12-hour light and dark cycles and fed using recommended feed. Female FVB/NJ mice from 8 - 9 weeks of age were used in the work (Jackson Labratories, Bar Harbor, ME). Devices were attached for 5 days post amputation (5 DPA) and then removed. For short term analyses, animals were sacrificed after device removal. For longer term assessments, animals were sacrificed at 15 days and 28 DPA. Four groups were used for each time point of the study. The first group were animals that had the digit amputated but had no device attached (ND). The second group were animals that wore the device with a silk hydrogel scaffold without drug (sham). The last

two groups wore devices that had either IFN-y, IL-4, or IL-10 pre-loaded into the silk elastomeric scaffold (IFN-y, IL-4, and IL-10, respectfully).

*4.3.5. Tissue Processing*

Animals were sacrificed using $CO_2$ asphyxiation and spinal dislocation. Amputation digits were collected and fixed for 12- 24 hours using a 4% paraformaldehyde solution (Sigma-Aldrich, St. Louis, MO). The tissue was then moved to a decalcification solution for 12 hours (Decal I, Roche, Basel, Switzerland) and placed through a series of sucrose then sucrose and Optimal cutting temperature compound (OCT) gradients then embedded into OCT to be sectioned at 10 um thick sections using a cryotome (Model CM1950, Lecia Biosystems Buffalo Grove, IL).

*4.3.6. Histology and Immunohistochemistry*

The tissue sections were rehydrated in PBS before staining. For general morphology and collagen fiber alignment, samples were stained with Masson's Trichrome (Sigma-Aldrich, St. Louis, MO) according to the manufacturer's instructions. For immunohistochemistry analysis, antigen retrieval was carried out either by a (1:1) ratio of methanol and acetone for 10 to 20 minutes at -20ºC or 1% sodium dodecyl sulfate solution for 5 minutes at room temperature. Non-specific antibody binding was blocked using a buffer that consisted of 10% goat (Sigma-Aldrich, St. Louis, MO), 0.1% triton-10X (Sigma-Aldrich St. Louis, MO), and 0.1% sodium-azide (Sigma-Aldrich St. Louis, MO). The slides were then incubated at 4ºC overnight with the following primary antibodies: CD31 (10 µg/ml, mouse anti-human Cat# 555444, BD Bioscience Franklin Lakes, NJ), F4/80 (5 ug/mL, rat, anti-mouse, Cat# ab6640, Cambridge, MA), PGP9.5

(1:250 dilution, Cat# NE1013, Millipore Sigma, Billerica, MA), iNOS (0.5 ug/ml, rabbit, anti-mouse, Cat# ab15323, Abcam, Cambridge, MA), CD206 (5 µg/mL, mouse, anti-mouse, Cat# ab8918, Abcam, Cambridge, MA), and CD163 (4.65 ug/mL rabbit, anti-mouse, Cat# ab182422, Abcam, Cambridge, MA), Primary antibodies were conjugated to Alexa Fluor 488 nm anti-rat raise in goat (Abcam, Cambridge, MA) and 488nm and 594 nm for anti-rabbit raised in goat or anti-mouse raise in goat (Thermo-Scientific, Waltham, MA).

*4.3.7. Image Analysis*

All Images from the *in vivo* work were taken using a Keyence microscope (model BZ-X710, Keyence, Osaka, Japan) at 10x and 20x. Image analysis was carried out using ImageJ (National Institute of Health Rockville, MD)[54], or by the manufacture's software. For immunohistochemistry analysis, the regions of interests (ROI) were define within the tissue surrounding and distal the amputation site of the P2 bone. Histological and immunohistochemistry analysis used 20X images. Three to five 20x images takes within the ROI were taken as a representative sample of the tissue and used for analysis. For immunohistochemistry analysis, the total area of the fluorescent signal was calculated and then normalized to total 4',6-diamidino-2-phenylindole (DAPI) area (i.e. % Counted Cell Area = (Positive Fluorescent Signal of Antibody in ROI)/ (Total Area of DAPI in ROI)).

*4.3.8. Statistical Analysis*

ANOVA statistical analysis followed by a student's t-test was performed to determine statistical significance of the different sub populations. This process was accomplished

using the data analysis package added to excel (Microsoft, Seattle, WA). All trials, unless otherwise indicated, had at least a population (N) of 4. Statistical significance was rated at $p<0.05$, 0.01, and 0.001 and this is indicated in the Figures by one, two, and three stars, respectively.

## 4.4 Results

### *4.4.1. Release Studies Confirm Technical Capability of Cytokine Delivery*

Release studies performed on the loaded cytokine showed a typical diffusion-based release profile, with the majority of the cytokine released by the third day of the study. Results from chapter three demonstrated that the hydrogel was incorporated into the wound-bed upon device removal. To confirm that the embedded hydrogel would not release biologically relevant amount cytokine at later time points *in vivo*, 15 and 30 day time points were also collected in the release studies. The 15 day time point demonstrated that there was no additional release of cytokine. The resultant release curves and release efficiencies for each cytokine are presented in Figure 4.1. This information, in conjunction with literature, was used to determine a high and low dose for the *in vivo* studies. A concentration of 50 ng/gel[77–79] was used for all three cytokines and 250 ng/gel[78,80–82] for IFNy and IL-4.Only the lower concentration of IL-10 was used for the study. Reported concentrations were lower for IL-10 and the higher concentration did not fit within the reported therapeutic range.

**A. Bulk Release:**

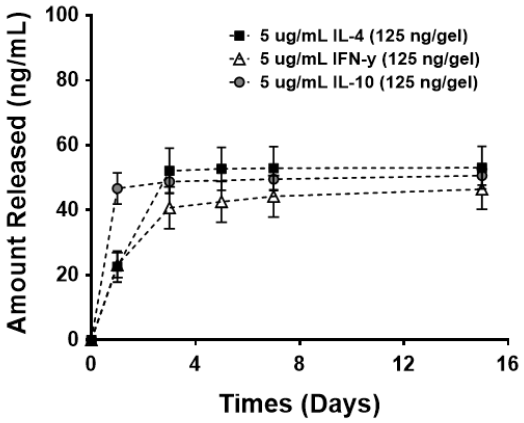


**B.** Percent for Bulk Loaded Hydrogels

| Cytokine | Release Percent |
|---|---|
| *IFN-γ (5 ug/mL)* | 42% ± 4% |
| *IL-4 (5 ug/mL)* | 36% ± 6% |
| *IL-10 (5 ug/mL)* | 28% ± 3% |

**C. Silk Hydrogel Scaffold Fabrication Techniques:**

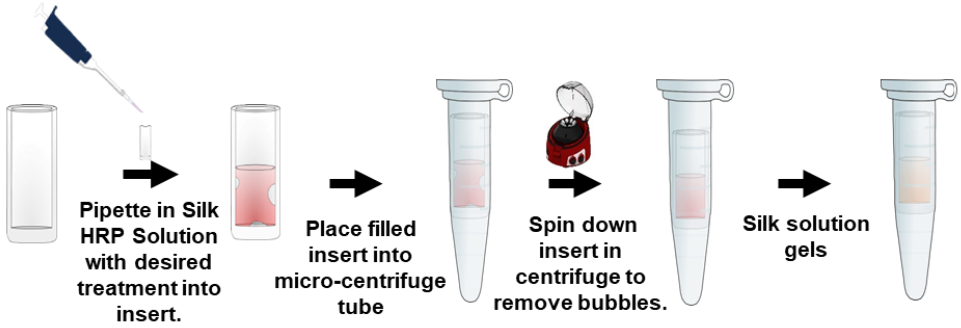


**Figure 4.1. Release Profile of Bulk Loaded Cytokine and experimental design. (A – B).** Release profile of the three bulk loaded cytokines.

### *4.4.2. Short Term Single Loaded Hydrogels Show Ability to Recruit Macrophages and Induced Desired Polarization:*

At 5 DPA each cytokine treated group displayed unique morphologies and hydrogel interactions. IFN-y and IL-10 showed cell infiltration into the hydrogel, while IL-4 treated animals showed little sign of cells inside the hydrogel. Conversely, IL-4 animals presented enhanced tissue growth past the cut site which was not seen in the other groups. There were histological differences observed between the high and low dose of IFNy and IL-4, with the high doses showing variability in results.

Immunohistochemistry (IHC) was used to assess macrophage recruitment at 5 DPA with the macrophage marker F4/80 and the general leukocyte marker CD45. Results showed a statistical significant increase in all cytokine treated groups compared to both controls for both markers. The IL-10 treated groups showed statistically lower F4/80 and CD45 expression than IL-4 and IFNy treated animals, which might reflect that IL-10 is not directly chemotactic to macrophages[83]. Macrophage recruitment differed in the the high and low doses of IL-4, but not IFNy (Supplementary Figure 1). Increasing the dose for IFNy did not affect overall macrophage recruitment, the higher IL-4 group showed an increase, but much more inconsistent level of F4/80 and CD45 expression. Due to the variability in macrophage recruitment and morphological outcome in the higher dose, the lower dose was used exclusively moving forward.

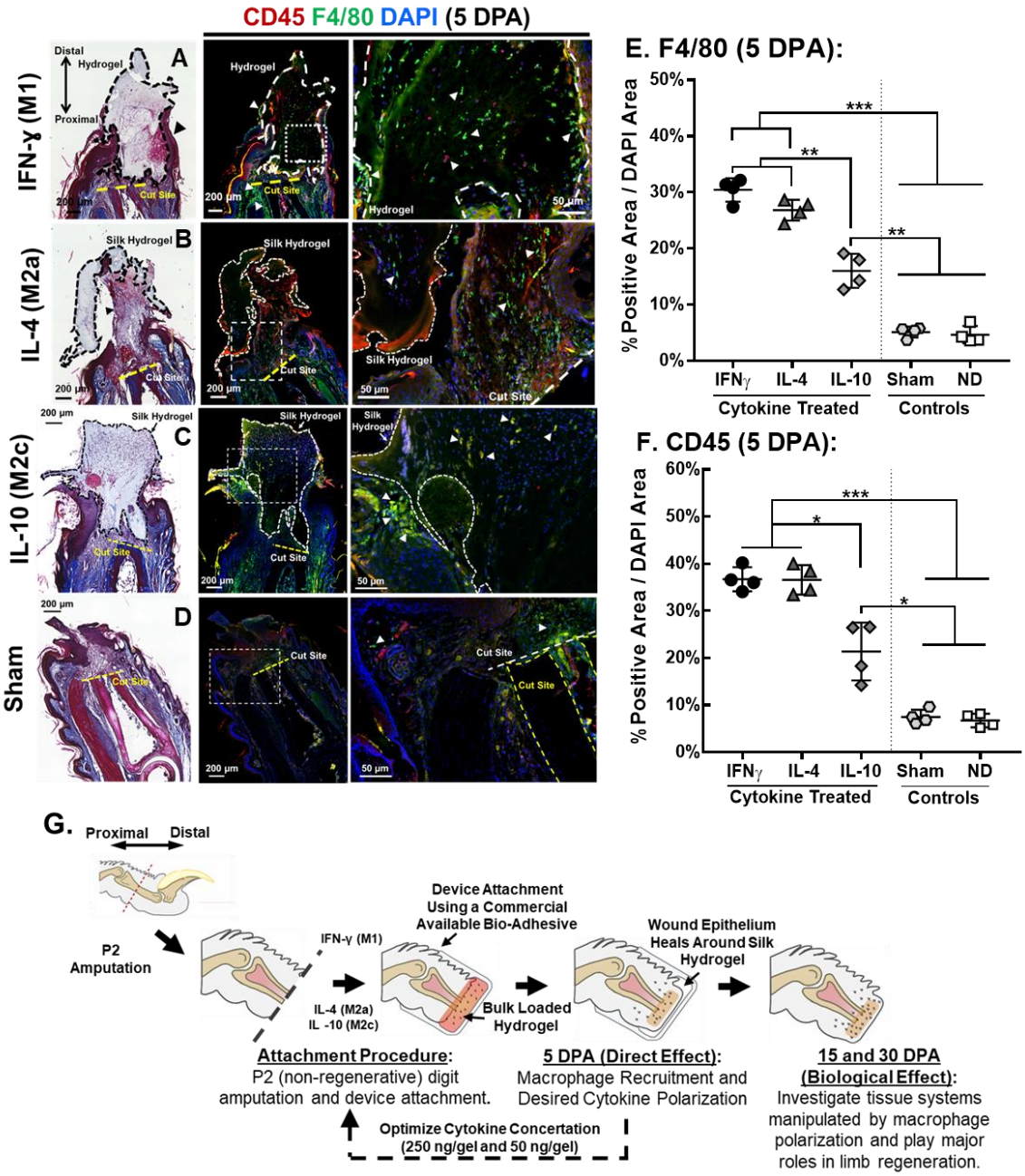
CD45 F4/80 DAPI (5 DPA)
IFN-γ (M1)
IL-4 (M2a)
IL-10 (M2c)
Sham
A
B
C
D
Distal
Proximal
Hydrogel
Silk Hydrogel
Cut Site
200 µm
50 µm
E. F4/80 (5 DPA):
% Positive Area / DAPI Area
50%
40%
30%
20%
10%
0%
***
**
**
IFNγ
IL-4
IL-10
Sham
ND
Cytokine Treated
Controls
F. CD45 (5 DPA):
% Positive Area / DAPI Area
60%
50%
40%
30%
20%
10%
0%
***
*
*
IFNγ
IL-4
IL-10
Sham
ND
Cytokine Treated
Controls
G.
Proximal
Distal
P2
Amputation
IFN-γ (M1)
IL-4 (M2a)
IL -10 (M2c)
Device Attachment
Using a Commercial
Available Bio-Adhesive
Bulk Loaded
Hydrogel
Wound Epithelium
Heals Around Silk
Hydrogel
Attachment Procedure:
P2 (non-regenerative) digit
amputation and device attachment.
5 DPA (Direct Effect):
Macrophage Recruitment and
Desired Cytokine Polarization
15 and 30 DPA
(Biological Effect):
Investigate tissue systems
manipulated by macrophage
polarization and play major
roles in limb regeneration.
Optimize Cytokine Concertation
(250 ng/gel and 50 ng/gel)

**Figure 4.2. Macrophage Recruitment at 5 DPA. (A -D).** Immunohistochemistry of the different cytokine treated groups for the macrophage marker F4/80 and general leukocyte marker CD45. **E.** Quantification of F4/80 expression. **F.** Quantification for CD45 Statistical Analysis was performed using ANOVA single factor followed by a student's t-test to compare groups. Significance to the control group is measured as following p-values * ≤ 0.05, ** ≤ 0.01, and *** ≤ 0.001. Population of each group is N ≥ 3.

To confirm if the desired polarization was achieved in the different cytokine treated groups, three known polarization associated markers (iNOS, CD206, and CD163) were utilized to assess the different polarization states (M1, M2a, and M2c, respectfully). The results presented in Figure 4.3. show a statistically significant increase in iNOS for IFNy compared to all the other groups and a statistically significant decrease in IL-4 compared to the other groups. Both IL-4 and IL-10 showed a significant increase in CD206 expression compared to the other groups. There was no significant difference between IL-10 and IL-4 animals. IL-10 has been shown to upregulate CD206 in certain tissue systems[84]. In order to further discern the difference between the two M2 polarization states, the ratio of iNOS to CD206 was determined. As shown below, IL-10 lost the significant difference in comparison to the control groups while IL-4 maintained that difference.

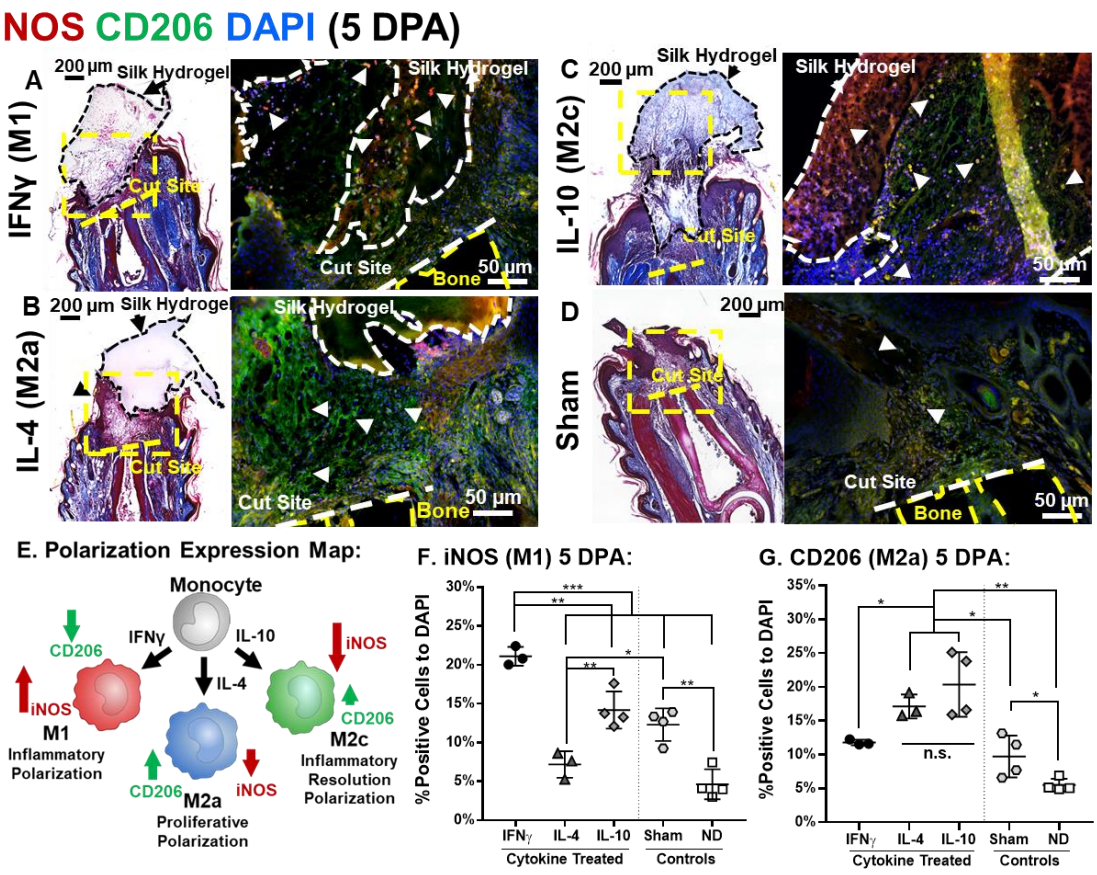


**Figure 4.3. Macrophage Polarization at 5 DPA**. Immunohistochemistry of the different cytokine treated groups for M1 polarizing marker iNOS (red) and the M2a polarizing marker CD206 (green). **G.** Quantification of iNOS expression. **H.** Quantification for CD206 expression. Quantification for CD45 Statistical Analysis was performed using ANOVA single factor followed by a student's t-test to compare groups. Significance to the control group is measured as following p-values * ≤ 0.05, ** ≤ 0.01, and *** ≤ 0.001. Population of each group is N ≥ 3.

CD163 is a scavenger receptor that is upregulated in M2c polarized macrophages compared to M1 and M2a macrophages and was used to further discern between the IL-4 and Il-10 treated groups. Both the location and amount of expression differed between the different animal groups. While there was little expression in the two controls and IFNy groups, both IL-4 and IL-10 showed an increase in CD163 expression with IL-10 showing a statistically higher increase in expression compared to IL-4. The expression of CD163 in IL-10 was observed throughout the tissue, with the most intense signal within or near the hydrogel. Interestingly, CD163 expression in IL-4 treated animals was located at or proximal the cut site, with very little to no expression in the new tissue growth or area near the incorporated hydrogel (Figure 4.4).

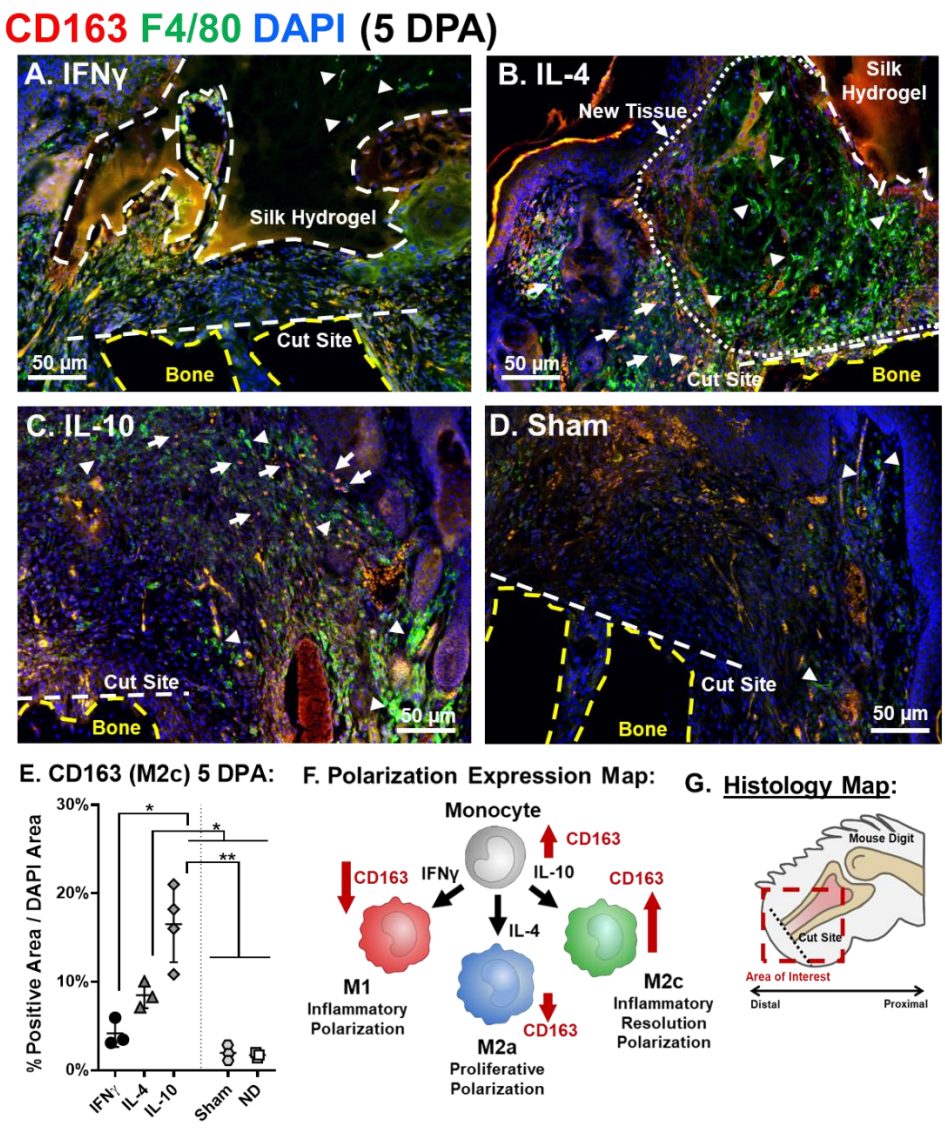


**Figure 4.4. CD163 Immunohistochemistry for M2c Macrophage Polarization. (A – D).** Immunohistochemistry of the different cytokine treated groups for M2c polarization marker CD163. **E.** Quantification of CD163 expression. **F.** Polarization map of the different cytokine treatments. **G.** Histology map of the region of interested in the IHC presented in (A – D). Statistical Analysis was performed using ANOVA single factor followed by a student's t-test to compare groups. Significance to the control group is measured as following p-values * ≤ 0.05, ** ≤ 0.01, and *** ≤ 0.001. Population of each group is N ≥ 3.

*4.4.3. Single Dose Shows Different Long Term Effects for Each Cytokine:*

Direct and indirect effects were assessed at 15 DPA. Histologically there were observed differences in how the tissue interacted with the embedded hydrogel (Figure 4.5). IFNy had a large inclusion around the hydrogel filled with small mononuclear cells, IL-4 showed almost no capsule formation, and the sham was in between the two with a moderate sized inclusion surrounding the incorporated hydrogel. The L-10 treated animals showed a unique morphology with regard to the incorporated hydrogel. Compared to the other device wearing groups, IL-10 animals showed a much higher amount of incorporated hydrogel with signs of tissue invasion in the material. In addition, these larger hydrogel pieces also showed signs of multi-nucleated cells at its edges, most likely foreign body cells(FBC) [85].

The presence of macrophages and other immune cells was assessed with IHC using the markers CD45 and F4/80 (Figure 4.5). Results from IHC reflected what was observed in the histology with the majority of F4/80 and CD45 expression centered around the encapsulated areas of the hydrogel. For the IL-10 treated group, expression of F4/80 and CD45 was not associated with any observed capsule. Rather, positive expressing cells were seen through the tissue and in particular around and in the hydrogel itself. The expression within the hydrogel tended to be in the same location that invading tissue growth was observed in histology. The observed multi-nucleated cells observed in histology were shown in the IHC to be a collection of F4/80 positive cells. As these cells merged together they tended to lose this expression (Figure 4.5). This is a characteristic of FBC cells[85] and it can be concluded that what was observed is a typical foreign body response (FBR) to the implanted material[86].

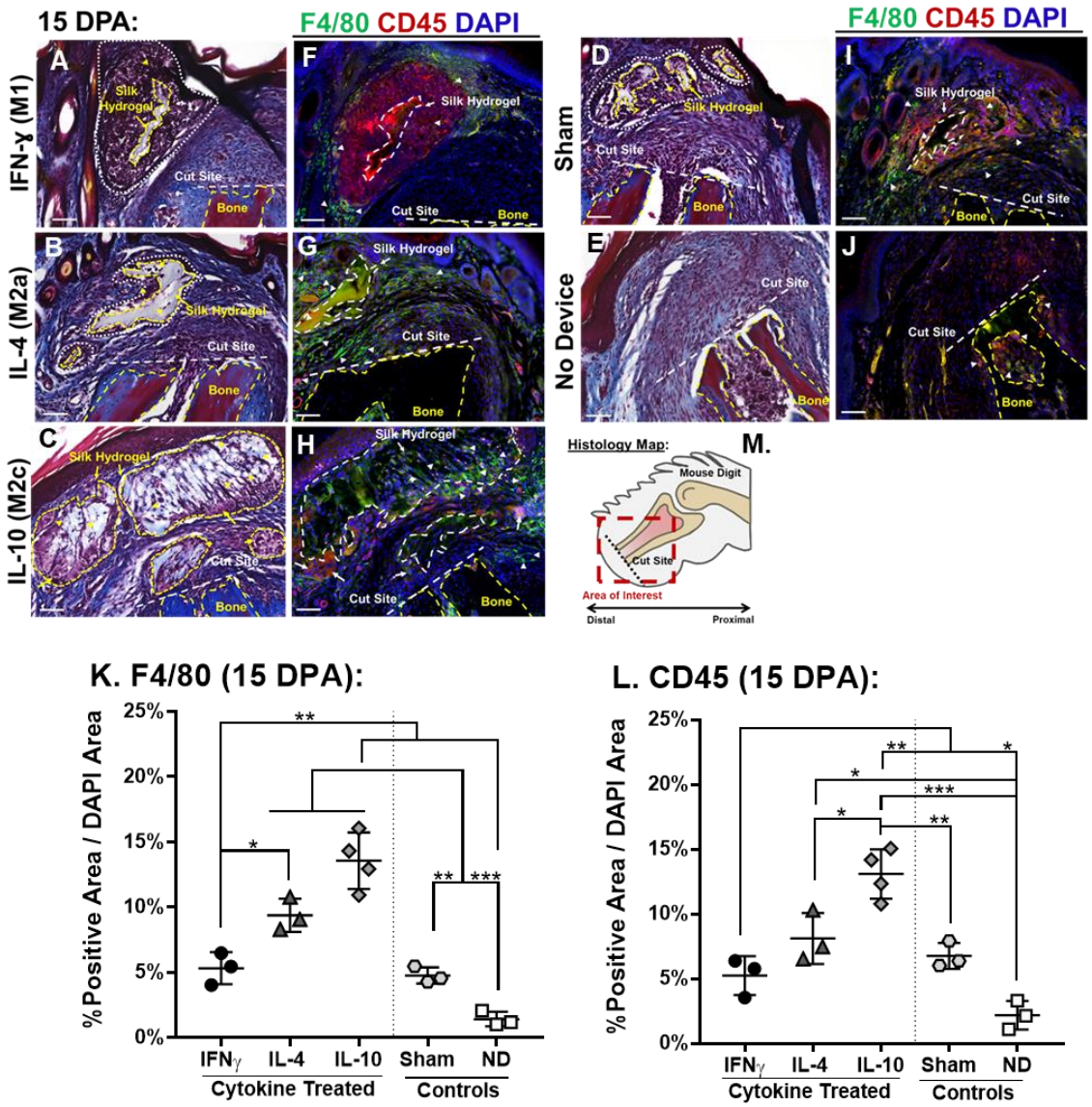


**Figure 4.5. Analysis of Immune Response at 15 DPA. (A - E).** Masson trichrome stain of the different groups at 15 DPA. **(F - J).** Immunohistochemistry of the different cytokine treated groups for the macrophage marker F4/80 and general leukocyte marker CD45. **K.** Quantification of F4/80 expression. **L.** Quantification for CD45. **M.** Histological map of the area of interest of the presented IHC in (A – E) Statistical Analysis was performed using ANOVA single factor followed by a student's t-test to compare groups. Significance to the control group is measured as following p-values * ≤ 0.05, ** ≤ 0.01, and *** ≤ 0.001. Population of each group is N ≥ 3.

Indirect effects on the wound healing process were evaluated in the areas of innervation and angiogenesis. This was accomplished with the IHC nerve marker PGP9.5 and the vascular marker CD31 (Figure 4.6). The nerve marker could be discerned from the surrounding tissues, CD31 was harder to distinguish from red blood cells in the IL-4 animal groups. As a result, CD31 was assessed qualitatively, while PGP9.5 was quantified. As presented in Figure 4.6, all device wearing animals appeared to have an in increase in CD31 expression compared to the no device wearing group. IHC for the nerve marker PGP9.5 showed the no device animal group to have the expression with a statistical decrease in the sham and IFNy groups. There was no statistical decrease in nerve marker for the interleukin groups (Figure 4.6).

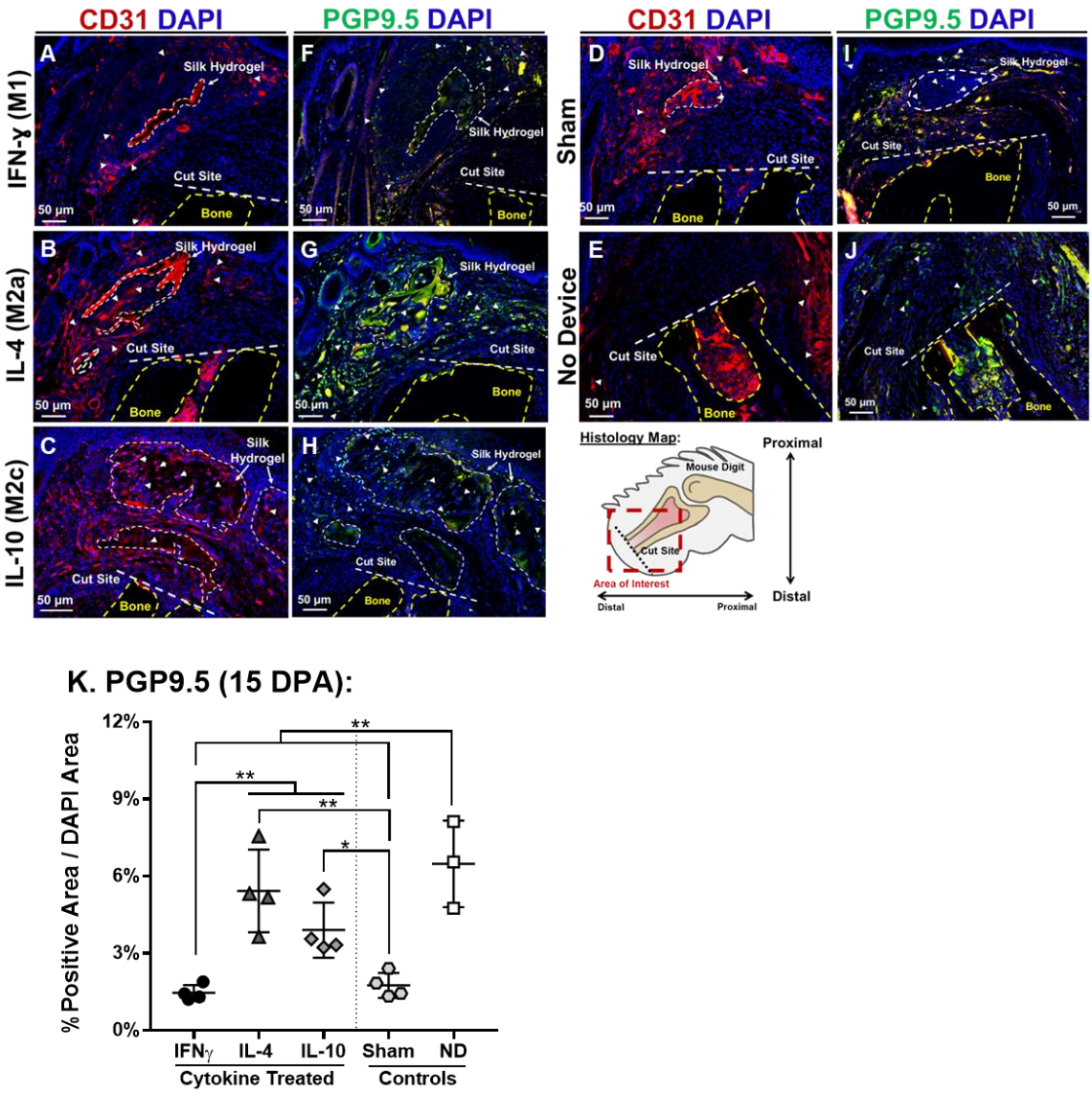


**Figure 4.6. Analysis of Angiogenesis and Innervation at 15 DPA. (A – E).** Immunohistochemistry of the different cytokine treated groups for vasculature marker CD31. **(F – J).** Immunohistochemistry of the different cytokine treated groups for nerve marker PGP9.5. **K.** Quantification for CD45 Statistical Analysis was performed using ANOVA single factor followed by a student's t-test to compare groups. Significance to the control group is measured as following p-values * ≤ 0.05, ** ≤ 0.01, and *** ≤ 0.001. Population of each group is N ≥ 3.

The location of expression for these two markers reflected what was observed with the immune related markers and the interactions with the implanted hydrogels. In the IFNy, IL-4, and sham groups the areas of encapsulation and highest expression of CD45 and F4/80 were areas where differences in CD31 and PGP9.5 IHC expression were seen.

A final time-point was taken at 28 DPA to assess the changes in morphology resulting from the various cytokine treatments (Figure 4.7). Little difference could be seen between the groups histologically with the exception of observed incorporated hydrogel at 28 DPA. Besides one animal in the IL-10 group, the only samples that showed any residual hydrogel at 28 DPA was the sham group. This was in contrast to what is observed at 15 DPA, and in particular the IL-10 group, where almost all the animals showed signs of incorporated hydrogel (Figure 4.5).

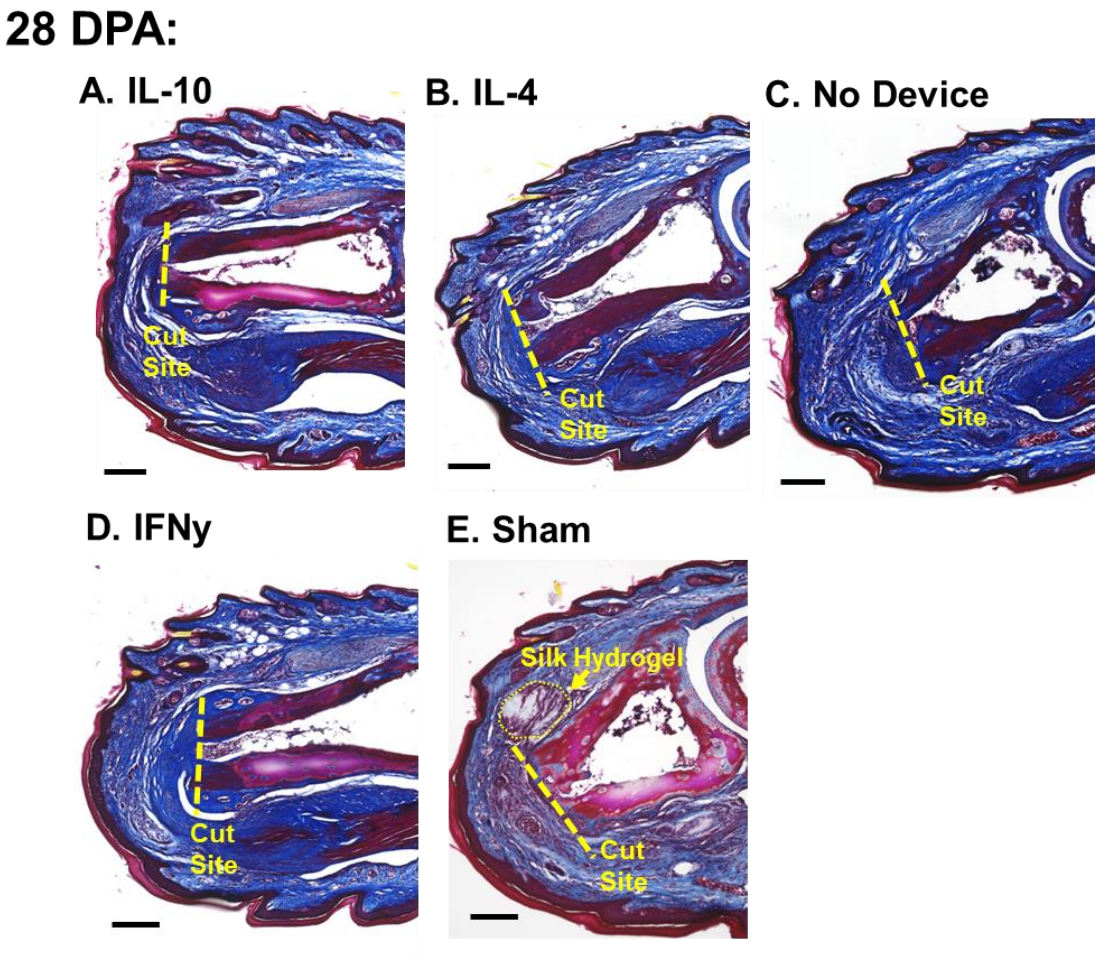


**Figure 4.7. Histology for 28 DPA time point.** Representational Trichrome stains of each of the animal groups for single cytokine delivery. Scale represents 200 μm. Population of each group is N ≥ 3.

## 4.5. Discussion

Macrophages act as the initiators of limb regeneration processes in mice[16]. How a macrophage reacts is determined upon its polarization state[87]. To understand the role of macrophages in limb regeneration we need to understand the role of macrophage polarization in the process. The current technology used to deliver biomolecules to the wound site, agarose beads, is limited to studying macrophage polarization in limb regeneration due to the need to be implanted underneath the skin. Simkin et al. was able to circumvent this by using a cyano-acrylate to close the skin around the cut site, but this was also shown to alter biological processes[18]. Our wearable bioreactor effectively delivered three different macrophage polarizing cytokines without the need to prematurely close the amputation site, a major improvement over current technology.

### *4.5.1. Improve Delivery by In Situ Characterization*

Since the hydrogel release profile could be characterized, the amount of cytokine released of could be predicted and dosing could be optimized. This is in contrast to the typically used method of implanting agarose beads (affi-bead), were only report the concentration of the concentrated solution which the particle was soaked in prior to implantation is typically reported. Affi bead loading is based surface adsorption to the bead, and while the concentration can be characterized, is not something that is typically done. The amount loaded into an affi-bead cannot be controlled, given that the amount adsorbed onto the bead is based on surface area, not concentration. The concentration of a delivered cytokine is critical, and this trend was seen in the high doses of IFNy and IL-4 (Supplementary Figure 1). The tunability in concentration that the wearable hydrogel bioreactor provides is essential for studying macrophage polarization in limb regeneration.

*4.5.2. 5 DPA shows Effective Delivery and Macrophage Polarization*

The initial 5 DPA time-point provided us with direct confirmation of macrophage polarization and a chance to optimize cytokine concentration (Figures 4.2 -4 and Supplementary Figure 1). Each cytokine resulted in a unique morphology and phenotype that was not observed in the control groups. What defined each of these phenotypes reflected the macrophage polarization state for the given cytokine. IFNy causes the M1 inflammatory state, and these animals showed hyper-epithelization[87] and enhanced recruitment of macrophage cells that were able to infiltrate the hydrogel. IL-4 polarizes macrophages to the proliferative regenerative M2a state. The animals in the IL-4 group showed no hydrogel infiltration[76], but enhanced tissue growth[87]. IL-10 resolves inflammation and induces the M2c state. These animals showed a significant decrease in macrophage recruitment[88,89] compared to the other cytokine treated groups (though statistically higher than the control groups) and infiltration of non-F4/80 positive cells into the hydrogel.

Polarization markers were able to confirm what was shown in histology and macrophage recruitment. While CD206 is associated with M2a activation, there was no statistical difference discerned between the interleukin animal groups. IL-10 has been shown to upregulate CD206 expression[84] so the lack of statistical difference can be explained. CD163 was used to discern M2c activation, and the IL-10 had the highest expression of all the animal groups (Figure 2.4). Another difference between the two interleukin groups is the location of CD163 expression in the tissue. While the IL-10 treated animals showed expression throughout the tissue, IL-4 exhibited CD163 expression in areas

proximal the cut site. The areas around the hydrogel and new tissue growth were mostly devoid of CD163 expressing cells. IL-4 suppresses CD163 signaling[90], but recruits CD163 expressing monocytes to a given location[91]. Seeing this trend in IHC confirmed the effective delivery of IL-4 in a localized manner, and the observed new tissue was most likely due to IL-4 delivery.

In relation to limb regeneration, the relationship between the lack of CD163 expression and the new tissue growth was noted. While tissue growth is considered a useful requirement for limb regeneration, too much fibrotic tissue growth can actually hinder this outcome. Bryant et al**.** showed that the lost ability of an axolotl to regenerate due to multiple amputations was closely associated with the up-regulation of ampihregulin and fibrotic tissue build up at the amputation site[6]. Prolonged or premature M2a activation leads to build-up to fibrotic scar tissue[92]. There is a trend to assume that the key to better regeneration is the rapid resolution of inflammation. However, as seen with the inhibition of limb regeneration in axolotl due to dysregulation of a regenerative associated cytokine and excessive scar tissue, quick resolution does lead to excessive regenerative polarization. In future work, our wearable bioreactor can be utilized to probe the relationship with CD163 suppression and effective IL-4 delivery on the regenerative outcome.

### *4.5.3. Longer Time Points Present Changes in Healing Tissue and Hydrogel Interactions*

The 15 DPA time point was chosen as an intermediate point between amputation and the end of the regenerative event at 28 DPA[10]. This allowed us to assess both the direct and indirect effect of macrophage polarization on the wound healing process. At this

time-point the incorporated hydrogel became a useful tool in discerning differences in morphology and phenotypic expression between the different treatment groups. IFNy, IL-4, and sham treated animal responses to the hydrogel reflected what is seen with immune responses to small biomaterial implants and their polarization state[85,93–95]. IL-10 on the other hand showed enhanced hydrogel incorporation and better tissue infiltration into the hydrogel (Figure 4.5). One of the roles of IL-10 in inflammation is immune tolerance[93]. By resolving the initial inflammatory response, we might have improved the incorporation of the hydrogel into the wound-bed and allowed for initial tissue infiltration to occur. Signs of FBC around the hydrogel and enhanced immune response at 15 DPA is typical of larger implants[96]. Thus, whatever initial deviation was caused by IL-10 does not active at 15 DPA. However, this does indicate how the initial modulation can affect later responses.

Towards innervation and angiogenesis, all device wearing animals showed increased expression of CD31, while the IFNy and sham groups showed a decrease in nerve marker PGP9.5 expression compared to the no device group. One of the macrophage's most defining roles in the wound healing process is how it can dictate what other cells are recruited to the wound site, and how those other cells react at the site of injury[87]. If there is a prolonged inflamed response, then the ability to recruit needed cell types will be delayed. Regeneration is time sensitive as well and that delay might alter the final result.

While all animal groups show an increase in hydrogel incorporation at 15 DPA, only the sham animals showed signs of hydrogel still present at 28 DPA (Figure 4.7.). While not

conclusive, this does point to better hydrogel incorporation with the immune modulated treatments. Given that we want to minimize the effect that our system intrinsically has on the biological outcome, enhance hydrogel degradation could be a useful tool to utilize in future work.

## 4.6. Conclusions

The work in this chapter established effective macrophage polarization using the wearable bioreactor. We were able to optimize dose concentration and deliver 3 polarizing cytokines that showed signs of unique morphology and polarizing phenotypes at 5 DPA. This effect extended to the direct immune response and nerve expression at 15 DPA. and potentially improved hydrogel breakdown as seen with the results at 28 DPA. More work needs to be done in characterizing the effect that this has on the regenerative outcome, but the results demonstrate efficacy and capability that can be applied to future work**.**

# Chapter 5: Hydrogel Design for Dynamic Modulation of Macrophage Polarization

## 5.1. Abstract

Regeneration is a dynamic event that requires a combination of temporal and spatial cues to succeed. To understand the whole story of what drives limb regeneration and the role which the immune system plays in it, the method of stimulation needs to be dynamic. The purpose of presented work in this chapter was to design, optimize, and apply two methods of drug delivery to dynamically manipulate the local macrophage population is a mouse digit tip amputation model. The first method focused on temporal control while the second focused on spatial control. Temporal control was performed with a modification to the surgical techniques that added an additional cytokine treatment following the initial attachment (reattachment). Spatial control was achieved by application of a composite hydrogel composed of silk polyvinyl micro-particles soaked in interleukin 4 (IL-4) encapsulated in a hydrogel bulk loaded with either interferon gamma (IFNy) or interleukin 10 (IL-10). Results to confirm efficacy of both treatment styles at 5 DPA showed differences in morphology as well as variations in the immune profile. Temporal control displayed order dependency in all areas of macrophage polarization and recruitment for IL-4 and IFNy and enhanced M2a polarization in IL-10 and IL-4 treatments. The composite hydrogel showed an attenuated polarization profile for the IFNy and IL-4 composite hydrogel that did not impact macrophage recruitment. Overall, these findings verify two successful techniques to modulate the local wound environment that can be applied to study limb regeneration in future work.

## 5.2. Introduction

Limb regeneration is by definition epimorphic[4]. It relies on the ability of the amassed cells in the blastema to recreate the complex structure of the limb. For limb regeneration to succeed these cells must execute a spatially specific series of events in a very certain order[97]. To understand limb regeneration, understanding the different steps in limb regeneration, as well as how these steps work together over space and time to form the new limb is needed. As such, the system used to stimulate the limb must be able to do so dynamically. Current delivery systems used to study regeneration currently only stimulate with a bolus single release, such as agarose beads soaked in the compound to be delivered.

Macrophages are dynamic by nature, so it is essential that we understand their role in limb regeneration in that regard. Each of the three explored macrophage polarization states (M1, M2a, and M2c) has unique traits associated with different with stages of the wound healing cycle (inflammation, proliferation, and remodeling)[98]. M1 macrophages are critical for inflammation and needed histolysis[98], M2a has the ability to secrete ECM and recruit progenitor cells[87], and M2c provides both resolution of inflammation and ability to remodel the newly formed ECM[87,89]. Each polarization state plays a critical role at a given time and location for both wound healing and regeneration to occur. Additionally, macrophage polarization *in vivo* is environmentally sensitive, time dependent, and spatially heterogeneous[89]. This complicated response cannot be mimicked by a single cytokine treatment alone[99]. This dynamic response also makes macrophage polarization difficult to characterize *in vitro* and challenging to study with current methods *in vivo*.

The hydrogel based bioreactor can provide temporal and spatial control of delivery through the protective hardware and tunable hydrogel medium. The hydrogel used in the system can be modified to alter how a drug is spatially and temporally delivered. The field of drug delivery and material engineering has utilized this approach to provide complex delivery of different treatments *in vivo*. This knowledge can be applied in this system to study limb regeneration. Some notable examples include immunotherapies that combine either two different chemo drugs in a composite gel format[100], pH sensitive hydrogels that released drug based on changes in the local tissue environment[101], or genetically modified T-cells with an attached nanogel loaded with an interleukin-15 super-agonist complex that enhance effective delivery while minimizing toxicity[102]. Each one of these examples demonstrates different techniques that provided that needed level of control in delivery to study limb regeneration. And, each of these examples could be used with the hydrogel in the wearable bioreactor.

The presented work in this chapter presents two methods of dynamic delivery to study how spatial and temporal manipulation of macrophage polarization would affect the regenerative outcomes. The first involves application of two different polarizing cytokine treatments. The second provided spatial delivery of two different cytokines through the use of a silk particle (SP) composite hydrogel that had one cytokine adsorbed to the particle, and another bulk loaded into the hydrogel. SPs were synthesized via phase separation induced with the addition of the polymer polyvinyl alcohol (PVA) to silk solution which is then cast into a film. As the blended solution dries the two polymers will phase separate, which results in the formation of the SP. These particular particles were chosen based on previous work which demonstrated effective long drug delivery *in vivo,*

a design requirement in the given study[103]. The work presented here demonstrates effective manipulation of the immune response at the 5 DPA time point.

## 5.3. Methods and Materials

### *5.3.1. Polyvinyl Alcohol Silk Particle Fabrication and Encapsulation*

The process to fabricate polyvinyl alcohol silk particle has been described in previous work[103]. In brief, a 5% polyvinyl alcohol (PVA) solution was formed by dissolving 30,000 – 70,000 molecular weight solid PVA (Millipore-sigma, St. Louis MO) in distilled water. This solution is then mixed with either 5%(w/v) 60 or 45 mb silk solution in a (1:5) ratio and cast into 100 mm petri-dishes, which are set to dry in the fume hood for 48 hours. After this, PBS is added to the dishes to dissolve the silk and PVA under agitation for 1 – 4 hours. When the films have completely dissolved then the solution is collected, centrifuged, and re-suspended multiple times to remove the PVA. After this, the particles were chilled for 2 hours in -20°C then overnight in -80°C. To induce beta-sheet formation, the SP slurry was lyophilized for 24 hours (Labconco, Kansas City, MO). For *in vivo* use the particles were sterilized for 24 hours using UV light.

For drug loading, the particles were re-suspended at 10 mg/mL in a Hanks buffer solution (HBS) with either 10 ug/mL of IL- 4 or HBS solution only, then placed on a shaker for 24 – 48 hours in 4°C. After this, the slurry was spun down with the loading buffer collected and stored in -80°C for later analysis. The particles where also washed multiple times to remove any loosely bound cytokine. Finally, the particles were re-suspended at a desired concentration for *in vivo* use or were stored at -80°C.

To ensure that the particles were loaded in a homogenous manner, a new method of hydrogel insert fabrication was optimized. Prior to loading the composite hydrogel solution, a bulk loaded ‘only’ or sham hydrogel solution was cast into the insert to coat the bottom of the insert and allowed to gel. This “wetted” the inside of the insert which made it easier to load the hydrogel solution with minimal bubble formation. Encapsulation of the silk particles involved

modifying the loading procedure for the hydrogel solution. Gelation was initiated in the hydrogel solution prior to particle loading. After the solution reacted for 2 to 5 minutes, the particles were added to the gelling solution and cast into the insert. This allowed the particles to be suspended in the hydrogel, rather than sink to the bottom of the insert.

### *5.3.2. Assessment and Optimization of SP Encapsulation and Retention in the Silk Hydrogel*

To verify that the particles remained in the hydrogel after encapsulation a release study was performed. Silk particles at a concentration of 20 mg silk particles/mL hydrogel were cast into 2.0 mL micro-centrifuge tubes at a volume of 0.3 mL. After gelation, 1 mL of PBS solution was added to the tubes ansd placed on a shaker in 37°C for 24 hours. After that the solution was collected and stored in -20°C for later use. This step was repeated again for 48 hours. The collected solution at 24 hours was spun down using a table-top centrifuge and the supernatant was removed with the pellet being re-suspended in 0.1 mL of PBS. 10 µL of the concentrated solution was then pipetted into a hemocytometer, which was placed under a bright-field microscope to check for particles.

An additional control of pure PBS solution and 20 mg/mL silk slurry was assessed in the same manner.

### *5.3.3. Drug Release Studies for SP and Composite Hydrogel*

Release studies were performed for the bulk loaded, silk particles alone, and composite hydrogel. In addition, the loading efficiency of IL-4 to the silk particles was also calculated. Both the methods used for the particles and hydrogel release studies have been described in previous work[103]. In brief, the silk particles were loaded with IL-4 as described in section 5.2.1. After multiple washes the silk particles were spun down and re-suspended in HBS. Part of the slurry was used for the particle release study and re-suspended to a final concentration of 10 mg SP/mL buffer. The other part of the slurry was encapsulated into the silk hydrogel at a final concentration of 10 mg SP/mL silk hydrogel. Each sample had 50 µL of hydrogel cast into a 1.5 mL micro-centrifuge tube, in which 1 mL of PBS was added to each sample after gelation. The experimental hydrogel sets consisted of 5 µg/mL IL-10 or IFNy loaded hydrogels with and without the IL-4 absorbed particles, while the control sets consist of unloaded hydrogels with and without unloaded particles. All samples were placed on a shaker at 37°C with samples taken and media refreshed at 1,3,5,7, and 15-day time points. The amount of IFN-y, IL-10, and IL-4 in each sample was determined using ELISA (Peprotech, Princeton NJ). Values were obtained at a N = 3 with technical replicates for each time point with the control value subtracted from the corresponding experimental sample.

*5.3.4. In Vivo Experimental Design*

All experiments were conducted under the approval of Tuft's IACUC. All animals were treated fairly and housed in 12-hour light and dark cycles and fed using recommended feed. Female FVB/NJ mice from 8 - 9 weeks of age were used in the work (Jackson Laboratories, Bar Harbor, ME). Three study groups were included into this study. The first was the no device (ND) group, the second a composite hydrogel group, and final the reattachment hydrogel group. The composite group consisted of bulk loaded IFNy with particle absorbed IL-4 (IFNy comp), bulk loaded IL-10 with particle absorbed IL-4 (IL-10 comp), and an unloaded hydrogel with unloaded particles (sham comp). Reattachment included five sub-groups each group differing on cytokine treatments and the order of which the animal received the treatments (nomenclature is "insert attached at amputation" to "inserted attached at 3 DPA"). These groups included IFNy to IL-4, IL-4 to IFNy, IL-10 to IL-4, IL-4 to IL-10, and finally sham to sham. Bulk loaded IL-4, IL-10, and IFNy were used as an additional control. A list of names of the different animal groups are presented in Table 5.1.

Animal trial devices were attached for 5 days and then removed. In the reattachment trial, devices were attached for 3 days' post amputation, replaced with a new hydrogel insert and then removed 2 days later (total of 5 days attached). A 3 day wait period for reattachment was chosen since the release profile from bulk release studies showed that the majority of the cytokine was released from the hydrogel by 3 days. The 2-day time point for the second attachment allowed for a total of 5 days' attachment. This time point was chosen in the case of reattachment to assess macrophage polarization during the initial immune response which happens within the first week of amputation[16,87,89]**.** The 5 day attachment was decided for the composite hydrogel group to allow for comparison

between the bulk loaded and composite groups. Amputation and initial device attachment followed earlier described methods. The reattachment procedure was performed similarly to the previously reported removal procedure, with a second device attached following removal. The embedded hydrogel from the first treatment was left attached and the second insert placed on top.

## **Table 5.1.** Animal Group Nomenclature

| Name | Description |
|---|---|
| Reattachment: | |
| IFNγ to IL-4 | Treated for 3 days with IFNγ then 2 days with IL-4 |
| IL-4 to IFNγ | Treated for 3 days with IL-4 then 2 days with IFNγ |
| IL-10 to IL-4 | Treated for 3 days with IL-10 then 2 days with IL-4 |
| IL-4 to IL-10 | Treated for 3 days with IL-4 then 2 days with IL-10 |
| Sham to Sham | Treated for 3 days with an unloaded hydrogel (sham) then 2 days an unloaded hydrogel (sham) |
| Composite: | |
| IFNγ Comp | Bulk loaded IFNy hydrogel with IL-4 absorbed silk particles encapsulated into the hydrogel |
| IL-10 Comp | Bulk loaded IL-10 hydrogel with IL-4 absorbed silk particles encapsulated into the hydrogel |
| Sham Comp | Unloaded hydrogel with unloaded silk particles encapsulated into the hydrogel |
| Bulk Loaded: | |
| IFNγ | Hydrogel bulk loaded with IFNγ |
| IL-10 | Hydrogel bulk loaded with IL-10 |
| Sham | Unloaded hydrogel |
| Control: | |
| No Device (ND) | Animal who received an amputation but had no device attached |

**Table 5.1. Animal Groups used in Reattachment and Composite Hydrogel Studies.**

This table provides the short hand names for each animal group along with a description of what that treatment is.

*5.3.5. Tissue Processing, Histology, and Immunohistochemistry*

Animals were sacrificed using $CO_2$ asphyxiation and spinal dislocation. Amputation digits were collected and fixed for 12- 24 hours using a 4% paraformaldehyde solution (Sigma-Aldrich, St. Louis, MO). The tissue was then moved to a decalcification solution for 12 hours (Decal I, Roche, Basel, Switzerland) and placed through a series of sucrose then sucrose and optiminal cutting temperature compound (OCT) gradients, which was then embedded into OCT to be sectioned at 10 um thick sections using a cryotome (Model CM1950, Lecia Biosystems Buffalo Grove, IL).

The tissue sections were rehydrated in PBS before staining. For general morphology and collagen fiber alignment, samples were stained with Masson's Trichrome (Sigma-Aldrich, St. Louis, MO) according to the manufacturer's instructions. For immunohistochemistry analysis, antigen retrieval was carried out either by a (1:1) ratio of methanol and acetone for 10 to 20 minutes at -20ºC or 1% sodium dodecyl sulfate solution for 5 minutes at room temperature. Non-specific antibody binding was blocked using a buffer that consisted of 10% goat (Sigma-Aldrich, St. Louis, MO), 0.1% Triton-10X (Sigma-Aldrich St. Louis, MO), and 0.1% sodium azide (Sigma-Aldrich St. Louis, MO). The slides were then incubated at 4ºC overnight with the following primary antibodies: F4/80 (5 ug/mL, rat, anti-mouse, Cat# ab6640, Cambridge, MA), iNOS (0.5 ug/ml, rabbit, anti-mouse, Cat# ab15323, Abcam, Cambridge, MA), CD206 (5 µg/mL, mouse, anti-mouse, Cat# ab8918, Abcam, Cambridge, MA), and CD163 (4.65 ug/mL rabbit, anti-mouse, Cat# ab182422, Abcam, Cambridge, MA). Primary antibodies were conjugated to Alexa Fluor 488 nm anti-rat raise in goat (Abcam, Cambridge, MA) and 488nm and 594 nm for anti-rabbit raised in goat or anti-mouse raise in goat (Thermo-Scientific, Waltham, MA).

### *5.3.6. Image Analysis*

All Images from the in vivo work were taken using a Keyence microscope (model BZ-X710, Keyence, Osaka, Japan) at 10x and 20x. Image analysis was carried out using ImageJ (National Institute of Health Rockville, MD), or by the manufacture's software. For immunohistochemistry analysis, the regions of interests (ROI) were define within the tissue surrounding and distal the amputation site of the P2 bone. Histological and immunohistochemistry analysis used 20X images. Three to five 20x images takes within the ROI were taken as a representative sample of the tissue and used for analysis. For immunohistochemistry analysis, the total area of the fluorescent signal was calculated and then normalized to total 4',6-diamidino-2-phenylindole (DAPI) area (i.e. % Counted Cell Area = (Positive Fluorescent Signal of Antibody in ROI)/ (Total Area of DAPI in ROI)).

### *5.3.7. Statistical Analysis*

ANOVA statistical analysis followed by a student's t-test was performed to determine statistical significance of the different sub populations. This process was accomplished using the data analysis package added to excel (Microsoft, Seattle, WA). All trials, unless otherwise indicated, had at least a population (N) of 4. Statistical significance was rated at $p<0.05$, 0.01, and 0.001 and this is indicated in the figures by one, two, and three stars, respectively.

## 5.4. Results

### *5.4.1. In Situ Composite Hydrogel Assessment and Surgical Technique*

*In situ* assessment was carried out to confirm the technical ability for the composite hydrogel design to achieve spatial delivery before *in vivo* use. This included retention of the physical particles in the hydrogel and effective delivery of the two cytokines. Physical entrapment was assessed by a release study. Only after centrifuging the collected solution at 24 hours and re-suspending at a concentration 1/10 the initial volume was there a noticeable concentration of particles observed with the hemocytomer (Figure 5.1)**.** This result indicated that while there was some release of the entrapped particles, the majority of the encapsulated particles stayed in the hydrogel, with the observed release particles most likely from the surface of the hydrogel.

Release and loading efficiency studies on the IL-4 absorbed particles and composite hydrogels confirmed a loading efficiency of around 30% of the 10 ug/mL of IL-4 to the loaded 10 mg SP/mL solution with a release of at 11% to 20% of its loaded amount (about 120 ng/mL) over the first two weeks of release, most within the first three days. This correlates to the typically observed burst release of any unbound IL-4 from the surface of the particles. In the composite release studies, the amount of bulk loaded IFNy and IL-10 released were at values around 42% and 30%, with no difference between the control and composite loaded hydrogel groups. The release IL-4 amount was detected around 2.5% load, which indicated that most of the lL-4 remained in the hydrogel itself.  Taken together, the particles themselves were able to load, release, and absorbed concentrations of IL-4 that are biologically effective, and the cytokine but for the most part remains in the hydrogel and does not impact the bulk release of a given

compound. These results verify the desired traits that is required to be utilized in vivo. Two different minute boils (mb) of silk were assessed to see if changes in boiling time (a processing step in silk material generation) would affect the release. As seen in Figure 5.1 did not have any effect on release and so moving forward used only the 60 mb particles

Reattachment involved modifying the previously reported surgical technique used with this device to include an additional attachment and removal step. During reattachment it was observed that the hydrogel from the first insert remained attached to the wound-bed upon removal. This could have been removed, but it was decided that by leaving the initial hydrogel attached to the wound-bed with a new hydrogel placed on top that the transition between polarization states might be more gradual. Overall, this added an additional tunable option to treatment that could use taken advantage of in future work.

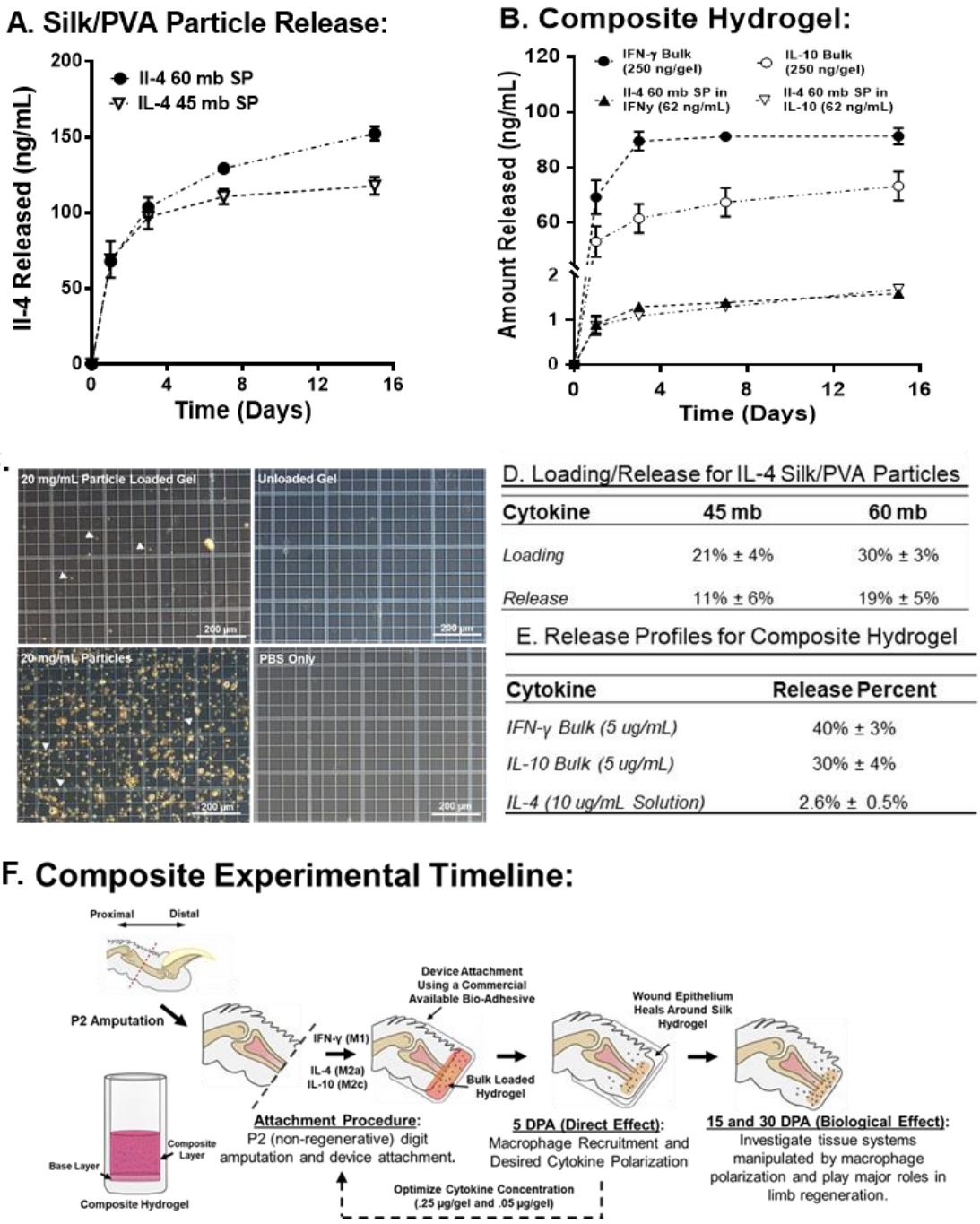


**Figure 5.1. *In Situ* Assessment of the Composite Hydrogel and Experimental Design**. **A.** Release profile of the composite hydrogel. **B.** Release profile of the Silk/PVA particles. **C.** Representational images from the particle release studies. **(D – E).** Table that summarizes the release and loading efficacies of the silk particles and composite hydrogels. **F.** Composite experimental design schematic.

*5.4.2. Reattachment In Vivo Results*

Histologically differences were hard to discern with the exception of the IL-10 to IL-4 and sham animal groups. The IL-10 to IL-4 animals showed an increase in new tissue growth (seen in Figure 5.2.A and Supplementary Figure 5.1) as well as hydrogel invasion (Supplementary Figure 5.1) at 5 DPA.

The treatments were evaluated for changes in macrophage recruitment and polarization. For macrophage recruitment the macrophage marker F4/80 and general leukocyte marker CD45 were used. Presented in Figure 5.2, the reattachment alone statistically altered the expression of both markers with a statistically significant increase in F4/80 and statistically significant decrease in CD45 compared to the no device group. Regardless, with the exception of the IFNy to IL-4 group, all cytokine treated animals showed a significant increase in the expression of both markers compared to the no device control. In comparison to the sham control, all cytokine reattachment treatments showed a statistically significant increase or decrease in expression, with the exception of IFNy to IL-4 for F4/80. IFNy to IL-4 had lower expression in both F4/80 and CD45 compared to the inverse IL-4 to IFNy, while IL-10 to IL-4 and its inverse IL-4 to IL-10 did not. Finally, IFNy to IL-4, which is the treatment that followed the same cytokine profile seen in traditional wound healing, showed similar expression of CD45 and F4/80 to the no device control group.

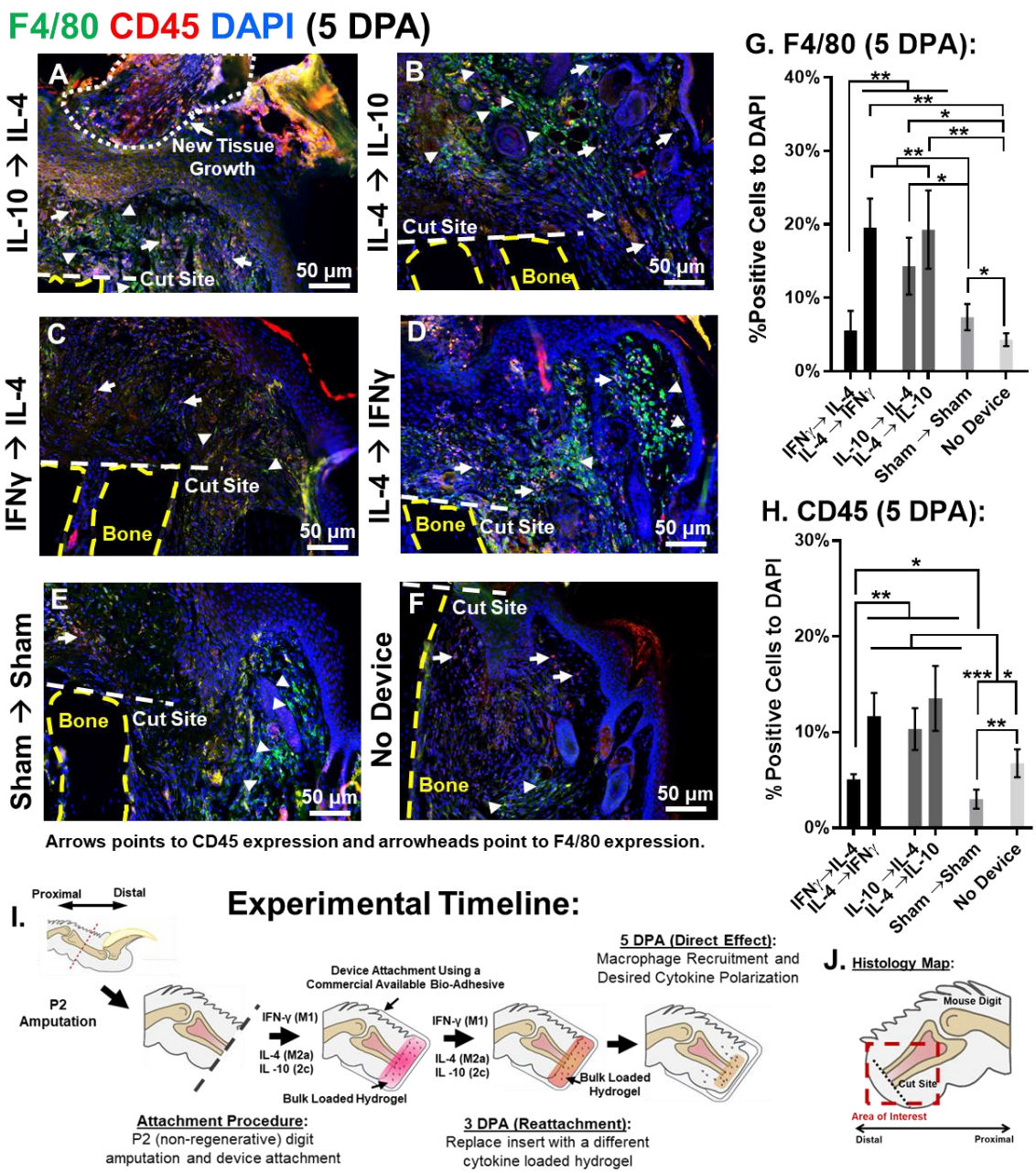
F4/80 CD45 DAPI (5 DPA)
A
New Tissue Growth
Cut Site
50 µm
IL-10 → IL-4
B
Cut Site
Bone
50 µm
IL-4 → IL-10
C
Cut Site
Bone
50 µm
IFNγ → IL-4
D
Bone
Cut Site
50 µm
IL-4 → IFNγ
E
Bone
Cut Site
50 µm
Sham → Sham
F
Cut Site
Bone
50 µm
No Device
Arrows points to CD45 expression and arrowheads point to F4/80 expression.
G. F4/80 (5 DPA):
%Positive Cells to DAPI
40%
30%
20%
10%
0%
IFNγ → IL-4
IL-4 → IFNγ
IL-10 → IL-4
IL-4 → IL-10
Sham → Sham
No Device
H. CD45 (5 DPA):
% Positive Cells to DAPI
30%
20%
10%
0%
IFNγ → IL-4
IL-4 → IFNγ
IL-10 → IL-4
IL-4 → IL-10
Sham → Sham
No Device
I.
Experimental Timeline:
Proximal
Distal
P2 Amputation
Device Attachment Using a Commercial Available Bio-Adhesive
IFN-γ (M1)
IL-4 (M2a)
IL -10 (2c)
Bulk Loaded Hydrogel
5 DPA (Direct Effect):
Macrophage Recruitment and Desired Cytokine Polarization
IFN-γ (M1)
IL-4 (M2a)
IL -10 (2c)
Bulk Loaded Hydrogel
Attachment Procedure:
P2 (non-regenerative) digit amputation and device attachment
3 DPA (Reattachment):
Replace insert with a different cytokine loaded hydrogel
J. Histology Map:
Mouse Digit
Cut Site
Area of Interest
Distal
Proximal

**Figure 5.2. Macrophage Recruitment for Reattached Animal Group at 5 DPA. (A – F).** Immunohistochemistry of the different reattachment groups for the macrophage marker F4/80 and general leukocyte marker CD45. **G.** Quantification of F4/80 expression. **H.** Quantification for CD45 expression. **I.** Experimental design and time-line for the reattachment animal groups. **J.** Histological map representing the area of interest of immunohistochemistry images presented in A – F. Statistical Analysis was performed using ANOVA single factor followed by a student's t-test to compare groups. Significance to the control group is measured as following p-values * ≤ 0.05, ** ≤ 0.01, and *** ≤ 0.001. Arrows points to CD45 expression and arrowheads point to F4/80 expression. Population of each group is N ≥ 4.

Macrophage polarization was assessed using the IHC markers iNOS, CD206, and CD163 for M1, M2a, and M2c respectively. As presented in Figure 5.3, the results indicate that reattachment induced an increase in CD163 expression regardless of treatment, as seen with the increased expression of CD163 in the sham group. IL – 4 to IFNy resulted in an increase in iNOS and CD163. Conversely, the inverse treatment, IFNy to IL-4, had the opposite effect with a statistically significant decrease in iNOS and CD163 expression compared to all other groups except the No Device group. In this regard, IFNy to IL-4 showed no significant difference in expression in any of the polarization markers to the no device group. There was a statistically significant difference in expression of all the polarization markers between the IFNy to IL-4 group compared to the IL-4 to IFNy group. Finally, IL-10 to IL-4 showed statistically higher expression of CD206 compared all other groups. Other than that difference, IL -10 to IL – 4 and its reverse treatment of IL-4 to IL-10 demonstrated no difference in polarization marker expression between the two.

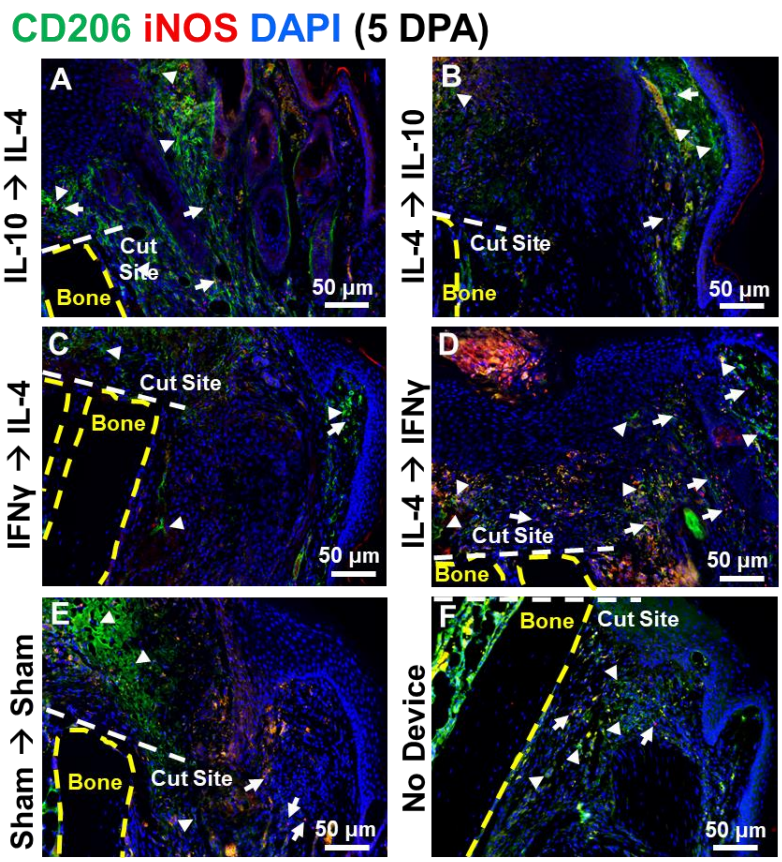


Arrows points to iNOS expression and arrowheads point to CD206 expression.

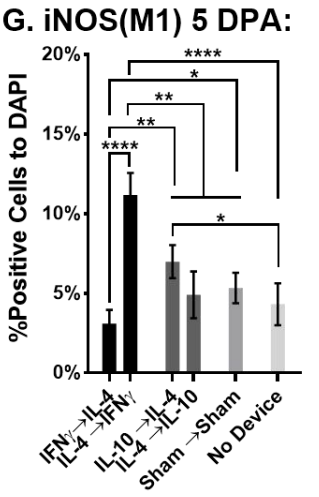


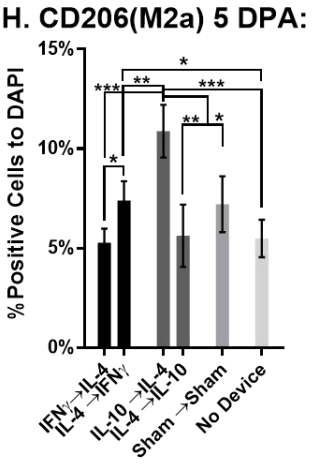


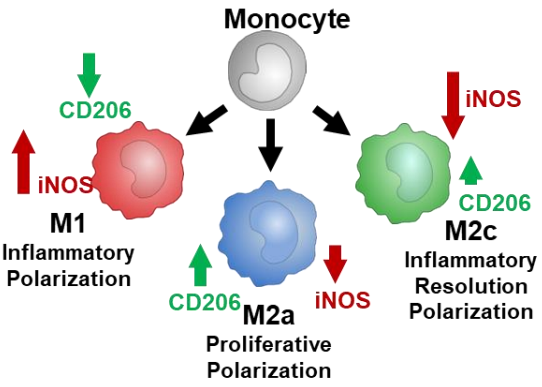


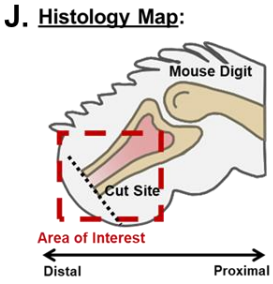

**Figure 5.3. Macrophage Polarization Reattached Animal Group at 5 DPA. (A – F).** Immunohistochemistry of the different reattachment groups for M1 polarizing marker iNOS (red) and the M2a polarizing marker CD206 (green). **G.** Quantification of iNOS expression. **H.** Quantification for CD206 expression. **I.** Polarization expression map. **J.** Histological map representing the area of interest of immunohistochemistry images presented in A –F. Statistical Analysis was performed using ANOVA single factor followed by a student's t-test to compare groups. Significance to the control group is measured as following p-values * ≤ 0.05, ** ≤ 0.01, and *** ≤ 0.001. Arrows points to CD45 expression and arrowheads point to F4/80 expression. Population of each group is N ≥ 4.

In conclusion, the results in the sham group demonstrated that the act of reattachment alone altered macrophage and leukocyte recruitment and an increase in CD163 expression. The results demonstrated that in IFNy and IL-4 treatments there was an order dependence, with differences in macrophage recruitment and polarization. In particular, IFNy to IL-4 treatment and the reverse IL-4 to IFNy demonstrated an inverse trend of iNOS and CD163 expression compared to all device wearing animals. The IFNy to IL-4 group mimicked the same cytokine profile as the typical wound healing cycle. This treatment recreated the temporal transition seen natively well enough to have similar expression in both macrophage recruitment and polarization as with the no device control group. Finally, while no difference was observed between IL-10 to IL-4 and its inverse IL4 to IL-10, IL-10 to IL-4 showed a statistically significant increase in CD206 expression compared to all other groups.

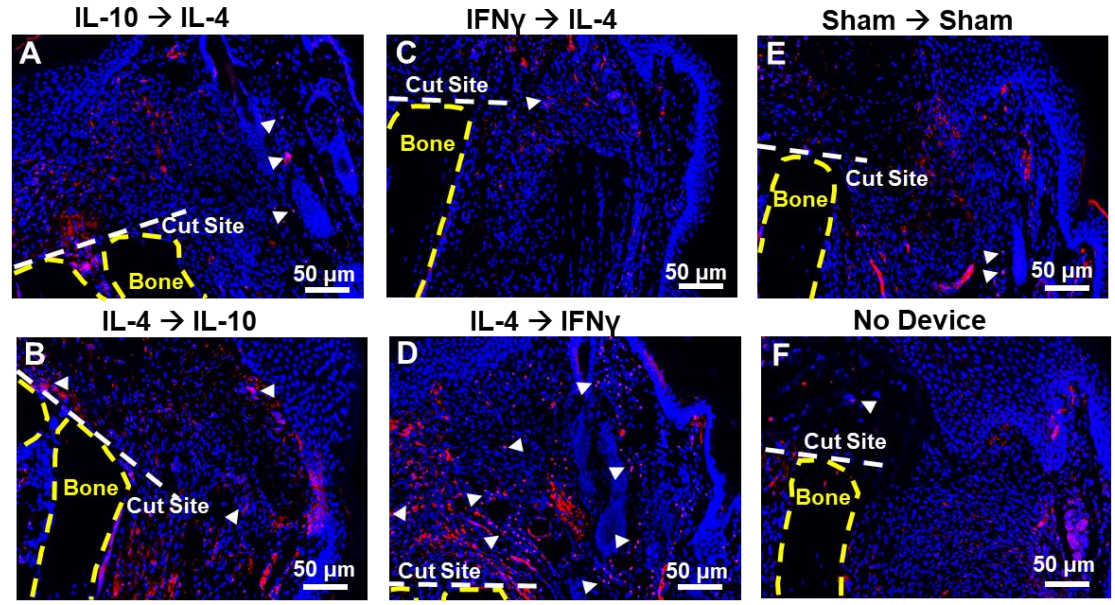
CD163 DAPI (5 DPA)
IL-10 → IL-4
IFNγ → IL-4
Sham → Sham
A
C
E
Cut Site
Bone
50 µm
IL-4 → IL-10
IL-4 → IFNγ
No Device
B
D
F

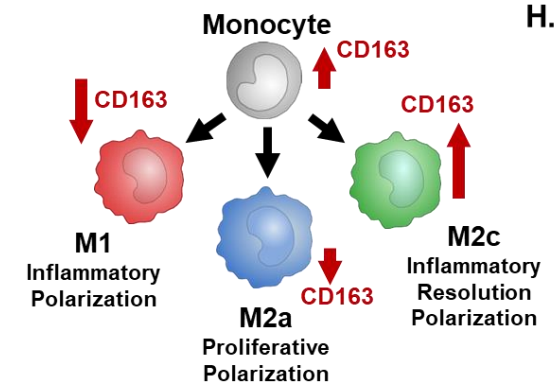
G. Polarization Expression Map:
Monocyte
CD163
M1
Inflammatory
Polarization
M2a
Proliferative
Polarization
M2c
Inflammatory
Resolution
Polarization

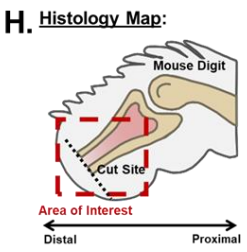
H. Histology Map:
Mouse Digit
Cut Site
Area of Interest
Distal
Proximal

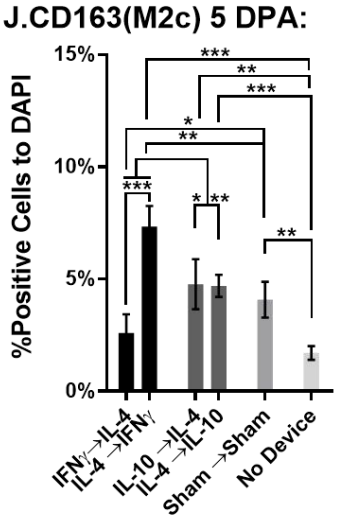
J.CD163(M2c) 5 DPA:
%Positive Cells to DAPI
15%
10%
5%
0%
IFNγ→IL-4
IL-4→IFNγ
IL-10→IL-4
IL-4→IL-10
Sham→Sham
No Device

**Figure 5.4. Macrophage M2c polarization in the Reattached Animal Group at 5 DPA. (A – F).** Immunohistochemistry of the different reattachment groups for M2c polarization marker CD163. **G.** Polarization map. **H.** Histological map representing the area of interest of immunohistochemistry images presented in A –F **J.** Quantification of CD163 expression. Statistical Analysis was performed using ANOVA single factor followed by a student's t-test to compare groups. Significance to the control group is measured as following p-values * ≤ 0.05, ** ≤ 0.01, and *** ≤ 0.001. Arrows points to CD45 expression and arrowheads point to F4/80 expression. Population of each group is $N \geq 4$.

*5.4.3. Composite In Vivo Results*

The composite hydrogel group histology showed differences to its bulk loaded counterparts in the relationship between the treatment given versus incorporation and wound closure at 5 DPA (Figure 5.5). The typical sham hydrogel group had little hydrogel incorporation into the wound-bed at 5 DPA. In contrast, 5/6 animals in the composite sham hydrogel group showed both increased hydrogel incorporation and cell invasion into the hydrogel (Figure. 5.4.). Histology for the cytokine treated groups, both the IL-10 comp and IFNy comp displayed enhanced wound closure and decreased hydrogel incorporation compared to their bulk counterparts and the sham composite group.

For macrophage recruitment, with the exception of the composite sham group for CD45 expression, all animals that received a composite hydrogel treatment had higher expression of CD45 and F4/80 compared to the no device group (Figure 5.4.). IFNy and IL-10 comp showed statistically significant increased F4/80 expression compared to the sham group and the IFNy comp showed statistically significant increase in CD45 expression compared to the sham comp (Figure. 5.4). In comparison with the bulk counterparts, the only difference observed for macrophage recruitment was a significant decrease in IFNy comp in the CD45 and a statistically significant increase in F4/80 for the sham comp. These results indicated that the composite gel increased macrophage recruitment in comparison with the neat silk hydrogel, but the drug loaded composite hydrogels did not improve macrophage recruitment compared to their bulk loaded counterparts.

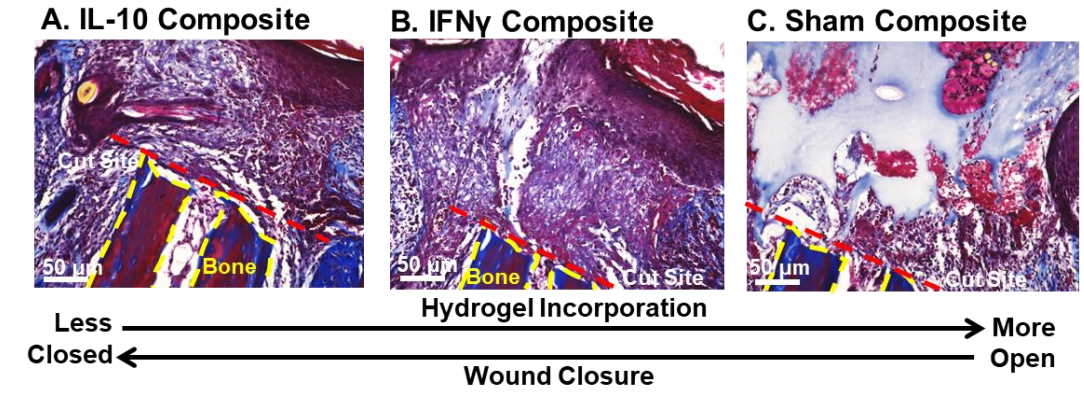


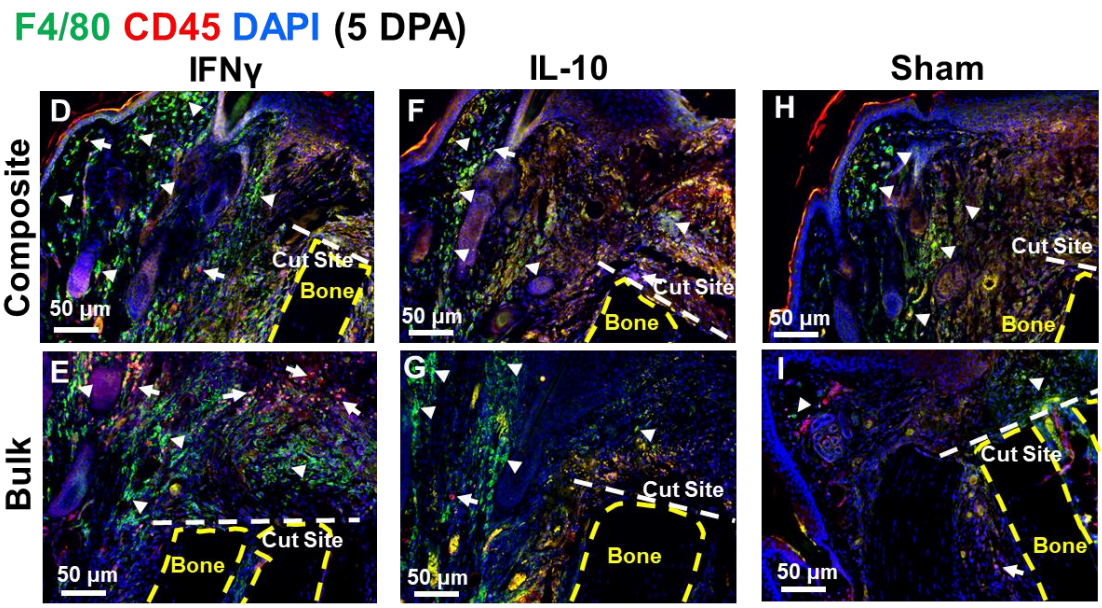


Arrows points to CD45 expression and arrowheads point to F4/80 expression.

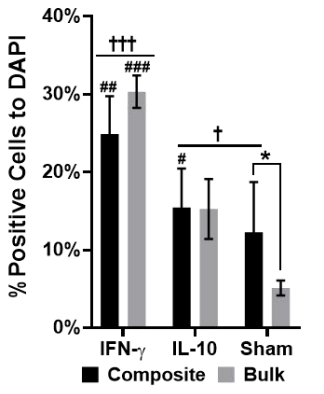


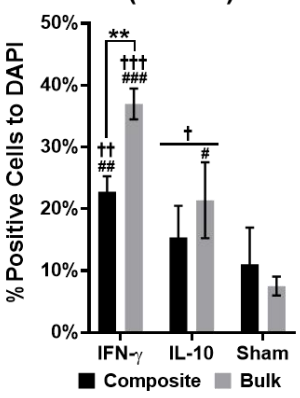


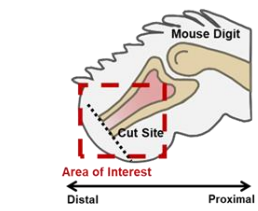


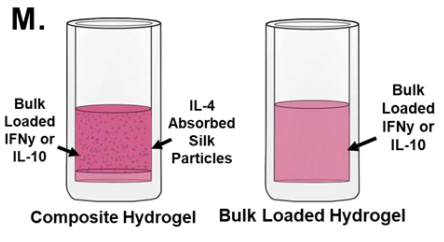

**Figure 5.5. Macrophage Recruitment and Histological Differences for Composite** Hydrogel Treatment. **(A – C).** Masson Trichrome images that represents the typically observed morphology in the three composite hydrogel groups. **(D – I).** Immunohistochemistry of the different reattachment groups for the macrophage marker F4/80 and general leukocyte marker CD45. **J.** Quantification of F4/80 expression. **K.** Quantification for CD45 expression. **L.** Histological map representing the area of interest of immunohistochemistry images presented in D -I. **M.** Schematic of the two hydrogel treatments used in the composite animal trials. Statistical Analysis was performed using ANOVA single factor followed by a student's t-test to compare groups. Significance to the control group is measured as following p-values * ≤ 0.05, ** ≤ 0.01, and *** ≤ 0.001. † is statistical significance compared to No Device group, p-values are † ≤ 0.05, †† ≤ 0.01, and ††† ≤ 0.00.1.# is statistical significance compared to the Sham group, p-values are # ≤ 0.05, # ≤ 0.01, and # ≤ 0.00.1**.** Arrows points to CD45 expression and arrowheads point to F4/80 expression. Population of each group is N ≥ 4.

In terms of macrophage polarization, the composite hydrogel alone resulted in an increase in iNOS expression (Figure 5.5.). Though still statistically higher than the sham comp group, IFNy comp demonstrated a statistical decrease in iNOS expression compared to the IFNy bulk loaded counterpart. Additionally, IFNy comp showed a statistical increase in both CD206 and CD163 expression in comparison to bulk loaded IFNy and both the sham and no device control groups (Figure. 5.5.). This result suggests that the IFNy composite group demonstrated an altered polarization profile that cannot be attributed to the bulk loaded IFNy or the composite hydrogel alone. The IL-10 comp group resulted in increases in all polarization markers compared to the two control groups. The only significant difference that the IL-10 comp group had to the bulk loaded IL-10 group was a decrease in CD206 expression. This result indicated that whatever difference was observed in the IL10 composite group was due to the bulk loaded treatment and not was not due any additional benefits from the composite treatment.

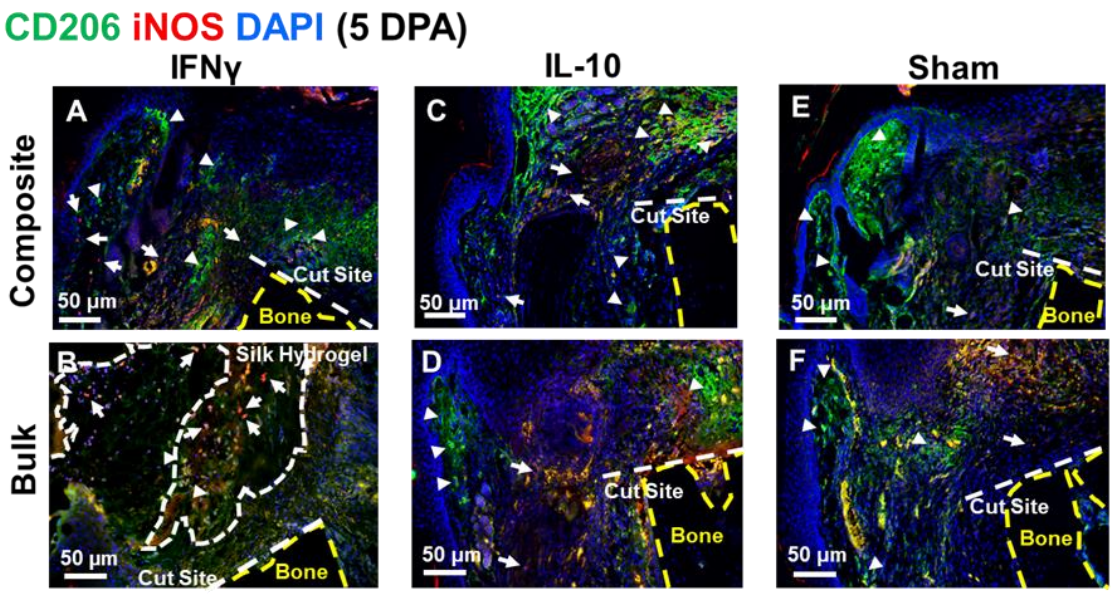


Arrows points to iNOS expression and arrowheads point to CD206 expression.

H. Histology Map:

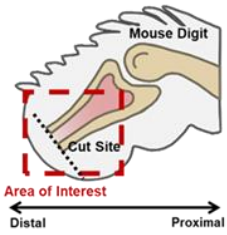


I. iNOS(M1) 5 DPA:

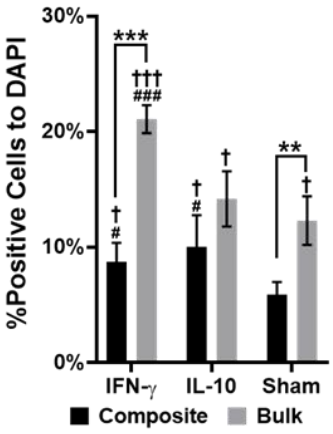


J. CD206(M2a) 5 DPA:

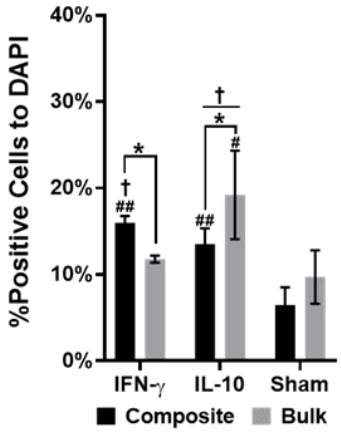

**Figure 5.6. Macrophage Polarization M1 and M2a for the Composite Animal Group at 5 DPA. (A – F).** Immunohistochemistry of the different reattachment groups for M1 polarizing marker iNOS (red) and the M2a polarizing marker CD206 (green). **G.** Quantification of iNOS expression.**H.** Histological map representing the area of interest of immunohistochemistry images presented in A –F. **I.** Quantification for CD206 expression. **J.** Polarization expression map. Statistical Analysis was performed using ANOVA single factor followed by a student's t-test to compare groups. Significance to the control group is measured as following p-values * ≤ 0.05, ** ≤ 0.01, and *** ≤ 0.001. † is statistical significance compared to No Device group, p-values are † ≤ 0.05, †† ≤ 0.01, and ††† ≤ 0.00.1.# is statistical significance compared to the Sham group, p-values are # ≤ 0.05, # ≤ 0.01, and # ≤ 0.00.1**.** Arrows points to CD45 expression and arrowheads point to F4/80 expression. Population of each group is N ≥ 4.

In summary, the neat composite hydrogel increased hydrogel incorporation and cell infiltration. IHC showed that this resulted in an increase in macrophage recruitment and decrease in iNOS expression. The composite treatments did not significantly alter macrophage recruitment, but the IFNy composite hydrogel did alter the polarization profile with decreased iNOS expression and increased CD206 and CD163 expression. Overall, the composite hydrogel treatment altered the initial macrophage immune profile.

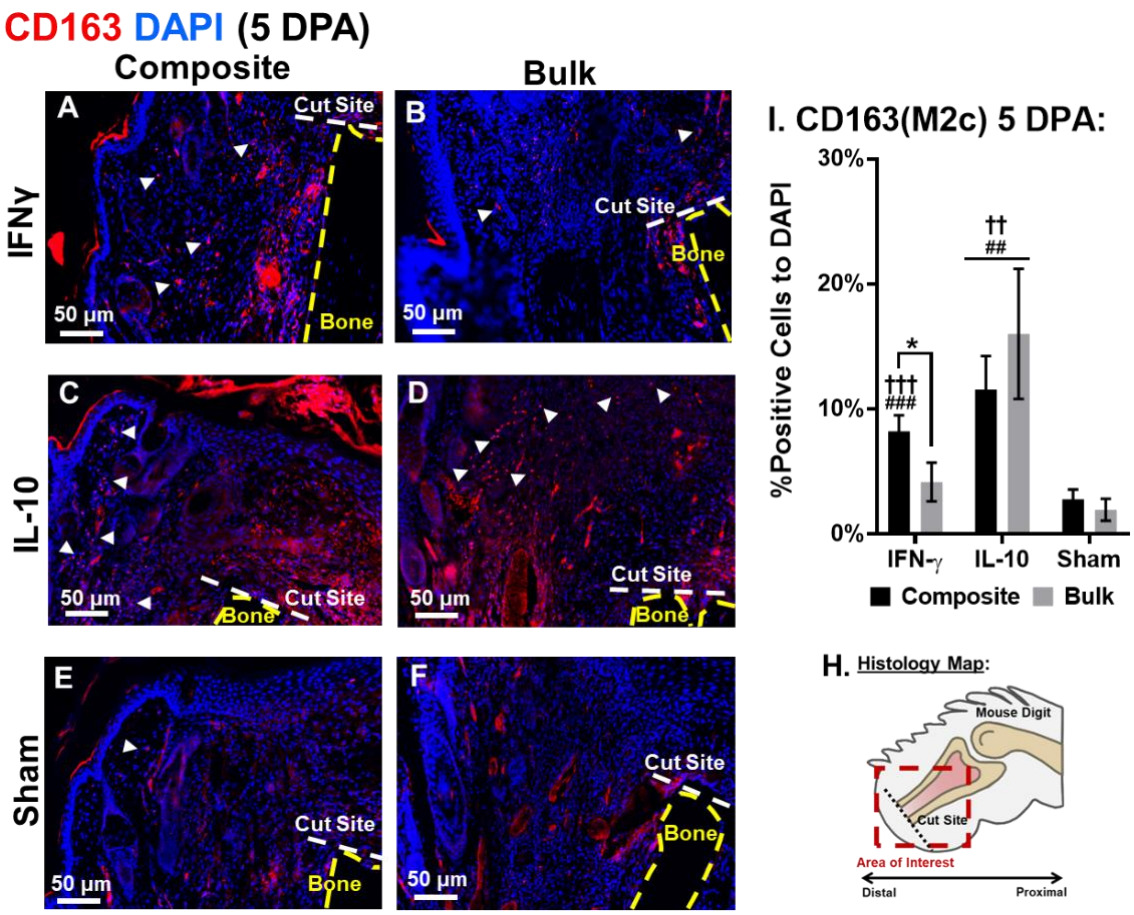


**Figure 5.7. Macrophage M2c polarization in the Composite Animal Group at 5 DPA. (A – F).** Immunohistochemistry of the different reattachment groups for M2c polarization marker CD163. **G.** Polarization map. **H.** Histological map representing the area of interest of immunohistochemistry images presented in A –F **J.** Quantification of CD163 expression. Statistical Analysis was performed using ANOVA single factor followed by a student's t-test to compare groups. Significance to the control group is measured as following p-values * ≤ 0.05, ** ≤ 0.01, and *** ≤ 0.001. † is statistical significance compared to No Device group, p-values are † ≤ 0.05, †† ≤ 0.01, and ††† ≤ 0.00.1.# is statistical significance compared to the Sham group, p-values are # ≤ 0.05, # ≤ 0.01, and # ≤ 0.00.1**.** Arrows points to CD45 expression and arrowheads point to F4/80 expression. Population of each group is N ≥ 4.

## 5.5. Discussion

The ability to modulate the amputation site dynamically is essential to study limb regeneration in the mouse digit tip model. Current techniques utilized to study limb regeneration are incapable of providing dynamic control when stimulating the amputation site. Limb regeneration is a dynamic event and its success relies on a set of spatially and temporally fluid cues from the wound-bed environment and cell population[21,89]. Macrophage polarization  is the reaction to the environment; which is changing as the wound transitions from the injured to healed state[21,104]. It is unclear if it necessary to modulate initial steps or the full temporal and spatial spectrum that a macrophage experiences in order to characterize their role in limb regeneration. To this end we implemented two approaches to tackle the challenge of dynamic delivery and were successful in modulating macrophage recruitment and polarization in a tunable manner.

### *5.5.1. Benefits of the Hydrogel Device and Resultant Tunability from In Situ Characterization*

Tunability of stimulation for *in vivo* systems is almost impossible to achieve outside of selective skin injury models[105,106]. Even with those systems, the control of delivery of the therapeutic compound is still limited[3]. For most studies to be successful the material or method of stimulation needs to be injected or implanted into the animal or risk premature removal by animal tampering[37,107]. This type of experimental design limits the ability to tune the treatment during the experiment. The design of our wearable bioreactor allows for secure attachment of the device to the hind paw of the mouse. This robust method allows us to focus our work on implementing material designs to modulate the wound bed dynamically.

In the reattachment work, temporal control was achieved by characterizing the bulk loaded cytokine release profile over time in chapter 4, and optimizing surgical techniques with the hydrogel. By characterizing the release profile, we were able to design an experimental timeline that let us delivery sequential doses of two cytokines that maximized dose efficacy while the wound-bed was still open. Choosing a hydrogel system with optimized surgical techniques presented the option to leave or remove the partially incorporated initial hydrogel treatment. In this study we decided to leave the initial hydrogel and attached the new insert over this. This most likely provided a more gradual transition between the two polarization treatments, mimicking the typically observed wound healing cytokine profile (IFNy to IL-4) and achieving similar macrophage recruitment and polarization states as in our no device control.

For the composite hydrogel it was necessary to verify that the silk particles were retained in the hydrogel, and that the resultant hydrogel was able to deliver the two cytokines in a spatially controlled manner (i.e., one remained in the hydrogel, while the other was released). The results demonstrated that the hydrogel was able to retain the silk particles and the particles were able to deliver effective doses of cytokine, with the composite hydrogel able to release one cytokine in the bulk while retaining the other**.** This result confirmed the technical capability of the composite hydrogel, and also provided information and a means to optimize future designs to improve *in vivo* results.

*5.5.2. Temporal Delivery Allows for Manipulation of the Cytokine Profile and Alters Macrophage Recruitment and Polarization.*

In limb regeneration, the role of macrophages is time dependent, with the most critical functions occurring right after amputation[16]**.** Polarizing macrophages with a sequential switch of polarization state is a commonly used technique to study macrophage functions *in vitro*[108]. However, *in vitro* assays cannot recapitulate the complex and diverse microenvironment presented *in vivo*[21]. Like-wise many of the animal injury models used in prior studies lack the control needed to study macrophage polarization dynamically[20]**.** The reattachment work presented in this chapter allowed us to perform a temporal polarization switch *in vivo* with the tunability akin to the related *in vitro* experiments.

Two cytokine treatment pairs were selected; IFNy and IL-4 were used to explore the effect of inverting the typically observed wound healing cytokine profile[89]. The IL-10 and IL-4 pair was chosen to observe what would occur if the initial inflammation step was removed, and to recapitulate a cytokine profile observed during development, which consists of a reduced M1 stage in an environment that is high in IL-10[109]**.** IFNy and IL-4 were order dependent. IFNy to IL-4 treatments had the opposite effect to IL-4 to IFNy in macrophage recruitment and expression of the polarization markers iNOS and CD163. The upregulation of both iNOS and CD163 would seem counter-intuitive given that iNOS is expressed only in the M1 state and is down regulated when a macrophage is polarized to M2a and M2c[76,90,91]. Additionally, CD163 is repressed in the presence of IFNy[91]. While this is true, most of the results were obtained with *in vitro* experiments. A

typical wound-bed tends to exhibit heterogeneous macrophage polarization which varies based on location in the tissue and the type of tissue[76,110].

One possibility is that IFNy effect might be attenuated or altered, given that it was applied at a later time-point with the initial IL-4 hydrogel still attached. In Chapter 4, we observed that IL-4 treated animals showed increased recruitment of macrophages that arrived to the amputation site expressing CD163. Only when these macrophages entered the newly grown tissue or were close to the embedded hydrogel did they lose this expression. The initial IL-4 treatment promoted an influx of CD163 positive macrophages. With the addition of the IFNy, this could cause these CD163 rich macrophage to switch polarization state and lose expression, or recruit a new population of iNOS producing M1 macrophages[76]. Histologically both CD163 and iNOS positive cells were observed in the IL-4 to IFNy animal group with iNOS expression highest distally to the cut site. CD163 was expressed in all areas of the tissue, but the density of expression was higher proximal to the cut site. Both theories are possible with the current information and additional time points would be needed to clarify mechanisms.

Results with the IFNy to IL-4 treatment showed levels of expression for both the macrophage recruitment and polarization markers similar to the no device control. This treatment mimics the typically observed M1 to M2a shift observed in native wound healing. For the IFNy to IL-4 animal treatment to have similar expression in both the macrophage and polarization markers to the no device wearing animal group, effective delivery in a timely manner was required. The results indicate that we were able to

achieve the time-dependent delivery needed to mimic the native wound healing event using the reattachment method with our wearable bioreactor.

The other pair of cytokines used was IL-10 to IL-4. Histologically, when delivered in the order of IL-10 to IL-4 this demonstrated cell invasion witnessed in single IL-10 bulk delivery combined with the observed tissue growth that results from the single delivery of IL-4 reported in Chapter 3. In contrast, the inverse showed little forward tissue growth, but increased wound epithelium (Supplementary Figure 5.1). This make sense since CD163 would resolve the initial immune response and allow for cell infiltration, and the following IL-4 treatment would result in enhanced tissue growth. Immunohistochemistry presented little difference with the exception of an increase in CD206 expression in the IL-10 to IL-4 group. This group was the only group to show a statistically higher expression of this marker to both the controls. This result appears to be order dependent, with the inverse showing no increase of CD206 expression. This result indicates that even with the initial IL-4 hydrogel still attached to the animal, sequential IL-10 would not heighten CD206 expression.

*5.5.3. Composite Hydrogel was able to attenuate IFNy effect on the system*

The macrophage population at an injury site is heterogeneous, with the polarization state location dependent. Limb regeneration has also demonstrated spatial dependent aspects that would apply to the initial immune response. As in the case of temporal control, *in vitro* cell and tissue models lack the complexity of the *in vivo* system, while *in vivo* lacks the control to begin to characterize this dynamic aspect of macrophage polarization[21]. To accomplish spatial control of delivery we designed a composite

hydrogel that was able to co-deliver two polarizing cytokines simultaneously, with the particle absorbed cytokine trapped in the hydrogel and the bulk loaded cytokine released in the burst.

The initial goal was to promote invasion as seen with the single treatment of either IL-10 or IFNy, and then switch the polarization state to M2a via the implanted IL-4 silk particles. However, hydrogel incorporation into the wound bed did not occur with the drug treated animals, and in fact histologically there were signs of enhanced wound closure in the drug treated animals. What is interesting to note is that the composite gel alone resulted in increased hydrogel incorporation and cell invasion into the hydrogel not seen in the neat sham hydrogel treated animals. The trend of wound closure and hydrogel incorporation for all the group was inverse to what was observed in the bulk loaded groups.

Mixed macrophage phenotypes will form a gradient of multiple polarizing cytokines[111]. This mixed signal might of lead to a wound healing response not predicted with the given cytokine treatment. The majority of the bulk loaded cytokine remains in the hydrogel. This means that the hydrogel would have both cytokines present rather than just the absorbed IL-4. It would make sense that the effect observed would either be of the bulk released hydrogel or a combination effect. Combination treatments of IL-4 and IL-10 have shown enhanced M2 polarization better than a single cytokine alone in inflammatory diseases such as osteoarthritis[79]. With this in mind the combined treatment presented with the composite hydrogel might have resulted in an enhanced M2 treatment, which accelerated wound healing. IHC showed the only statistically significant

difference between the IL-10 composite and IL-10 bulk hydrogel to be in CD206 expression. Taken together with the enhanced wound closure speed it is most likely that the IL-10 composite gel supported an enhanced M2 polarization state.

The IFNy composite treatment displayed a distinct change in the polarization profile from the IFNy bulk animal group. IFNy comp displayed a sharp decrease in iNOS, and statistically significant increase in CD206 and CD163 expression compared to the bulk loaded IFNy group. Both iNOS and CD163 expression were observed mostly proximal or at the cut site. The location of iNOS expression contrasted with what was observed in the IFNy bulk loaded hydrogels where iNOS was expressed distally to the cut site. IL-4 and IFNy have a destructive effect on macrophage polarization when combined[78,79,112]**.** It would make sense that the composite hydrogel would demonstrate this effect. It also should be noted that this attenuation was location dependent with iNOS expression suppressed in the areas distal the cut site and near the hydrogel. This composite hydrogel design resulted in spatial control of a typically seen M1 result proximal the cut site and an attenuated M1 and weak M2 polarization state distal the cut site. To that end, while the initial goal was not met, this design did induce a spatially-dependent polarization profile and modulating the immune profile in a dynamic manner.

### 5.6. Conclusions

The work presented in this chapter details two new methods of dynamic drug delivery to be used with the wearable bioreactor to study limb regeneration *in vivo* in the mouse digit tip amputation model. By utilizing both the tunability that the hardware and hydrogel provide, we were able to temporally modulate cytokine delivery with reattachment and

induce location specific immune response with the composite hydrogel. The composite hydrogel and combination therapies have been pursued previously, but never in a limb regeneration context. The macrophage polarization switch performed with reattachment is widely used *in vitro* but not performed *in vivo* as far as we know. Future work will be needed to add later time points to the overall effects beyond technical capability but this work demonstrates the technical capability for the wearable bioreactor to deliver dynamic treatments needed to study limb regeneration.

# Chapter 6: Conclusion, Future Directions, and Potential Areas of Interest

## 6.1. Conclusion and Next Steps

The purpose of this thesis was to create and optimize a wearable bioreactor for studying limb regeneration *in vivo* using a mouse digit tip amputation model. Here we demonstrated a device capable of fulfilling that goal with the additional benefit of both dynamic and static modes of stimulation. While this system has proven to be robust and effective, there are areas that need to be improved upon to allow for this device to be used to its full potential. The two areas that need to be addressed before additional projects undertaken are: 1) Expansion on the tools used to study the biological outcome, and 2) Improve degradation rate of the material. Moving beyond basic improvement, a proposed next project would be to deliver limb progenitor cells and enhancing the delivery with the immune modulating techniques developed in chapters 4 and 5.

## 6.2. Expanding Biological Analysis

Another technical area that needs to be improved on is the means to assess the biological outcomes. The presented protocols relied heavily on histology and immunohistochemistry. This alone cannot really assess what is happening biologically. The system can be easily utilized in conjunction with transgenic mice for knock in and knock out experiments. In addition, other means of assessment need to be applied such as genomic analysis or *in vitro* assessment to confirm and better understand the observed phenotypic changes.

### 6.3. Tunable Degradation of the Silk Hydrogel Insert

One area of importance that should be addressed is hydrogel degradation. If the hydrogel does not degrade over time, then this will have a long term impact on the regenerative outcome of the system. Typically, covalently linked hydrogels do not degrade *in vivo* at a rate that avoids encapsulation and exclusion from the body. Immune modulation can help improve initial cell and tissue incorporation, however this can be improved. Recent work has shown that altering the concentration of HRP and $H_2O_2$ can help reduce the cross-linking density, however this has already been implemented in the presented work. One area of particular interest would be to incorporate cleavable peptide links into the hydrogel. These linkers would be cleaved with enzymes that are already present in the mouse system (e.g. MMPs). This would provide a powerful tool given that the enzyme chosen could be upregulated at a certain time of the wound healing process, thus potentially providing some temporal control over degradation

### 6.4. Enhanced Limb Progenitor Cell Delivery by Immune Modulation

Limb progenitor (LP) cells collected from the embryonic limb bud are capable of patterning limbs when engrafted onto chicks and adult frogs[35,113]. This has been attempted before in mice with minimal success, most likely due to a delay in attachment[26]. Proof of concept work has already shown that our system is capable of delivering limb progenitor cells to the amputation site (Figure 6.1). With improved scaffold design and a more expansive set of tools to assess the outcome, our device can be used to study limb progenitor cells in a mouse digit amputation model.

Past work in both delivery of LP cells in xenopus, as well as cell delivery in tissue engineering, has shown that the interaction of the delivered cells with immune cells was one of the major factors in effective delivery. In xenopus, the animals had to be thymectomized to allow for successful incorporation into the amputation site[26]. Additionally, research in biomaterial based cell delivery has shown that the cross-talk between delivered stem cells and macrophages had a pro-healing effect. Delivered stem cells in a m infracted model showed that the delivered cells recruited and polarized the local macrophage population to a M2 state via secretion of IL-10[114]. Additional work has shown that M2 macrophages secrete growth factors (e.g. VEGF, TGFB1, IL-10) that improve delivered stem and progenitor cell viability while M1 macrophage cytokine secretion (IL-1b, IL-6, TNF-a) inhibited proliferation and viability of the delivered progenitor and stem cells[114]. Finally, work done in which delivered stem cells in a TGF-B1 fibrin cardiac *in vivo* showed increased migration into the tissue in correlation with crosstalk between the local immune population and the delivered cells[114]. If this crosstalk is characterized, then it could be manipulated to enhance the final outcome. *The goal of the proposed future work is to characterize the cross-talk between the immune system and limb progenitor cells in a P2 amputation model. Following this we then propose applying temporal delivery of cytokines to polarize the tissue macrophage population prior to cell delivery and see if we can alter this cross-talk and improve the regenerative outcome*. ***We hypothesize that if we modulate the immune profile prior to delivery we will create a pro-regenerative environment more akin to what is witnessed during development, and enhance the overall regenerative cross-talk between the delivered cells and endogenous cell population.*** The proposed work would be accomplished in three aims.

**Aim 1**: Use the wearable bioreactor to deliver limb progenitor cells and characterize the resultant immune and regenerative profile. The purpose of this aim is to establish the baseline impact that the limb progenitor cells have on the system in immune response and changes in biological outcomes. This aim would follow earlier work and apply a more rigorous method of biological characterization for both the initial 5 DPA time point with intermediate and long term time-points of 15 DPA and 1 month, respectfully. In addition to histological and immunohistological analysis, this aim would also assess changes at the genomic level with qPCR. The markers at 5 DPA would focus on immune responses, then transition to more regenerative associated biomarkers such as ECM components, cartilage, bone, nerve, and vasculature markers. This more in-depth profile will then be compared to the controls and a baseline library can be established. The method of delivery has been effective and qPCR analysis protocols have been established by other labs. However, if this cannot be done other method of analysis can be performed such immunohistochemistry.

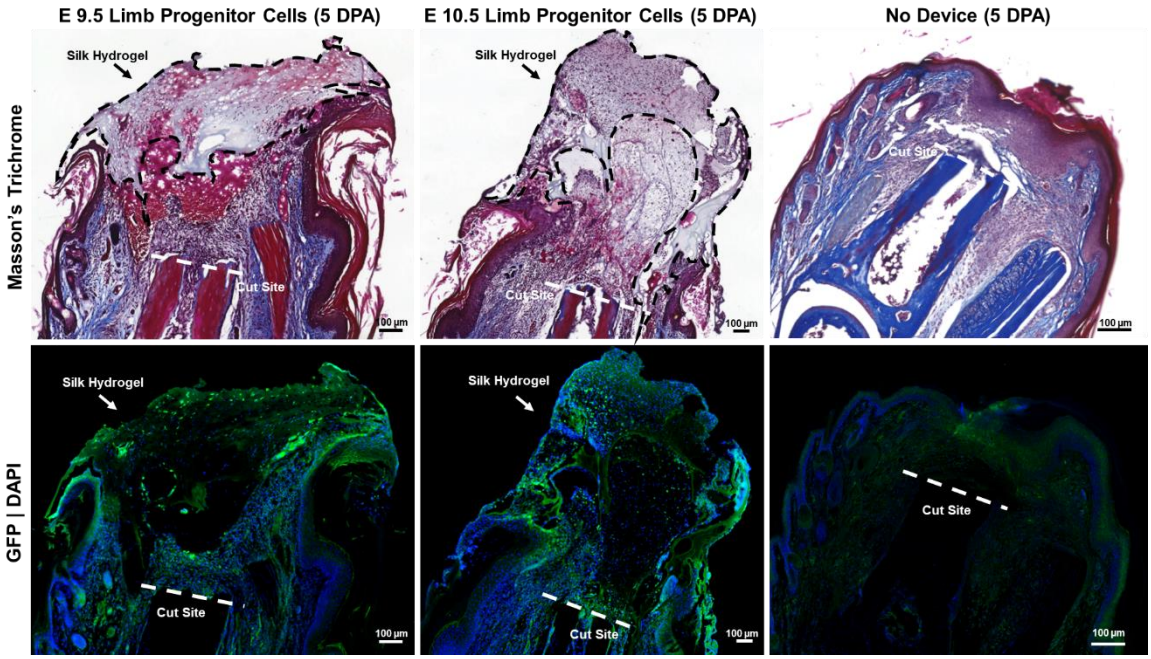


**Figure 6.1. Preliminary data of Limb Progenitor Cell Delivery (collected at embryonic stages E9.5 and E10.5) at 5 DPA**. Masson trichrome stains show that the cell loaded hydrogels have enhanced interaction with the tissue and the immunohistochemistry shows the green fluorescence protein (GFP) labeled limb progenitor cells have been successfully delivered to the wound site.

**Aim 2:** Characterize the indirect effect of macrophage polarization on LP cells *in vitro.* If we assess how the different polarized macrophage states affect LP cells *in vitro* we can limit the number of polarization conditions attempted *in vivo*. The proposed method to accomplish this would be to isolate primary monocytes from FVB/Nj mice and polarize them *in vitro* to M1, M2a, and M2c polarization states using Interferon gamma (IFNy) for M1, interleukin 4 (IL-4) for M2a, and interleukin 10 (IL-10), respectfully. Following polarization, the media would be collected and added to culture of isolated LP cells. Time points would be taken at 24, 48, and 72 hours post media addition to assess viability of the cells and changes in expression of known limb mesenchyme markers *Meis1, Hoxa11, and Hoxa13*, and differentiation markers for cartilage Transcription factor *Sox9* (Sox9), bone marker Transcription factor *Sp7/Osterix* (Sp7), and tendon marker *Scleraxis* (Scx). Changes in viability would indicate which treatments to pursue, while qPCR would help characterize potential results seen *in vivo*. What a macrophage secretes from polarization is time and cytokine concentration dependent *in vitro*[107,108]. If all polarization media treatments prove to be lethal or have no effect upon the LP cells, then these two variables can be altered. This is acceptable since we can alter both of these conditions *in vivo* with the amount of cytokine we load in the first dose and the time between delivery of the cytokine treatment and LP, these alternative measures make sense.

**Aim 3:** Use the sequential reattachment method *in vivo* to study the effect of priming the tissue system with different macrophage polarization states has to LP cell delivery. The goal of this aim would be to use the sequential reattachment protocol established in chapter 5 and deliver a polarizing treatment followed by LP cells. With the information obtained in aims 1 and 2 of the proposed work we could assess the changes in

biological outcomes. As presented in the experimental timeline (Figure 6.2), 3 time points will be taken (5 DPA, 15 DPA, and 30 DPA) to evaluate the direct and indirect effects *in vivo*. Analysis will be carried out with the methods optimized in aim one. Potential challenges include ineffective treatments, and adverse effects to the animal or LP cells. Changes in doses and attachment times can be modulated to address these issues.

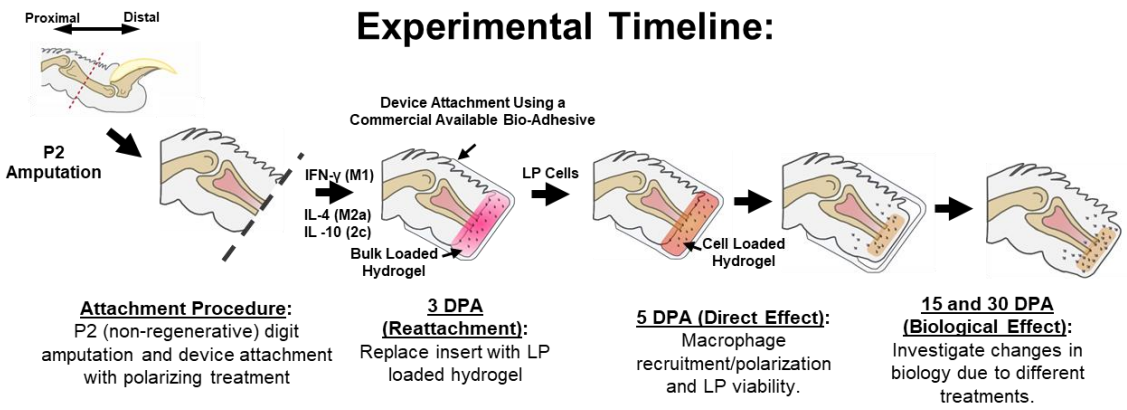


**Figure 6.2. Experimental Timeline of *In Vivo* Cell Delivery.** After attachment an insert with the desired cytokine treatment will be attached for 3 days. After this the insert will be replaced with the LP cell loaded insert. The device will remain attached for 2 days with removal at 5 DPA. Direct impact on the system will be evaluated at 5 DPA while intermediate and longer time points will be taken at 15 DPA and 30 DPA.

# Chapter 7: References


1. Reichert1, W. “Monty” *et al.* 2010 Panel on the Biomaterials Grand Challenges William. *J Biomed Mater Res A.* **96,** 275–287 (2011).

2. National Center for Health Statistics. Health, United States, 2016: With Chartbook on Long-term Trends in Health. *Cent. Dis. Control* 314–317 (2017). at <https://www.cdc.gov/nchs/data/hus/hus16.pdf#019>

3. Laurencin, C. T. & Nair, L. S. The Quest toward limb regeneration: a regenerative engineering approach. *Regen. Biomater.* **3,** 123–125 (2016).

4. Carlson, B. M. *Principles of Regenerative Biology*. (Elsevier/Academic, 2007).

5. McCusker, C., Bryant, S. V. & Gardiner, D. M. The axolotl limb blastema: cellular and molecular mechanisms driving blastema formation and limb regeneration in tetrapods. *Regeneration* **2,** 54–71 (2015).

6. Bryant, D. M. *et al.* Identification of regenerative roadblocks via repeat deployment of limb regeneration in axolotls. *npj Regen. Med.* **2,** 30 (2017).

7. Godwin, J. W., Pinto, A. R. & Rosenthal, N. A. Macrophages are required for adult salamander limb regeneration. **110,** (2013).

8. Quijano, L. M., Lynch, K. M., Allan, C. H., Badylak, S. F. & Ahsan, T. Looking Ahead to Engineering Epimorphic Regeneration of a Human Digit or Limb. **22,** 251–263 (2016).

9. Dolan, C. P. *et al.* Axonal regrowth is impaired during digit tip regeneration in mice. *Dev. Biol.* 0–1 (2018). doi:10.1016/j.ydbio.2018.11.010

10. Simkin, J. *et al.* The mammalian blastema: regeneration at our fingertips.

*Regeneration* **2,** 93–105 (2015).

11. Dolan, C. P., Dawson, L. A. & Muneoka, K. Digit Tip Regeneration: Merging Regeneration Biology with Regenerative Medicine. *Stem Cells Transl. Med.* **7,** 262–270 (2018).

12. Fernando, W. A. *et al.* Wound healing and blastema formation in regenerating digit tips of adult mice. *Dev. Biol.* **350,** 301–310 (2011).

13. Galliot, B., Crescenzi, M., Jacinto, A. & Tajbakhsh, S. Trends in tissue repair and regeneration. *Development* **144,** 357–364 (2017).

14. Reinke, J. M. & Sorg, H. Wound repair and regeneration. *European Surgical Research* **49,** 35–43 (2012).

15. Dawson, L. A. *et al.* The periosteal requirement and temporal dynamics of BMP2-induced middle phalanx regeneration in the adult mouse. *Regeneration* **4,** 140–150 (2017).

16. Simkin, J. *et al.* Macrophages are required to coordinate mouse digit tip regeneration. **4,** (2017).

17. Casas-engel, M. De & Corbí, A. L. of Macrophage Polarization : Infl ammation and Beyond. (2014). doi:10.1007/978-3-319-07320-0

18. Simkin, J. *et al.* Epidermal closure regulates histolysis during mammalian ( *Mus* ) digit regeneration. *Regeneration* **2,** 106–119 (2015).

19. Yu, L. *et al.* Angiogenesis is inhibitory for mammalian digit regeneration. *Regeneration* **1,** 33–46 (2014).

20. Das, A. *et al.* Monocyte and Macrophage Plasticity in Tissue Repair and

Regeneration. *Am. J. Pathol.* **185,** 2596–2606 (2015).

21. Sica, A. & Mantovani, A. Science in medicine Macrophage plasticity and polarization : in vivo veritas. **122,** 787–795 (2012).

22. Lehoczky, J. A., Robert, B. & Tabin, C. J. Mouse digit tip regeneration is mediated by fate-restricted progenitor cells. **108,** (2011).

23. Sammarco, M. C., Simkin, J., Cammack, A. J. & Fassler, D. Hyperbaric Oxygen Promotes Proximal Bone Regeneration and Organized Collagen Composition during Digit Regeneration. 1–16 (2015). doi:10.1371/journal.pone.0140156

24. Marrero, L., Simkin, J., Sammarco, M. & Muneoka, K. Fibroblast reticular cells engineer a blastema extracellular network during digit tip regeneration in mice. *Regeneration* **4,** 69–84 (2017).

25. Dawson, L. A. *et al.* Analogous cellular contribution and healing mechanisms following digit amputation and phalangeal fracture in mice. 39–51 (2016). doi:10.1002/reg2.51

26. Lin, G., Chen, Y. & Slack, J. M. W. Imparting regenerative capacity to limbs by progenitor cell transplantation. *Dev. Cell* **24,** 41–51 (2013).

27. Farkas, J. E. & Monaghan, J. R. A brief history of the study of nerve dependent regeneration. *Neurogenesis* **4,** e1302216 (2017).

28. Johnston, A. P. W. *et al.* Dedifferentiated Schwann Cell Precursors Secreting Paracrine Factors Are Required for Regeneration of the Mammalian Digit Tip. *Cell Stem Cell* **19,** 433–448 (2016).

29. Torossian, F. *et al.* Macrophage-derived oncostatin M contributes to human and mouse neurogenic heterotopic ossifications. *JCI insight* **2,** 2 (2017).

30. Guihard, P. *et al.* Oncostatin M, an inflammatory cytokine produced by macrophages, supports intramembranous bone healing in a mouse model of tibia injury. *Am. J. Pathol.* **185,** 765–775 (2015).

31. Demoulin, J. B. & Montano-Almendras, C. P. Platelet-derived growth factors and their receptors in normal and malignant hematopoiesis. *Am J Blood Res* **2,** 44–56 (2012).

32. Lee, J., Marrero, L., Yu, L., Dawson, L. A. & Muneoka, K. SDF-1 α / CXCR4 signaling mediates digit tip regeneration promoted by BMP-2. *Dev. Biol.* **382,** 98–109 (2013).

33. Yu, L., Han, M., Yan, M., Lee, J. & Muneoka, K. BMP2 induces segment-specific skeletal regeneration from digit and limb amputations by establishing a new endochondral ossification center. *Dev. Biol.* **372,** 263–273 (2012).

34. Han, M., Yang, X., Lee, J., Allan, C. H. & Muneoka, K. Development and regeneration of the neonatal digit tip in mice. *Dev. Biol.* **315,** 125–135 (2008).

35. Chen, Y., Xu, H. & Lin, G. Generation of iPSC-derived limb progenitor-like cells for stimulating phalange regeneration in the adult mouse. *Cell Discov.* **3,** 1–14 (2017).

36. Fernando, W. A. *et al.* Wound healing and blastema formation in regenerating digit tips of adult mice. **350,** 301–310 (2011).

37. Hechavarria, D., Dewilde, A., Braunhut, S., Levin, M. & Kaplan, D. L. BioDome regenerative sleeve for biochemical and biophysical stimulation of tissue regeneration. *Med. Eng. Phys.* **32,** 1065–1073 (2010).

38. Partlow, B. P. *et al.* Highly tunable elastomeric silk biomaterials. *Adv. Funct.*

*Mater.* **24,** 4615–4624 (2014).

39. Hassell, T., Gleave, S. & Butler, M. Growth inhibition in animal cell culture - The effect of lactate and ammonia. *Appl. Biochem. Biotechnol.* **30,** 29–41 (1991).

40. Kumar, M., Coburn, J., Kaplan, D. L. & Mandal, B. B. Immuno-Informed 3D Silk Biomaterials for Tailoring Biological Responses. (2016). doi:10.1021/acsami.6b09937

41. Gerhardt, L.-C. & Boccaccini, A. R. Bioactive Glass and Glass-Ceramic Scaffolds for Bone Tissue Engineering. *Materials (Basel).* **3,** 3867–3910 (2010).

42. Ferguson, M. W. J. & O 'kane, S. Scar-free healing: from embryonic mechanisms to adult therapeutic intervention. *Phil. Trans. R. Soc. Lond. B* **359,** 839–850 (2004).

43. Kasuya, A. & Tokura, Y. Attempts to accelerate wound healing. *J. Dermatol. Sci.* **76,** 169–172 (2014).

44. Boateng, J. & Matthews, K. H. Wound healing dressings and drug delivery systems : A review Wound Healing Dressings and Drug Delivery Systems : A Review. (2008). doi:10.1002/jps.21210

45. Phan, A. Q. *et al.* Positional information in axolotl and mouse limb extracellular matrix is mediated via heparan sulfate and fibroblast growth factor during limb regeneration in the axolotl ( *Ambystoma mexicanum* ). *Regeneration* **2,** 182–201 (2015).

46. Wu, Y. *et al.* Connective Tissue Fibroblast Properties Are Position-Dependent during Mouse Digit Tip Regeneration. *PLoS One* **8,** (2013).

47. Cooper, K. L. *et al.* Initiation of Proximal-Distal by Signals and Growth.

48. Einhorn, T. A. & Gerstenfeld, L. C. Fracture healing: Mechanisms and interventions. *Nat. Rev. Rheumatol.* **11,** 45–54 (2015).

49. Satoh, A., Suzuki, M., Amano, T., Tamura, K. & Ide, H. Joint development in Xenopus laevis and induction of segmentations in regenerating froglet limb (spike). *Dev. Dyn.* **233,** 1444–1453 (2005).

50. Lin, G., Chen, Y. & Slack, J. M. W. Imparting Regenerative Capacity to Limbs by Progenitor Cell Transplantation. *Dev. Cell* **24,** 41–51 (2013).

51. Rockwood, D. N. *et al.* Materials fabrication from Bombyx mori silk fibroin. *Nat Protoc* **6,** 1612–1631 (2011).

52. Pritchard, E. M., Dennis, P. B., Omenetto, F., Naik, R. R. & Kaplan, D. L. Review: Physical and chemical aspects of stabilization of compounds in silk. *Biopolymers* **97,** 479–498 (2012).

53. Liu, X., Sun, Q., Wang, H., Zhang, L. & Wang, J. Y. Microspheres of corn protein, zein, for an ivermectin drug delivery system. *Biomaterials* **26,** 109–115 (2005).

54. ImageJ. ImageJ User Guide. *IJ 1.46r* 187 (2003). doi:10.1038/nmeth.2019

55. Sfeir, C., Ho, L., Doll, B., K, A. & Hollinger, J. Fracture Repair. *Bone Regen. Repair Biol. Clin. Appl.* 21–44 (2005). doi:10.1385/1-59259-863-3:021

56. Satoh, A., Graham, G. M. C., Bryant, S. V. & Gardiner, D. M. Neurotrophic regulation of epidermal dedifferentiation during wound healing and limb regeneration in the axolotl (Ambystoma mexicanum). *Dev. Biol.* **319,** 321–335 (2008).

57. Markeson, D. *et al.* Scarring , stem cells , scaffolds and skin repair. **552,** 649–668 (2015).

58. Lin, A., Hokugo, A. & Nishimura, I. Wound closure and wound management. *Cell Adh. Migr.* **4,** 396–399 (2010).

59. SHIMOKAWA, T., YASUTAKA, S., KOMINAMI, R. & SHINOHARA, H. Wound epithelium function in axolotl limb regeneration. *Okajimas Folia Anat. Jpn.* **89,** 75–81 (2012).

60. Numata, K. & Kaplan, D. L. Silk-based delivery systems of bioactive molecules. *Adv. Drug Deliv. Rev.* **62,** 1497–1508 (2010).

61. Laing, R., Gillan, V. & Devaney, E. Ivermectin – Old Drug, New Tricks? *Trends Parasitol.* **33,** 463–472 (2017).

62. Lerchner, W. *et al.* Reversible Silencing of Neuronal Excitability in Behaving Mice by a Genetically Targeted, Ivermectin-Gated Cl- Channel. *Neuron* **54,** 35–49 (2007).

63. Melotti, A. *et al.* The river blindness drug Ivermectin and related macrocyclic lactones inhibit WNT-TCF pathway responses in human cancer. *EMBO Mol Med* **6,** 1263–1278 (2014).

64. Sharmeen, S. Activation of chloride channels with the anti-parasitic agent ivermectin induces membrane hyperpolarization and cell death in leukemia cells Activation of chloride channels with the anti-parasitic agent ivermectin induces membrane hyperpolarization and ce. **116,** 3593–3603 (2010).

65. Jin, L. *et al.* The antiparasitic drug ivermectin is a novel FXR ligand that regulates metabolism. *Nat. Commun.* **4,** 1–8 (2013).

66. Seil, M. *et al.* Ivermectin-dependent release of IL-1beta in response to ATP by peritoneal macrophages from P2X7-KO mice. *Purinergic Signal.* **6,** 405–416

(2010).

67. Zhang, X. *et al.* Inhibitory effects of ivermectin on nitric oxide and prostaglandin E2production in LPS-stimulated RAW 264.7 macrophages. *Int. Immunopharmacol.* **9,** 354–359 (2009).

68. Ventre, E. *et al.* Topical ivermectin improves allergic skin inflammation. *Allergy Eur. J. Allergy Clin. Immunol.* **72,** 1212–1221 (2017).

69. Miura, S., Takahashi, Y., Satoh, A. & Endo, T. Skeletal callus formation is a nerve-independent regenerative response to limb amputation in mice and Xenopus. 202–216 (2015). doi:10.1002/reg2.39

70. Richards, C. D. The Enigmatic Cytokine Oncostatin M and Roles in Disease. *ISRN Inflamm.* **2013,** 1–23 (2013).

71. Raggatt, L. J. *et al.* Fracture healing via periosteal callus formation requires macrophages for both initiation and progression of early endochondral ossification. *Am. J. Pathol.* **184,** 3192–3204 (2014).

72. Schlundt, C. *et al.* Macrophages in bone fracture healing: Their essential role in endochondral ossification. *Bone* **106,** 78–89 (2018).

73. Grässel, S. The role of peripheral nerve fibers and their neurotransmitters in cartilage and bone physiology and pathophysiology. *Arthritis Res. Ther.* **16,** 485 (2014).

74. Dubový, P., Jančálek, R. & Kubek, T. *Role of inflammation and cytokines in peripheral nerve regeneration*. *International Review of Neurobiology* **108,** (2013).

75. Gurtner, G. C., Werner, S., Barrandon, Y. & Longaker, M. T. Wound repair and regeneration. **453,** (2008).

76. Porcheray, F. *et al.* Macrophage activation switching: An asset for the resolution of inflammation. *Clin. Exp. Immunol.* **142,** 481–489 (2005).

77. Kwon, D. *et al.* Extra-Large Pore Mesoporous Silica Nanoparticles for Directing in Vivo M2 Macrophage Polarization by Delivering IL-4. *Nano Lett.* **17,** 2747–2756 (2017).

78. Spiller, K. L. *et al.* Sequential delivery of immunomodulatory cytokines to facilitate the M1-to-M2 transition of macrophages and enhance vascularization of bone scaffolds. *J. Biomater.* **1,** 194–207 (2015).

79. Eijkelkamp, N. *et al.* IL4-10 Fusion Protein Is a Novel Drug to Treat Persistent Inflammatory Pain. *J. Neurosci.* **36,** 7353–7363 (2016).

80. Girard, D., Ratthé, C., Ennaciri, J., Garcs Gonalves, D. M. & Chiasson, S. Interleukin (IL)-4 induces leukocyte infiltration in vivo by an indirect mechanism. *Mediators Inflamm.* **2009,** 1–11 (2009).

81. Segura, S., Gamazo, C., Irache, J. M. & Espuelas, S. Gamma interferon loaded onto albumin nanoparticles: In vitro and in vivo activities against Brucella abortus. *Antimicrob. Agents Chemother.* **51,** 1310–1314 (2007).

82. Kamaly, N. *et al.* Targeted Interleukin-10 Nanotherapeutics Developed with a Microfluidic Chip Enhance Resolution of Inflammation in Advanced Atherosclerosis. *ACS Nano* **10,** 5280–5292 (2016).

83. Duque, G. A. & Descoteaux, A. Macrophage cytokines: Involvement in immunity and infectious diseases. *Front. Immunol.* **5,** 1–12 (2014).

84. Siqueira Mietto, B. *et al.* Role of IL-10 in Resolution of Inflammation and Functional Recovery after Peripheral Nerve Injury. *J. Neurosci.* **35,** 16431–16442

(2015).

85. Sheikh, Z., Brooks, P. J., Barzilay, O., Fine, N. & Glogauer, M. Macrophages, foreign body giant cells and their response to implantable biomaterials. *Materials (Basel).* **8,** 5671–5701 (2015).

86. Ward, W. K. A review of the foreign-body response to subcutaneously-implanted devices: The role of Macrophages and cytokines in biofouling and fibrosis. *J. Diabetes Sci. Technol.* **2,** 768–777 (2008).

87. Wynn, T. A. & Vannella, K. M. Macrophages in Tissue Repair, Regeneration, and Fibrosis. *Immunity* **44,** 450–462 (2016).

88. David M. Mosser and Xia Zhang. Interleukin-10: new perspectives on an old cytokine. *Immunol Rev* 205–218 (2008). doi:10.1111/j.1600-065X.2008.00706.x.

89. Mescher, A. L. Macrophages and fibroblasts during inflammation and tissue repair in models of organ regeneration. *Regeneration* **4,** 39–53 (2017).

90. Etzerodt, A. & Moestrup, S. K. CD163 and Inflammation: Biological, Diagnostic, and Therapeutic Aspects. *Antioxid. Redox Signal.* **18,** 2352–2363 (2013).

91. Moeller, J. B. *et al.* CD163-L1 Is an Endocytic Macrophage Protein Strongly Regulated by Mediators in the Inflammatory Response. *J. Immunol.* **188,** 2399–2409 (2012).

92. Ogle, M. E., Segar, C. E., Sridhar, S. & Botchwey, E. A. Monocytes and macrophages in tissue repair: Implications for immunoregenerative biomaterial design. **241,** 1084–1097 (2016).

93. Higgins, D. M. *et al.* Localized immunosuppressive environment in the foreign body response to implanted biomaterials. *Am. J. Pathol.* **175,** 161–170 (2009).

94. Inardi, S. I. M. *et al.* IL-4 Release from a Biomimetic Scaffold for the Temporally Controlled Modulation of Macrophage Response. (2016). doi:10.1007/s10439-016-1580-z

95. Klopfleisch, R. Macrophage reaction against biomaterials in the mouse model – phenotypes, functions and markers. *Acta Biomater.* (2016). doi:10.1016/j.actbio.2016.07.003

96. Amy E. Thurber, Fiorenzo G. Omenetto, and D. L. K. In Vivo Bioresponses to Silkublic Access. *Biomaterials* **71,** 145–157 (2015).

97. Seifert, A. W. & Muneoka, K. The blastema and epimorphic regeneration in mammals. *Dev. Biol.* **433,** 190–199 (2018).

98. Rees, A. J. Macrophage Biology : An Overview. *YSNEP* **30,** 216–233 (2010).

99. Klopfleisch, R. Acta Biomaterialia Macrophage reaction against biomaterials in the mouse model – Phenotypes , functions and markers. *Acta Biomater.* **43,** 3–13 (2016).

100. Alberto Mantovani, Silvano Sozzani, Massimo Locati, P. A. and A. S. Macrophage polarization: tumor-associated macrophages as a paradigm for polarized M2 mononuclear phagocytes. *TRENDSin Immunol.* **23,** 549–555 (2002).

101. Li, J. & Mooney, D. J. Designing hydrogels for controlled drug delivery. *Nat. Rev. Mater.* **1,** 1–38 (2016).

102. Tang, L. *et al.* Enhancing T cell therapy through TCR-signaling-responsive nanoparticle drug delivery. *Nat. Biotechnol.* **36,** (2018).

103. Wang, X., Yucel, T., Lu, Q., Hu, X. & Kaplan, D. L. Silk nanospheres and microspheres from silk/pva blend films for drug delivery. *Biomaterials* **31,** 1025–

1035 (2010).

104. Biswas, S. K. & Mantovani, A. review Macrophage plasticity and interaction with lymphocyte subsets : cancer as a paradigm. *Nat. Publ. Gr.* **11,** 889–896 (2010).

105. Wang, X., Ge, J., Tredget, E. E. & Wu, Y. The mouse excisional wound splinting model, including applications for stem cell transplantation. *Nat. Protoc.* **8,** 302–9 (2013).

106. Farah, Z., Fan, H., Liu, Z. & He, J. Q. A concise review of common animal models for the study of limb regeneration. *Organogenesis* **12,** 109–118 (2016).

107. Dunn, L. *et al.* Murine Model of Wound Healing. *J. Vis. Exp.* 1–6 (2013). doi:10.3791/50265

108. David M. Mosser and Xia Zhang. in *Current protocols in immunology / edited by John E.Coligan ...[et al.]* 5447–5453 (2010). doi:10.1002/0471142735.im1402s83.Activation

109. King, A., Balaji, S., Le, L. D., Crombleholme, T. M. & Keswani, S. G. Regenerative Wound Healing: The Role of Interleukin-10. *Adv. Wound Care* **3,** 315–323 (2014).

110. Graney, P. L., Lurier, E. B. & Spiller, K. L. Biomaterials and Bioactive Factor Delivery Systems for the Control of Macrophage Activation in Regenerative Medicine. *ACS Biomater. Sci. Eng.* acsbiomaterials.6b00747 (2017). doi:10.1021/acsbiomaterials.6b00747

111. Mills, C. D. Anatomy of a discovery: M1 and M2 macrophages. *Front. Immunol.* **6,** 1–12 (2015).

112. So, E.-Y., Park, H.-H. & Lee, C.-E. IFN- and IFN- Posttranscriptionally Down-Regulate the IL-4-Induced IL-4 Receptor Gene Expression. *J. Immunol.* **165,**

5472–5479 (2000).

113. Cooper, K. L. *et al.* Initiation of proximal-distal patterning in the vertebrate limb by signals and growth. *Science (80-. ).* **332,** 1083–1086 (2011).

114. Aurora, A. B. & Olson, E. N. Immune modulation of stem cells and regeneration. *Cell Stem Cell* **15,** 14–25 (2014).

# Appendix A: Supplementary Information for Chapter 2

**Table S.2.1.** Material Used for Device and Hydrogel Fabrication

| Item(s) | Vendor | Catalogue Number |
|---|---|---|
| Outer Sleeve: | | |
| Form 2 SLA 3D-Printer | Formlabs | N/A |
| Dental SG Resin | Formlabs | RS-F2-DGOR-01 |
| MelodySusie 36W UV Nail Dryer | Amazon | B00NPW16QW |
| Isopropanol (ACS grade) | Fischer-Scientific | A416-4 |
| Soft Silicone Insert: | | |
| Dragon Skin™ 10 NV | Smooth-On | N/A |
| Polyether Ether Ketone Rod 1-Inch thick | McMaster-Carr | 7707T21 |
| Bel-Art™ Space Saver Vacuum Desiccators | Fischer-Scientific | 08-594-15B |
| Integra™ Miltex™ Standard Biopsy Punches | Fischer-Scientific | 12-460-409 |
| Protective Cap: | | |
| USA Scientific Inc 2.0 mL Flat Cap Tube | Fischer-Scientific | NC9558509 |
| Dental LT Clear Resin | Formlabs | RS-F2-DLCL-01 |
| Silk Hydrogel Solution: | | |
| DMEM Concentrated Media (10x) | MiliporeSigma | D2429-100ML |
| Dextrose (USP grade) | MiliporeSigma | D9434-250G |
| Hanks Buffer Salt Solution | MiliporeSigma | H9394-100ML |
| Sodium Bicarbonate | MiliporeSigma | S6297-250G |
| Gibco™ GlutaMAX™ Supplement | Fischer-Scientific | 35-050-061 |
| Hydrogen Peroxide | MiliporeSigma | H3410-500ML |
| Horseraddish Peroxidase | MiliporeSigma | P8375-5KU |
| Hydrogel Insert Loading: | | |
| Eppendorf™ Microcentrifuge Tubes | Fischer-Scientific | 05-402 |
| ARTEC EDUCATIONAL Mini Centrifuge | Amazon | B00ITX7XVE |
| Forceps Fine-tip (4SA) | Fischer-Scientific | 17-467-147 |

**Table S.2.1. Products used in Fabrication and Application of Wearable Bioreactor.**

**Table S.2.2.** Material Used for Animal Surgeries

| Item(s) | Vendor | Catalogue Number |
|---|---|---|
| General: | | |
| Surgical Drapes | Fischer-Scientific | 13-005-198 |
| Gauze | Fischer-Scientific | 22-037-975 |
| Beta Iodine Swabs | Fischer-Scientific | NC0116841 |
| Alcohol Pads | Fischer-Scientific | 19-090-833 |
| 1 mL syringe with 25 gauge needle | Fischer-Scientific | 14-823-30 |
| Skin-Tite BioAdhesive | Smooth-On | N/A |
| Bent Surgical Probe | Fischer-Scientific | 17-467-600 |
| Attachment: | | |
| Foreceps (Percise and Straight) | Fischer-Scientific | 22-327379 |
| 3.5-inch Spencer Suture Scissors | Henry Schien | 1006024 |
| Maintenance During Attachment: | | |
| Insulin Syringe | Fischer-Scientific | 14-829-1B |
| 25 Gauge Needle | Fischer-Scientific | 14-821-13D |
| Removal and Reattachment: | | |
| Forceps (Bent) | Fischer-Scientific | 16-100-110 |

**Table S.2.2. Products used in Surgery**

# Appendix B: Supplementary Information for Chapter 3

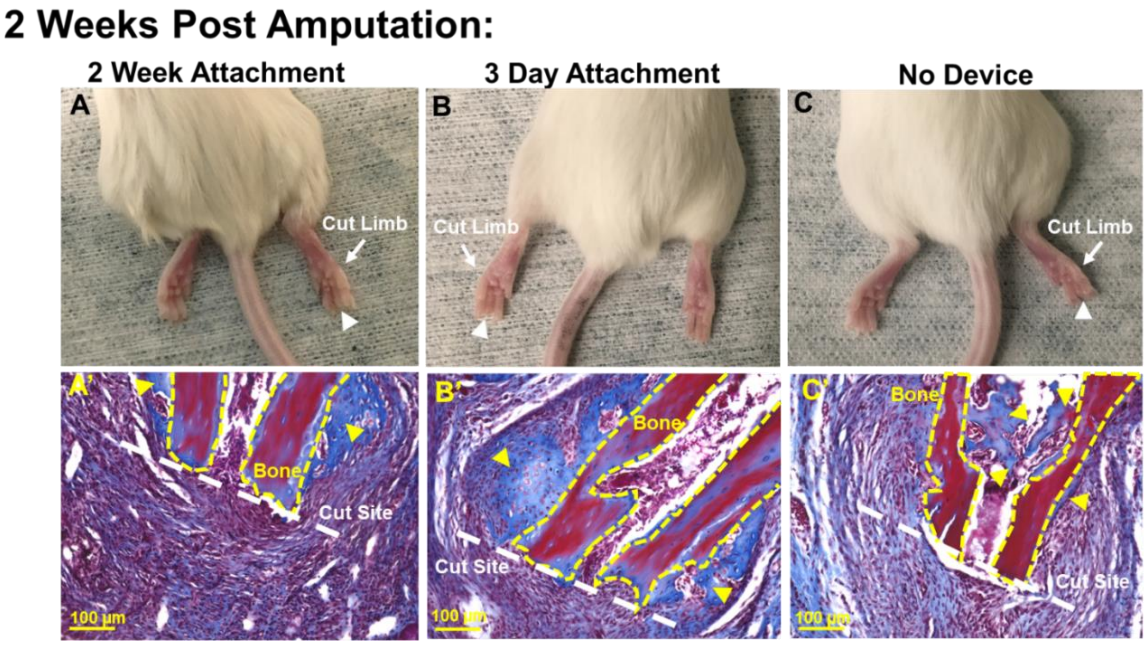


**Supplementary Figure 3.1. Evaluation of Device Attachment for Extended Time Periods.** The 2 week attachment shows almost no difference in morphology compared to the 3 day attached animals but improvement compared to the no device animals.

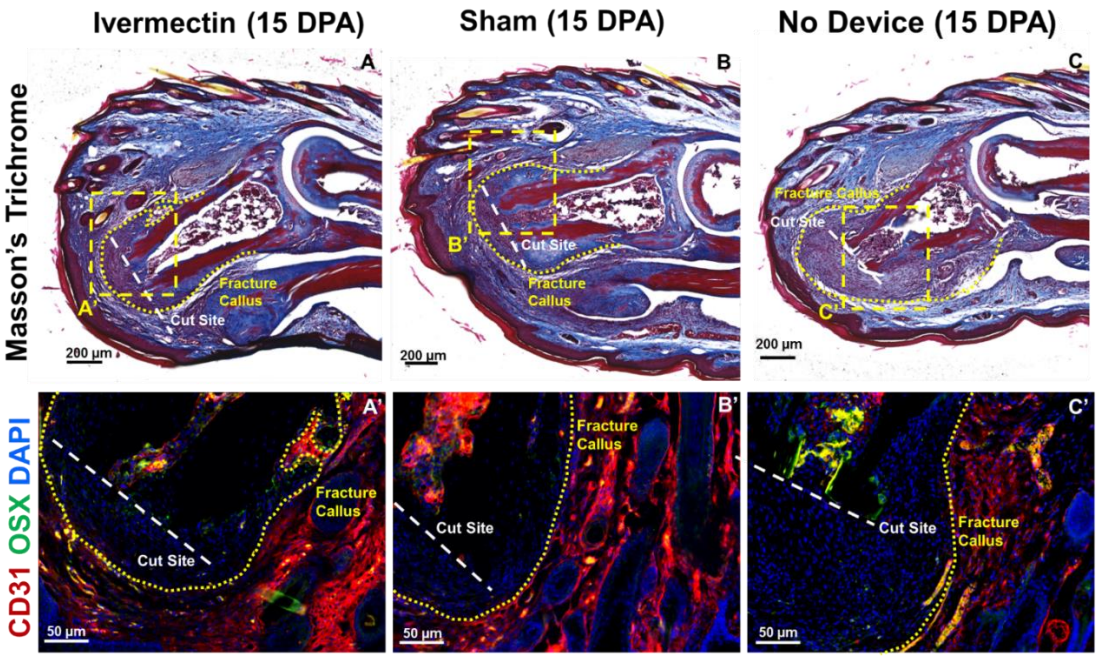


**Supplementary Figure 3.2. Example of Masson Trichrome and IHC for CD31 to Determine Fracture Callus Area.** The fracture callus is mostly avascular with vascularized tissue surrounding it at 15 DPA. As a result the vasculature marker CD31 can demarcate the fracture callus area.

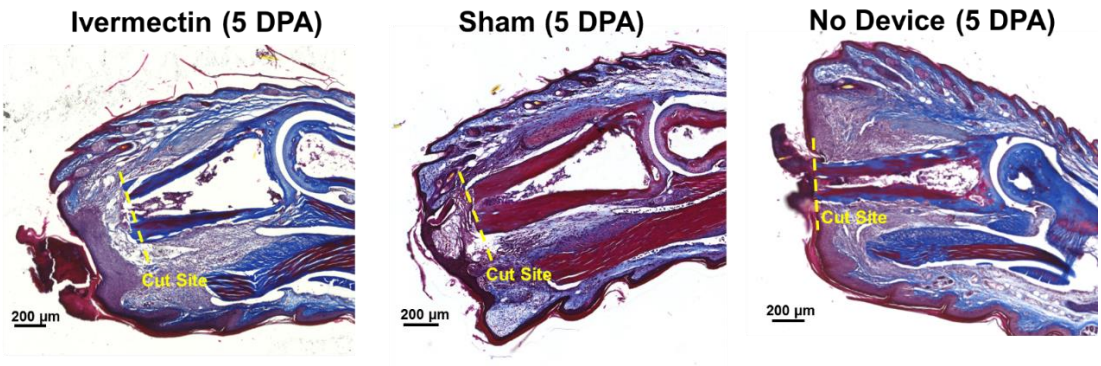


**Supplementary Figure 3.3. 5 DPA Histology**. Histology demonstrates little difference between the sham and ivermectin treated groups while the no device animal wound is still open.

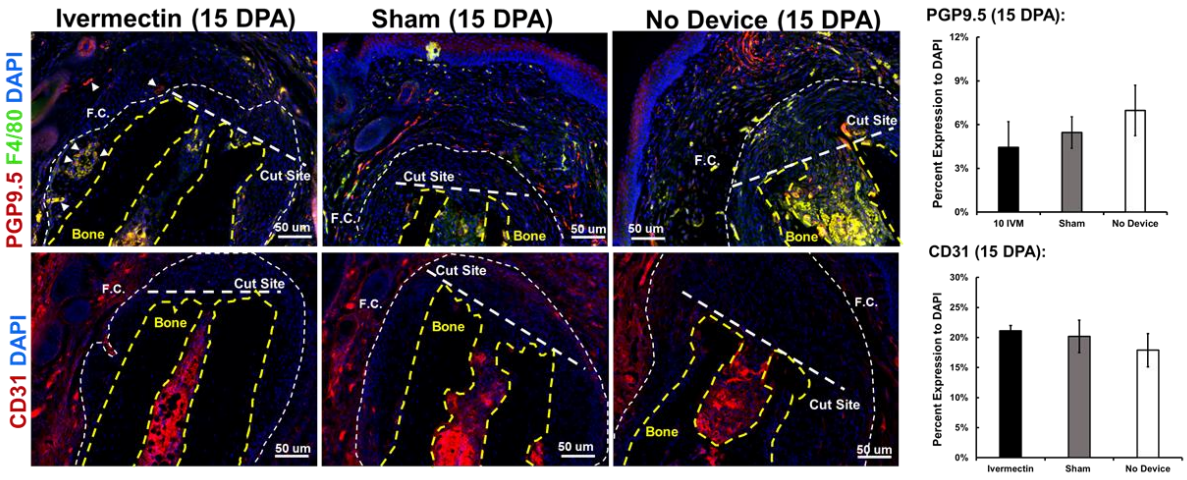


**Supplementary Figure 3.4. 15 DPA PGP9.5 and F4/80 stain.** Results demonstrate that there was no difference in the vasculature marker CD31, nerve marker PGP9.5, and macrophage marker F4/80 from Ivermectin treatments at 15 DPA.

# Appendix C: Supplementary Information for Chapter 4

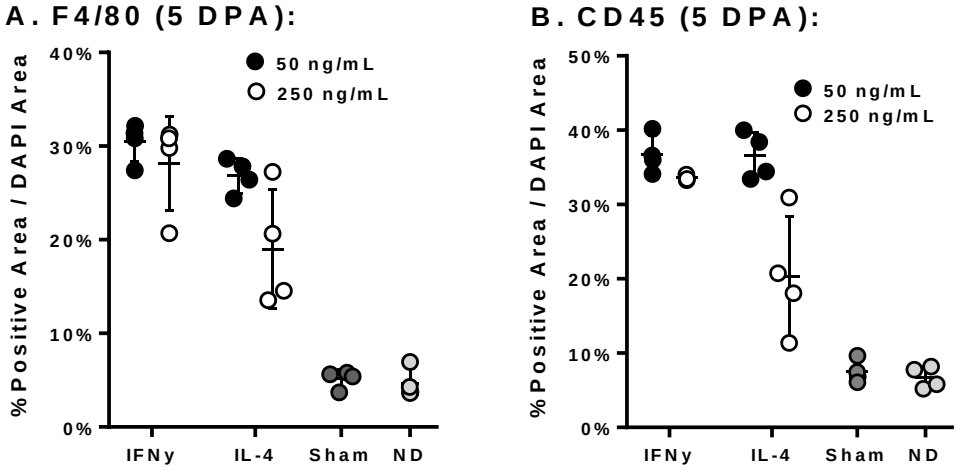


**Supplementary Figure 4.1. Quantification of F4/80 and CD45 for the high and low dose of IFNy and IL-4 at 5 DPA**. Statistical Analysis was performed using ANOVA single factor followed by a student's t-test to compare groups. Significance to the control group is measured as following p-values * ≤ 0.05, ** ≤ 0.01, and *** ≤ 0.001. Arrows points to CD45 expression and arrowheads point to F4/80 expression. Population of each group is N ≥ 3.

# Appendix D: Supplementary Information for Chapter 5

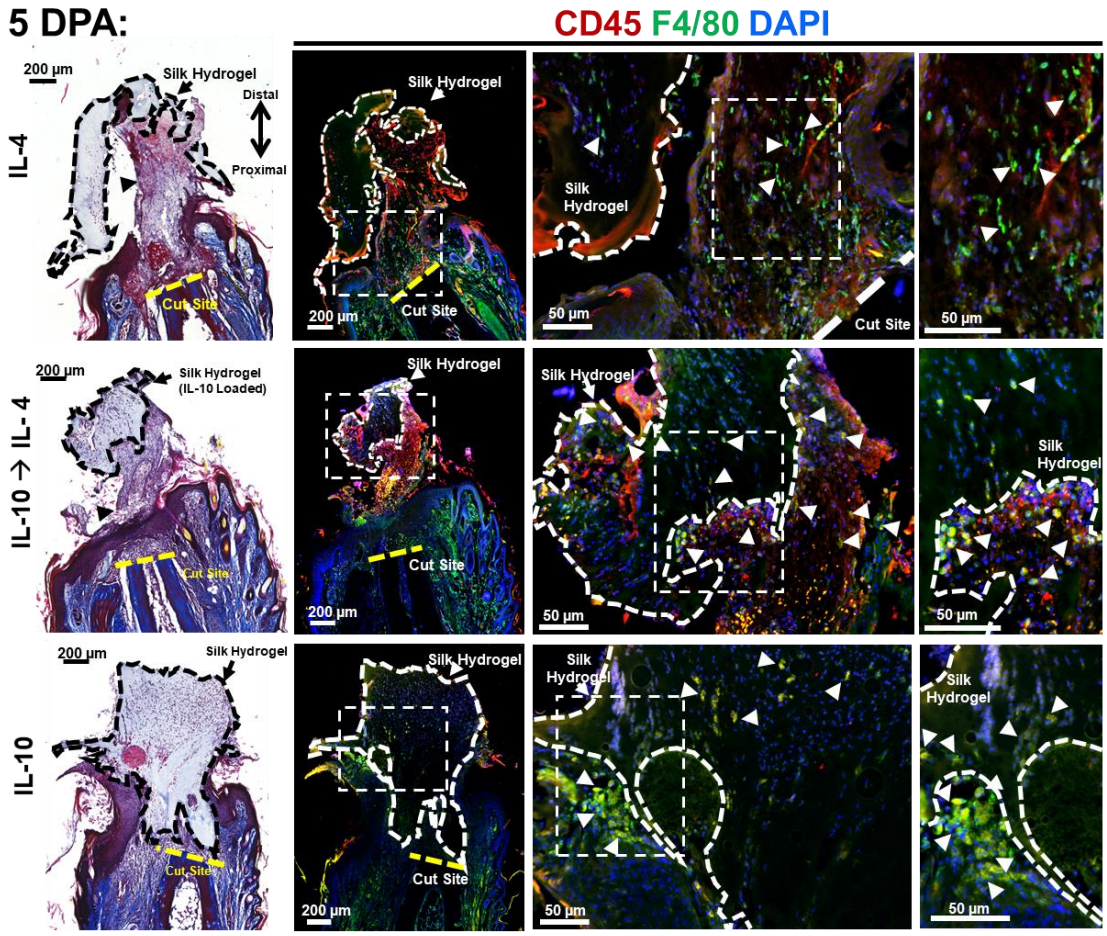


**Supplementary Figure 5.1. Morphology and IHC to represent changes in morphology observed in the IL-10 to IL-4 treated group.** When compared histologically to IL-4 and IL-10 bulk treated animal it becomes apparent that the IL-10 to IL-4 treated animals share a combined morphology with enhanced tissue growth and non-immune cells infiltrating into the hydrogel.